LYAPUNOV-BASED FAULT TOLERANT CONTROL

OF QUADROTOR UNMANNED AERIAL VEHICLES

Xiaobing Zhang

A Thesis

in

The Department

of

Mechanical and Industrial Engineering

Presented in Partial Fulfillment

of the Requirements

for the Degree of Master of Engineering

at Concordia University

Montreal, Quebec, Canada

March 2010

Your file Votre référence
ISBN: 978-0-494-71047-0
Our file Notre référence
ISBN: 978-0-494-71047-0

CONCORDIA UNIVERSITY

SCHOOL OF GRADUATE STUDY

This is to certify that the thesis prepared

By: **Xiaobing Zhang**

Entitled: **LYAPUNOV-BASED FAULT TOLERANT CONTROL OF QUADROTOR UNMANNED AERIAL VEHICLES**

and submitted in partial fulfillment of the requirements of the degree of

MASTER OF APPLIED SCIENCE (Mechanical Engineering)

Complies with the regulations of the university and meets the accepted standards with respect to originally and quality.

Signed by the final examining committee:

_____Chair

_____External Examiner

C. Wang

_____Internal Examiner

W. F. Xie

_____Co-supervisor

Y. M. Zhang

_____Co-supervisor

C. Y. Su

Approved by _____

Mar. 30, 2010

ABSTRACT

LYAPUNOV-BASED FAULT TOLERANT CONTROL OF QUADROTOR UNMANNED AERIAL VEHICLES

Xiaobing Zhang

This thesis presents the theoretical development, simulation study and flight tests of a Lyapunov-based control approach for the Fault Tolerant Control (FTC) of a quadrotor unmanned aerial vehicle (UAV). Based on the derivation of nonlinear model of the dynamics of the quadrotor UAV, a Lyapunov-based control approach with fixed controller gains is proposed and firstly demonstrated through simulations of the quadrotor UAV for handling system parameter uncertainties. Secondly, this proposed Lyapunov-based approach with the selected controller gains is applied as a fault tolerant controller in the framework of a passive Fault Tolerant Control System (FTCS), for handling less severe faults occurring in the quadrotor UAV. Thirdly, the proposed new controller by Lyapunov-based adaptive control method for fault tolerant control of the quadrotor UAV is proposed to handle more severe faults. Finally, the Lyapunov-based control method has been implemented to the test bed, Qball-X4 Unmanned Aerial Vehicle, and the acceptable performances on altitude control have been achieved.

In the thesis, simulation and flight testing results demonstrate that the FTCS with the Lyapunov-based approach has certain robustness for most of partial losses. However, the FTCS with Lyapunov-based adaptive control approach has advantages in accommodating more severe faults for, which may not be addressed by the Lyapunov-based approach.

Acknowledgments

This thesis would not have been possible without the very substantial support of the many individuals.

I owe my deepest gratitude to my supervisors, Professor Youmin Zhang and Professor Chun-Yi Su, thanks to whom I was offered this opportunity to study at Concordia University and work for the NSERC project. In addition, I greatly appreciate their invaluable assistance, encouragement and guidance, not only for the research work, but also for the writing of the thesis. Their passion for academic research and their rigorous scholarship attitude will have a long-lasting effect on me in the future.

I am also grateful for Dr. Ying Feng's considerable assistance through my entire research work. She always made herself ready, available and accessible to help me. I thank her generous assistance.

I am profoundly thankful to my family members for their everlasting love and support. Without their encouragement and support, it would have been impossible for me to complete this thesis work.

Lastly, I am happy to have had a chance to offer my respect and best wishes to all of colleagues and friends supporting me in every aspect during the completion of the thesis.

TABLE OF CONTENTS

List of Figures

List of Tables

Nomenclature

x_E, y_E, z_E	Inertial frame fixed with Earth along *x, y, z* axis
x_B, y_B, z_B	Body frame fixed with quadrotor UAV along *x, y, z* axis
x, y, z	Position of quadrotor UAV in Earth frame along *x, y, z* axis
l	Distance of motor from pivot centre
J_x	Moment of inertial in roll
J_y	Moment of inertial in pitch
J_z	Inertial moment in yaw
g	Gravity acceleration
F_1, F_2, F_3, F_4	Thrusts generated by corresponding rotor blades
L	Rolling moment
M	Pitching moment
N	Yawing moment
m	Mass of quadrotor UAV
$\ddot{\phi}$	Roll angular acceleration
$\ddot{\theta}$	Pitch angular acceleration
$\ddot{\psi}$	Yaw angular acceleration
$\dot{\phi}$	Roll angular velocity
$\dot{\theta}$	Pitch angular velocity
$\dot{\psi}$	Yaw angular velocity

ϕ	Roll angle fixed with Earth frame
θ	Pitch angle fixed with Earth frame
ψ	Yaw angle fixed with Earth frame
ω_B	Quadrotor UAV's angular velocity
P	Roll angular velocity of quadrotor UAV
Q	Pitch angular velocity of quadrotor UAV
R	Yaw angular velocity of quadrotor UAV
u	Velocity along x_B with body frame
v	Velocity along y_B with body frame
w	Velocity along z_B with body frame
k_{di} $(i=1,...,6)$	Drag coefficients

Acronyms

UAV	Unmanned Aerial Vehicle
VTOL	Vertical Taking-Off and Landing
FTC	Fault Tolerant Control
FTCS	Fault Tolerant Control System
PFTCS	Passive Fault Tolerant Control System
AFTCS	Active Fault Tolerant Control System
FDD	Fault Detection and Diagnosis

CHAPTER 1

INTRODUCTION

UAVs (Unmanned Aerial Vehicles) are aircraft with no pilot on board. Based on this definition, UAVs have a great family which includes flying robots (such as the Pointer, Javelin, and Black Pack Mini), the VTOL (Vertical Taking-Off and Landing) UAVs (including conventional helicopters, quadrotor helicopters, and two-tilt-rotor rotorcrafts), airships and others. Since UAVs have no crew, compared with manned airplanes, they are more desirable in implementing tasks in dangerous or inaccessible environments, and necessary in possessing autonomous and fault-tolerant capabilities for assigned missions.

In the Fault Tolerant Control System (FTCS) field, some UAVs have been chosen to be the research platforms, such as the fixed-wing aircraft, the conventional helicopter, the airship and the quadrotor helicopter. Compared with other aircrafts, the quadrotor helicopter has many advantages for being used as a university research platform. Firstly, its small rotor size is perfect for indoor flight, in comparison with the fixed-wing airplanes, which is capable of avoiding the less damage in the event of a collision; Secondly, simple design results in the less mechanical failure and low maintenance; Thirdly, its payload capacity allows researchers to do different tasks and implement more complicated missions.

1.1 Background

Research of the quadrotor helicopter has travelled a long path, which can be traced back to the beginning of last century. In the past, the most striking work had been done

by Etienne Oehmichen in 1920s, Dr. George de Bothezat and Ivan Jerome in 1922, and Convertawings Model "A" quadrotor helicopter, in Amityville in 1956.

Etienne Oehmichen designed and built two machines. The first one in the 1920s with six rotating wing machines had been tested and had failed because the lift generated by the twin rotors with a 25hp engine was less than the machine's gravity [1].

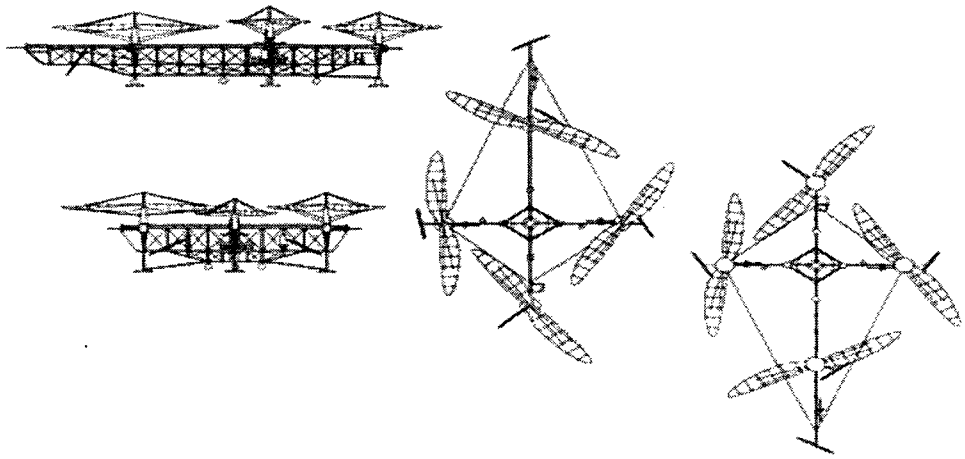

Figure 1-1 Oemichen No. 2 [1]

The second machine shown in Figure 1-1 had four rotors and eight propellers that were all driven by a single 120 hp Le Rhone rotary engine, which showed strong, stable and controllable ability, through the implementation of more than one thousand test flights during the mid-1920s. The most successful experiment was made on April 17, 1924 when Oemichen No. 2 established the first-ever 1 km flight for 7 minutes and 40 seconds. The success of the aircraft had made was attributed to its structure. Oemichen No. 2 was basically a steel-tube frame, with two blade rotors at the end of its four arms. The angle of these blades could vary by warping. One propeller located at the nose was for steering the helicopter; five of the propellers, turning in a horizontal plane, worked on stabilizing

the machine laterally; and the remaining pair acted as pusher propellers for forward propulsion.

During the same period, Dr. George de Bothezat and Ivan Jerome received a contract from the US Army Air Corps to develop a vertical flight machine [2]. The 1678 kg "X"-shaped structure in Figure 1-2 supported an 8.1m diameter six-blade rotor at each end of its 9m arms. Every rotor had been designed to occupy individual collective pitch control, and then it could produce differential thrust through vehicle inclination for translation. Its two small propellers with variable pitch were for producing the thrust and yaw control, and they were mounted at the ends of the lateral arms. The aircraft experienced its first flight in October 1922, and with a weight of 1700kg at take-off. This aircraft had been tested with one hundred flights, especially one experiment which had three "passengers" hanging on its airframe. At the highest altitude, it reached five meters. All of these efforts totally proved that practical helicopters would be theoretically possible and become a reality in the future.

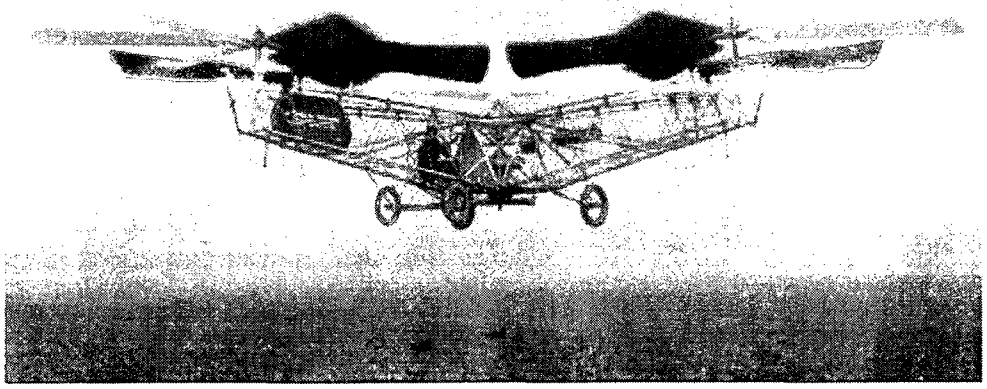

Figure 1-2 The "X"- shaped structure quadrotor [2]

Another stunning design for the quadrotor helicopter was the Convertawings Model "A" in 1956, shown in Figure 1-3, which was built for much larger civil and military quadrotor helicopters [3]. Unlike the former two varieties of quadrotor helicopters, this unique helicopter had additional wings mounted to help four rotors in achieving enough lift, and it had two engines to drive four rotors. Under this structure, Convertawings Model "A" quadrotor helicopter without a tail rotor was controlled by varying the thrust between the rotors. In the mid-1950s, this helicopter had undergone many experiments and successfully achieved its design objectives.

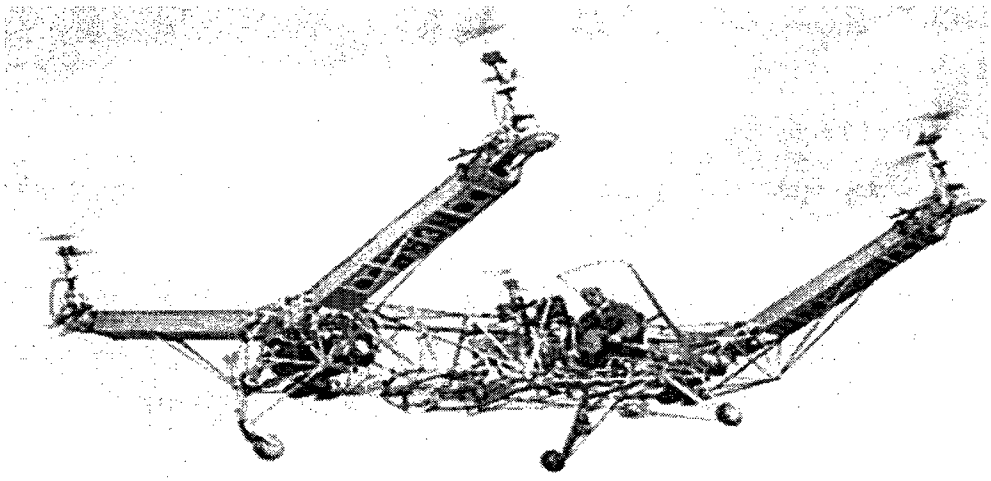

Figure 1-3 Convertawings quadrotor helicopter model A [3]

The quadrotor has undergone through two generations since 1920 [4]. The three quadrotors mentioned above belong to the first generation. They were intended to carry one or more passengers. Although these vehicles couldn't bear much pilot workload and increase their stability, they were still the first successful heavier-than-air Vertical Taking-Off and Landing (VTOL) machines. The current generation of quadrotor helicopters is called Unmanned Aerial Vehicles (UAVs), since they are without pilots.

Moreover, UAVs have dramatically improved in their maneuverability and have reduced their size simultaneously.

Following the success achieved by previous researchers, many universities and companies nowadays are working on the quadrotor UAV research projects. Meanwhile, commercial vehicles are designed by companies in a very popular manner.

One of the most famous companies is Draganfly Innovations Inc. in Canada. Since its founding in 1998, Draganfly Innovations Inc. has made great efforts to deliver products, from the hobby line to emergency services in dangerous environments. Recent machines designed by Draganfly Innovations Inc. are the Draganflyer X4 helicopter (a quadrotor helicopter) and the Draganflyer X6 helicopter (a six-rotor helicopter). Since the Draganflyer X4 presented in Figure 1-4 is an affordable, maintainable, stable UAV and a suitable platform for research and development [5], it has been adopted as a research platform by many research institutes, such as the Massachusetts Institute of Technology (MIT) [6], Vanderbilt University [7], Boeing Research and Technology [8] in USA, and most recently, by Concordia University in Canada [9].

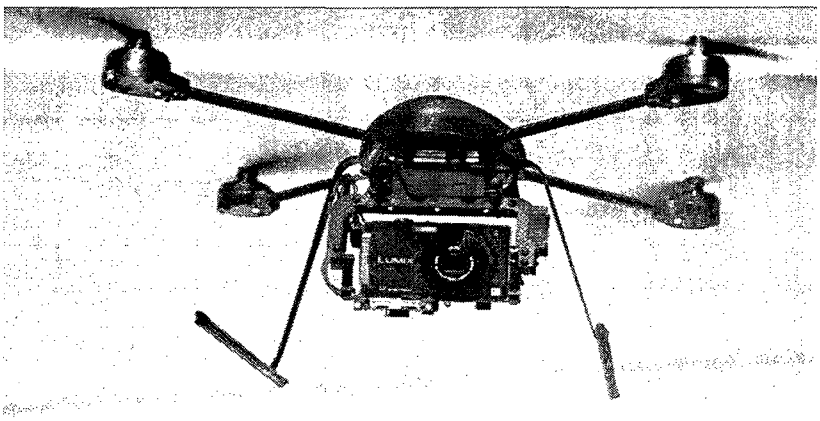

Figure 1-4 Dranganflyer X4 helicopter [5]

Equipped with ten sensors (three accelerometers, three gyroscopes, three magnetometers, and one barometric pressure sensor), the Draganflyer X4 can fly at a determined attitude and position, relying on the control software. It consists of quad super-quiet brushless motors, a quad counter-rotating carbon fiber rotor blade, eight color-coded day and night LED navigation lights, a flexible and shock-absorbing releasing and landing gear, RF Communication, and a digital still/video camera. Depending on an onboard wireless video camera which provides 1280*720 resolutions and can be used for night search and rescue, the Dranganflyer X4 is capable of reconnaissance tasks. Moreover, the simplicity of the quadrotor design, without any moving parts, provides less maintenance time and maintenance fees. The inherent structure of the quadrotor UAV, with two pairs of counter-rotating rotor blades, provides stability to the quadrotor UAV.

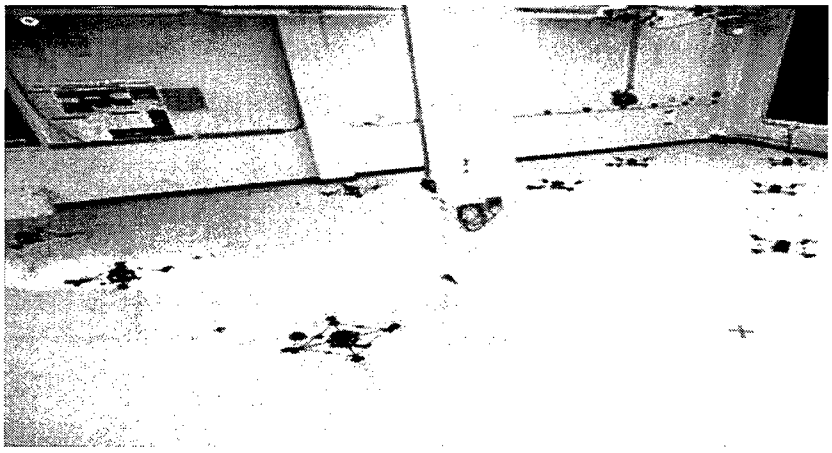

Figure 1-5 The quadrotor fleet of MIT [6]

Figure 1-5 shows MIT's first demonstration in March 2007 [6]. Ten quadrotor UAVs (model: Draganflyer V Ti Pro's) fly autonomously to surveil and monitor ground objects or vehicles. MIT's system makes it possible to have a number of aerial vehicles flying

completely under computer control, and it is able to do tasks like surveillance or tracking while keeping each individual vehicle from collision with any others. The vehicles can all be coordinated towards the same task, or be used in group or individually.

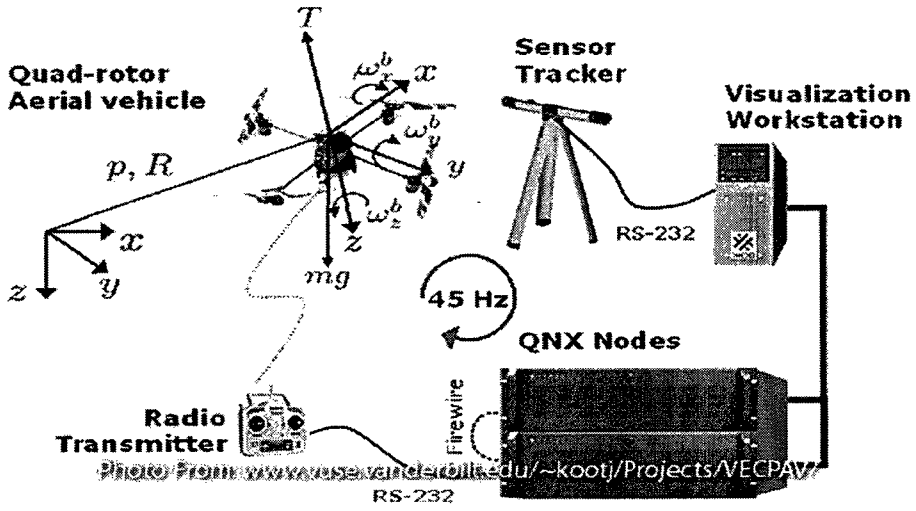

Figure 1-6 Embedded computing platform of Vanderbilt university [7]

In November 2007, Vanderbilt University employed Draganflyer RC helicopters to develop an Autonomous Control System (the VECPAV Project-Vanderbilt Embedded Computing Platform for Autonomous Vehicles) as shown in Figure 1-6 [7]. The VECPAV system applies a sensor tracker to obtain the motion and position of a Draganflyer RC helicopter, then analyzes these data and sends commands back to the Draganflyer RC helicopter through a radio control transmitter, telling the Draganflyer RC helicopter to maintain its position or to move through its flight plan.

Boeing Research and Technology has developed, collaborated with MIT, a test-bed in the Vehicle Swarm Technology Lab (VSTL) to support 13 vehicles' routine flights only from one human operator in 2009 [8]. The entire system includes several subsystems, and they are position reference subsystem, the vehicles subsystem, ground control computers

subsystem, and command & control computers subsystem. These subsystems communicate through the two network buses which are one network for position and altitude data, another network for health condition, capability data, and commands respectively. Moreover, the interaction between these subsystems is achieved in real-time environment.

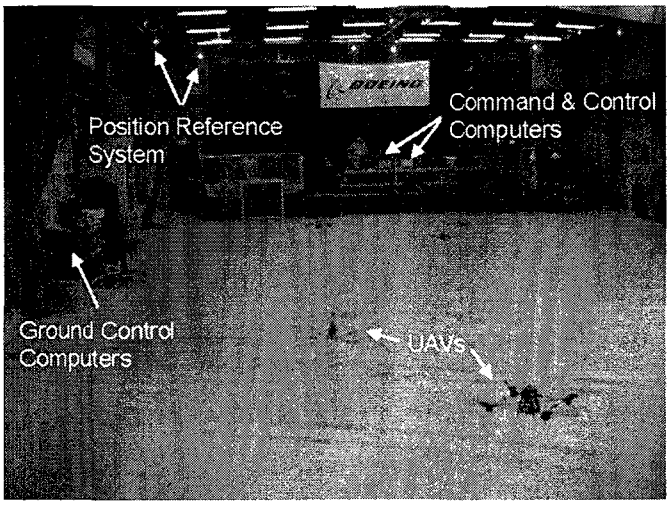

Figure 1-7 Test-bed of Boeing's vehicle swarm technology lab [8]

Supported by an NSERC (Natural Sciences and Engineering Research Council of Canada) Strategic Project Grant (SPG), the Networked Autonomous Vehicles Lab. (NAVL) at the Department of Mechanical and Industrial Engineering of Concordia University has worked on fault-tolerant cooperative control of Quadrotor UAVs since 2007 [9]. The test-bed available at the NAVL included several quadrotor UAVs based on the Draganflyer X4 UAV, "Qball" quadrotor UAV, and Wheeled Mobile Robots (WMR) developed by Quanser Innovations Inc. through the support of the NSERC SPG project led by Concordia University, as shown in Fig. 1-8.

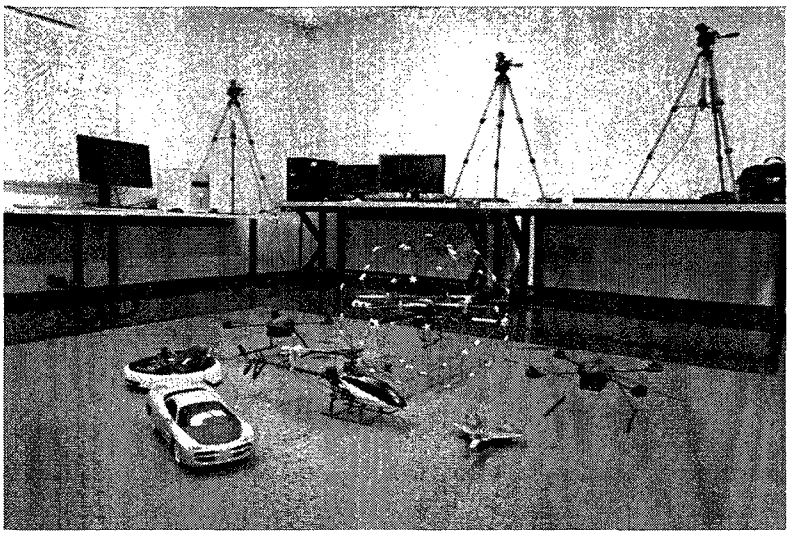

Figure 1-8 Test-bed of Concordia's networked autonomous vehicles lab [9]

When comparing current quadrotor helicopters with conventional ones, the quadrotor helicopters have distinct advantages as follows:

- Without pilots to be trained, swarm deployed vehicles can be controlled by one person through remote controller.
- Its smaller size, without mechanical linkages, makes the vehicles much safer (it does not easily damage itself and its surroundings), simplifies the design leading to reduced costs, and provides less maintenance requirements [10].
- It increases the payload capacity because of its multi-rotors.
- It is effective at surveillance, inspection and emergency tasks because of its capability at taking-off and landing in a smaller area and is easily able to hover above any targets [11].

However, in certain cases, some of its advantages become disadvantages. High agility is an excellent quality for implementing tasks, while it makes the control more difficult

because of dynamic instabilities and sensitivity to disturbances. Meanwhile, obtaining of higher payload capacity comes at the price of increasing energy consumption due to extra motors.

1.2 Literature Review

As one of the most complex flying machines, various control strategies have been investigated for controlling quadrotor UAVs to meet different control objectives. Since recent existing research works handle control designs mostly for normal flight conditions of UAVs, the literature review given in this section is firstly about control approaches without consideration of faults to be occurred in the quadrotor UAVs; Then the current fault tolerant control approaches are discussed in the following part.

For the control of the UAV system under normal case, various control methods have been explored to improve the control performance. Altug *et al* [12] utilized feedback linearization method to stabilize altitude and Euler angles, while Mistler *et al* [13] stabilized the position and yaw angle. Lee *et al* [14] designed output feedback (OFB) for a nonlinear UAV system and applied an observer to estimate the velocities of the UAV. Based on the above research, the PD^2 (proportional and twice derivative) feedback structure was used by Tayebi and McGilvray [15], where the two derivative actions offered the benefits to accommodate the transient performance and disturbances in the practical application. Since feedback linearization method relies on the access of accurate information or exact mathematical model, it degrades the robustness and performance of the system [20]. To ensure robustness to the uncertainty, Mokhtari *et al* [16] proposed a robust feedback linearization approach combining with H_∞ controller, where H_∞ strategy

made the controller more robust to handle aerodynamic force disturbances and 20% parameter uncertainties on mass and inertia. To achieve the same objective, Benallegue *et al* [17] attempted to combine the feedback linearization with the high-order sliding mode observer by utilizing the benefit of sliding mode control (insensitivity to the uncertainties and disturbances). High-order sliding mode observer worked as an observer and the estimator of the external disturbances. In addition, another challenge of the norm form of the feedback linearization method is that it includes zero dynamics that may be unstable [20]. In order to solve this problem, an integrator was placed in front of each control signal by Zhou *et al* [18], which avoids the zero dynamics since it increases the vector relative degree.

In order to ensure the system stability, the well-known concept about backstepping method was firstly proposed by Kanellakopoulos *et al* in 1991 [19]. Since it avoids cancelling the plant nonlinearities [20] and is not as strict as feedback linearization method for the nonlinear systems used, nowadays this control strategy has been utilized for the quadrotor UAV by the researchers. Madani and Benallegue [21] employed backstepping control scheme to control three interconnected systems of the quadrotor UAV since it is impossible for the under-actuated system to control all the outputs. Altug *et al* [22] used backstepping control for controlling pitch and roll angles in the x and y plane, and Altug *et al* [12] for x, y and Euler angles. By making use of the backstepping method with the integrator, Mian *et al* [23] stabilized the altitude. Meanwhile, they controlled Euler angles by backstepping method based PID. To improve system robustness, Raffo *et al* [24] proposed a backstepping nonlinear H_∞ control method to stabilize the rotation movement and uncertainty (nonlinear H_∞ scheme) and track the

reference trajectory (backstepping scheme). On the basis of work [21], a controller by combining the backstepping method and sliding mode control was proposed by Madani et Benallegue proposed [25] for the quadrotor UAV. The chattering phenomenon in sliding mode control was solved by using an approximation of a sign function. The challenge of the backstepping scheme is that the designed controller involves complicated constructure. To solve this challenge, most of research work attempted to design the controller separately [22, 23, 24] and connected them together, while Sharma and Ward [26] proposed a neuro-adaptive backstepping network where the network simplified the backstepping design. Moreover, the neuro-adaptive backstepping network addressed parametric uncertainties and the unmatched lift and side force uncertainties in the plant model.

The other methods utilized for the quadrotor UAV are Lyapunov analysis [27, 28], LQR (linear quadratic regulator) control [29], Nested-saturation techniques based on the Lyapunov analysis [30-31], MBPC (model based predictive control) / 2 DOF H_∞ controller [32], and sliding mode control [33]. Bouabdallah *et al* [27] described the whole design procedures of hardware test bench and the controller design for the altitude & Euler angles, while Castillo *et al* [28] employed the proposed controller to stabilize the altitude & yaw displacement and discussed the boundness of ψ, $\dot{y}$. The reasons to develop the nested-saturation techniques based on the Lyapunov analysis control method was that nested-saturation techniques enabled the global asymptotic stability and Lyapunov method ensured the convergence property [30, 31]. A practical quadrotor system by Chen and Huzmezan [32], including an experimental system including a flying mill, a DSP system, a programmed microprocessor and a wireless transmitter, was

presented to test their MBPC / 2 DOF H_∞ controller, where H_∞ loop shaping controller was for stabilization of speed, throttle and yaw control, and the MBPC was for longitudinal and lateral trajectory control. Based on the quadrotor UAV's characteristic which is an under-actuated system, Xu and Ozguner [33] divided the quadrotor UAV system into fully-actuated subsystem and under-actuated subsystem. The former subsystem constructed a PID controller to make altitude and roll angle approach to their desired values, and the latter developed sliding mode control method to stabilize x, y, θ, and ψ.

However, all above mentioned works deal with control of UAVs only for the UAVs flying under normal flight conditions, without consideration of potential faults to be occurred in the UAVs. Since the importance of safety and reliability of UAVs, the main motivation and objective of this thesis work is to investigate and develop nonlinear control schemes for quadrotor UAVs flying under certain fault conditions based on the powerful Lyapunov approach. It can be viewed as an extension of existing works for quadrotor UAVs to more challenging and practical flight conditions of quadrotor UAVs under various fault (abnormal) flight conditions. The following sections will introduce existing research work and control techniques in the fault tolerant control field.

As a comprehensive bibliographical review paper for the FTCS, Zhang and Jiang [34] clearly describes the background, classification, control schemes, current research activities and future challenges, and presents also many schemes for fault detection and diagnosis (FDD) and reconfigurable control employed by researchers in the FTCS area.

FDD strategies have been developed for many years. Relevant to aerospace field, Berbra *et al* [35] implemented a set of nonlinear estimators/observers to be sensitive to

faults, and use the switch strategy to choose each instant estimate to feed to the controller; Qi *et al* [36] introduced a novel adaptive unscented Kalman filter for online state and parameter estimation to be used for fault-tolerant control; Zhang and Jiang [37] presented a two-stage adaptive Kalman filter to observe the potential faults, and utilize these fault information to reconfigure controller; Boskovic and Mehra [38] proposed a new hybrid failure detection and identification method since its advantages are that only one fixed observer runs at most of time.

Compared with the FDD research, fault tolerant control researches are late for years and these techniques were initiated by aerospace systems study and application. An entire active fault tolerant control system is proposed by incorporating FDD, feedback controller, and reconfigurable feedforward controller with a command generator together, where the feedforward controller design is for steady-state reference tracking [37]. Since adaptive control strategy enables the system to accommodate more faults, Gayaka and Yao [39], Tao and Chen [40] choose adaptive controller based on output feedback to deal with the actuator failures. The linear control methods used for the fault tolerant control system are (LQ)/H∞ [41] and LQG control scheme [42], where Liao and Wang [41] used linear quadratic (LQ) and H∞ to track the reference inputs in the presence of actuator faults or control surface impaiements, and Yang *et al* [42] adopted LQG to accommodate sensor partial or outage faults. In addition, Ikeda and Shin [43] proposed an adaptive control based on backstepping scheme for the decentralized system to achieve the fault tolerances.

There are various types of faults in practical systems. The fault types taken into account in the literature are actuators outage [42, 43], sensors outage (zero output) [42],

transient fault and bias failure [35], control surface impairment [41], and partial actuator faults [39]. The different fault scenarios has been explained clearly [37], and it classifies faults as abrupt and incipient, single, multiple and consecutive faults.

Choosing one suitable model as a platform is important in evaluating performance when aircrafts undergo the wind disturbances, control surface impairments and hardware component failures. The platforms/aircraft models chosen for FTCS investigation in the literature are presented as below:

- Quadrotor helicopter [35]
- Rotorcraft or UAV helicopter [36]
- F/A-18C/D model (F-18 aircraft) [38]
- Boeing 747 [39]
- Lateral dynamic model of Boeing 747 [40]
- F-16 aircraft [41]

1.3 Scope and Objectives

1.3.1 Scope

The quadrotor UAV is a highly nonlinear, multi-variable, strong-coupled and under-actuated system. Judging from previous literature review study, it can be seen that researchers have managed to achieve a good performance by applying different control strategies (using linear control theory or nonlinear control theory).

However, the above existing works mostly are for controller design under normal situations, without consideration of any potential faults in quadrotor UAVs. Nevertheless, any kinds of faults, such as actuators, sensors and component malfunction, can happen in

any quadrotor UAV system and lead to unexpectedly reduced system performance, even crash of a UAV. Besides, it is impossible to predict in advance how worse the fault may become, and when and where the fault may take place. Therefore, Fault Tolerant Control (FTC) techniques have been greatly developed in recent years because of the increasing demands of reliability and safety for UAVs and aircrafts. However, not much work has been done for UAVs, especially for quadrotor UAVs, to accommodate faults for achieving an acceptable performance under varying fault conditions by employing a FTC strategy.

1.3.2 **Objectives**

The absence of FTC techniques for UAVs has motivated us to choose a quadrotor UAV for analysis and controller development using the FTC technique. The thesis addresses FTC design technique based on backstepping control method, or more generally Lyapunov-based nonlinear control techniques for achieving acceptable performance when anticipated or unanticipated faults may occur in the quadrotor UAV system. The specific objectives are as follows:

- Derive a nonlinear mathematical model of the quadrotor UAV, according to its particular physical structure and dynamics;
- Develop a Lyapunov-based controller without consideration of the faults;
- Design a Lyapunov-based controller as the fault tolerant controller for the quadrotor UAV with a PFTCS (Passive Fault Tolerant Control System) structure;

- Implement a range of partial loss situations and perform simulations by employing the Lyapunov-based method in the framework of PFTCS to analyze the performance of the FTC algorithm;
- Develop a Lyapunov-based adaptive controller for fault tolerant control of the quadrotor UAV; and validate its control performance through simulations under varying faults;
- Implement the Lyapunov-based control method on the test bed, Qball-X4 quadrotor UAV.

1.4 Outline

This thesis includes six chapters. Chapter 1 introduces the background, current research and literature review relevant to the existing control design techniques without faults for quadrotor UAVs. Chapter 2 describes the flight principle of quadrotor UAV on the basis of its physical structure and dynamics, and derives its six degree-of-freedom nonlinear mathematical model. Relying on these equations from Chapter 2, Chapter 3 develops a Lyapunov-based controller and demonstrates its effectiveness by simulations under system uncertainties. Since performance limitation is under fault conditions, Chapter 4 introduces PFTCS concept into the quadrotor UAV system. In addition, the controller with suitable controller gains has been adopted as a reliable controller for the PFTCS in simulations which consider most of the possible actuator partial losses. This reliable controller of the PFTCS can accommodate most of the partial losses. To improve system stability and reliability, Chapter 5 proposes a Lyapunov-based adaptive control method for fault tolerant control of the quadrotor UAV. The simulations prove that the

proposed new controller can deal with faulty system better than a PFTCS with Lyapunov-based control scheme. Based on the theoretical derivation of Section 3.1 in chapter 3, Chapter 6 briefly introduces Qball, a test bed from Quanser Innovation Company, and executes the Lyapunov-based control method on the Qball in order to stable the altitude. Chapter 7 highlights the main contributions of the thesis work, the conclusion and recommendations for future work.

CHAPTER 2

MODELING OF THE QUADROTOR UAV

The quadrotor UAV has attained much attention because of its merits in military and potential civilian applications. As indicated by its name, the quadrotor UAV has four rotors which are arranged as a "+" shape.

2.1 Mechanism of Quadrotor UAV

The quadrotor UAV obtains the thrust by the rotation of four rotors. The four rotors have been divided into two groups. One group is the front and back rotors (3&1), and the other group is the left and right rotors (2&4). The front and back rotors rotate in a counter-clockwise direction while the other two do so in clockwise direction.

All movements of the quadrotor UAV can be controlled by a change in each rotor speed. Vertical flight is the simplest one, and can be achieved by increasing the speed of all rotors to move up or by decreasing the speed to go down. Roll motion can be achieved by decreasing (increasing) the left rotor speed, while increasing (decreasing) the right rotor speed to make the quadrotor UAV roll left (right). Pitch motion can be controlled by decreasing (increasing) the front rotor speed while increasing (decreasing) the rear rotor speed to make the quadrotor UAV up (down). Yaw moment is a little different, and depends on the speed of all the rotors. When the front and rear pair spins more slowly (faster) than the left and right pair, the quadrotor UAV will move in a positive (negative) direction (counter clockwise/clockwise direction).

2.2 Mathematical Model of the Quadrotor UAV

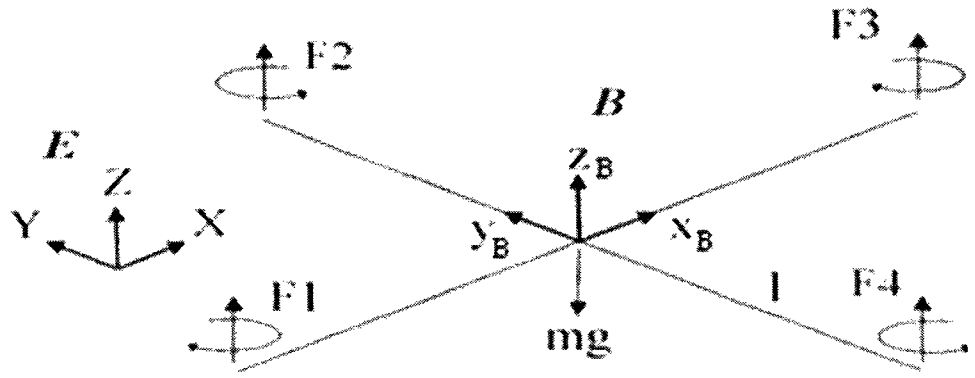

Figure 2-1 Physical structure of the quadrotor UAV

Figure 2-1 shows the structure of a quadrotor UAV. As a rigid body, the frames related to the quadrotor are defined as follows:

- $E = \{x_E, y_E, z_E\}$ denotes the inertial frame E which is fixed with the earth.
- $B = \{x_B, y_B, z_B\}$ represents the body frame B fixed with the quadrotor UAV body and is assumed to be at the center of the gravity of the quadrotor, where the Z axis is pointing upwards.
- $P = \{x, y, z\}$ is the position of the mass centre of the quadrotor UAV expressed in the inertial frame.

In Figure 2-1, F_1, F_2, F_3, and F_4 are the thrust generated by each corresponding rotor respectively, m is the mass of the quadrotor UAV, and g is the gravity acceleration.

Coordinate rotation

A ZYX right-hand rotation sequence has been chosen for the rotation from the reference Earth frame to a body-fixed coordinate system. Assumptions required for the rotations and the steps will be shown as below [44]:

- The Earth is flat, non-rotating, and an approximate inertial reference frame.
- The acceleration of gravity is constant and perpendicular to the surface of the Earth.
- The atmosphere is at rest relative to the Earth, and atmospheric properties are functions of altitude.

Rotation matrices from the earth-fixed frame to the body-fixed frame [44]

The earth-fixed frame is aligned with x-forward, y-left, and z-up. The body-fixed frame has the same definition. x_B points at the front of the quadrotor, y_B points at the left side of the quadrotor, and z_B points at up. The rotations based on an earth-fixed frame are explained as follows:

- Rotate around z axis (yaw angle $\psi \in (-\frac{\pi}{2}, \frac{\pi}{2})$ is positive if its angular velocity is consistent with the positive z axis)

$$L_z(\psi) = \begin{pmatrix} \cos\psi & \sin\psi & 0 \\ -\sin\psi & \cos\psi & 0 \\ 0 & 0 & 1 \end{pmatrix} \tag{2-1}$$

- Rotate around new y axis (pitch angle $\theta \in (-\frac{\pi}{2}, \frac{\pi}{2})$ is positive if its angular velocity is consistent with the positive y axis)

$$L_y(\theta)=\begin{pmatrix}\cos\theta & 0 & -\sin\theta\\ 0 & 1 & 0\\ \sin\theta & 0 & \cos\theta\end{pmatrix} \tag{2-2}$$

- Rotate around new x axis (roll angle $\phi \in (-\frac{\pi}{2},\frac{\pi}{2})$ is positive if its angular velocity is consistent with the positive x axis)

$$L_x(\phi)=\begin{pmatrix}1 & 0 & 0\\ 0 & \cos\phi & \sin\phi\\ 0 & -\sin\phi & \cos\phi\end{pmatrix} \tag{2-3}$$

Euler angles ϕ , θ , ψ represent roll angle, pitch angle and yaw angle, which rotates around the x-y-z body axis respectively. Therefore, the rotation matrices from earth-frame to body-frame can be obtained from the above equations.

$$\begin{aligned}L_{E\text{-}B} &= L_x(\phi)L_y(\theta)L_z(\psi)\\ &=\begin{pmatrix}\cos\psi\cos\theta & \cos\theta\sin\psi & -\sin\theta\\ \sin\phi\sin\theta\cos\psi-\cos\phi\sin\psi & \sin\phi\sin\theta\sin\psi+\cos\phi\cos\psi & \sin\phi\cos\theta\\ \cos\phi\sin\theta\cos\psi+\sin\phi\sin\psi & \cos\phi\sin\theta\sin\psi-\sin\phi\cos\psi & \cos\phi\cos\theta\end{pmatrix}\end{aligned} \tag{2-4}$$

Then the matrix $L_{B\text{-}E}$ can easily be written as below:

$$\begin{aligned}L_{B\text{-}E} &= {L_{E\text{-}B}}^T =\\ &\begin{pmatrix}\cos\psi\cos\theta & \sin\phi\sin\theta\cos\psi-\cos\phi\sin\psi & \cos\phi\sin\theta\cos\psi+\sin\phi\sin\psi\\ \cos\theta\sin\psi & \sin\phi\sin\theta\sin\psi+\cos\phi\cos\psi & \cos\phi\sin\theta\sin\psi-\sin\phi\cos\psi\\ \sin\theta & \sin\phi\cos\theta & \cos\phi\cos\theta\end{pmatrix}\end{aligned} \tag{2-5}$$

Force equation derivation procedure

From Newton's second law,

$$\begin{pmatrix}mI & 0\\ 0 & J\end{pmatrix}\begin{pmatrix}\dot{V}_B\\ \dot{\omega}_B\end{pmatrix}+\begin{pmatrix}\omega_B\times mV_B\\ \omega_B\times J\omega_B\end{pmatrix}=\begin{pmatrix}F_B\\ T_B\end{pmatrix} \tag{2-6}$$

where body force is $F_B \in \Re^3$, body moment is $T_B \in \Re^3$, body velocity is $V_B \in \Re^3$, body angular velocity is $\omega_B \in \Re^3$, $I \in \Re^3$ is an identity matrix, and $J \in \Re^3$ is an inertial matrix, the force equation derivation procedure can be shown as follows:

Since the resultant force acted on the quadrotor UAV body is

$$\sum F_B = F_T - D + L_{G-B} \times mg$$

where D denotes drag force which is opposite to the quadrotor UAV move direction, F_T represents the sum of thrusts from all of the propellers, mg is the gravity of the quadrotor UAV, it can be rewritten as:

$$\sum F_B = \begin{pmatrix} mg\sin\theta - k_{d1}\dot{x} \\ -mg\sin\phi\cos\theta - k_{d2}\dot{y} \\ F_T - mg\cos\phi\cos\theta - k_{d3}\dot{z} \end{pmatrix} \tag{2-7}$$

$k_{d1}\dot{x}$, $k_{d2}\dot{y}$, $k_{d3}\dot{z}$ in Eq. (2-7) are the drag along the body axis x_B, y_B, and z_B where k_{d1}, k_{d2}, and k_{d3} are coefficients. In addition, the sum of thrust F_T equals to:

$$F_T = F_1 + F_2 + F_3 + F_4$$

Define $V_B = \begin{pmatrix} u \\ v \\ w \end{pmatrix}$ where V_B is the velocity vector of body and u, v, w is the velocity along body axis x_B, y_B, and z_B respectively. From $\left.\frac{dv}{dt}\right|_E = \left.\frac{\partial v}{\partial t}\right|_B + \omega_B \times V_B$, the acceleration of the quadrotor UAV is:

$$a = \dot{V}_B + \begin{pmatrix} P \\ Q \\ R \end{pmatrix} \times \begin{pmatrix} u \\ v \\ w \end{pmatrix} = \begin{pmatrix} \dot{u} - Rv + Qw \\ \dot{v} - wP + Ru \\ \dot{w} - Qu + Pv \end{pmatrix} \tag{2-8}$$

where P , Q , and R represent three angular velocity vectors of the UAV body respectively.

Combine equations from Eq. (2-6) to Eq. (2-8), and the force equations can be obtained as follows:

$$\dot{u} = \frac{1}{m}(mg\sin\theta - k_{d1}\dot{x}) + Rv - Qw$$
$$\dot{v} = \frac{1}{m}(-mg\sin\phi\cos\theta - k_{d2}\dot{y}) + Pw - Ru$$
$$\dot{w} = \frac{1}{m}[(F_1 + F_2 + F_3 + F_4) - mg\cos\phi\cos\theta - k_{d3}\dot{z}] + Qu - Pv$$

Navigation equation derivation procedure

By employing Eq. (2-5) and $\sum F = L_{B\to E}(F_T - D) - mg$, the navigation equation is represented by:

$$\ddot{x} = \frac{F_1 + F_2 + F_3 + F_4}{m}(\cos\psi\sin\theta\cos\phi + \sin\psi\sin\phi) - \frac{k_{d1}\dot{x}}{m}$$
$$\ddot{y} = \frac{F_1 + F_2 + F_3 + F_4}{m}(\sin\psi\sin\theta\cos\phi - \cos\psi\sin\phi) - \frac{k_{d2}\dot{y}}{m}$$
$$\ddot{z} = \frac{F_1 + F_2 + F_3 + F_4}{m}\cos\theta\cos\phi - \frac{k_{d3}\dot{z}}{m} - g$$

Moment equation derivation procedure

Note that since each propeller inertial is comparably small to inertial moments of the quadrotor UAV which is shown in Table 1 in [45], this thesis does not take gyroscopic moments into account which are caused by four propeller rotations.

Moment equations can be defined as follows:

$$\frac{dH_B}{dt}/_G = \frac{\partial H_B}{\partial t}/_B + \omega_B \times H_B = T_B \qquad (2\text{-}9)$$

H_B represents the angular momentum vector of the quadrotor UAV body, and T_B represents the net torque acting about the cg (center of gravity) of the quadrotor UAV.

$$H_B = J\omega_B = \begin{pmatrix} J_{xx} & -J_{xy} & -J_{xz} \\ -J_{xy} & J_{yy} & -J_{yz} \\ -J_{xz} & -J_{yz} & J_{zz} \end{pmatrix} \begin{pmatrix} P \\ Q \\ R \end{pmatrix} \tag{2-10}$$

From (2-9) and (2-10), the moment of the quadrotor UAV is:

$$\dot{H}_B + \omega_B \times H_B = J\dot{\omega}_B + \omega_B \times H_B = T_B \tag{2-11}$$

where body moment can be defined as $T_B = \begin{pmatrix} L \\ M \\ N \end{pmatrix}$, L, M, N denote the roll moment, pitch moment and yaw moment respectively.

Because the quadrotor UAV has a symmetric structure, the inertial matrix of the rigid body is

$$J = \begin{pmatrix} J_x & 0 & 0 \\ 0 & J_y & 0 \\ 0 & 0 & J_z \end{pmatrix} \tag{2-12}$$

and

$$J^{-1} = \begin{pmatrix} \frac{1}{J_x} & 0 & 0 \\ 0 & \frac{1}{J_y} & 0 \\ 0 & 0 & \frac{1}{J_z} \end{pmatrix} \tag{2-13}$$

Then the equations from Eq. (2-10) to Eq. (2-13) can be combined into

$$\dot{\omega}_B = -J^{-1}\left(\omega_B \times \left(J\omega_B\right)\right) + J^{-1}T_B$$

Since

$$\omega_B \times H_B = \begin{pmatrix} i & j & k \\ P & Q & R \\ J_x P & J_y Q & J_z R \end{pmatrix} = \begin{pmatrix} RQ(J_z - J_y) \\ PR(J_x - J_z) \\ PQ(J_y - J_x) \end{pmatrix},$$

the angular accelerations $\dot{P}, \dot{Q}, \dot{R}$ of the quadrotor UAV become:

$$\begin{pmatrix} \dot{P} \\ \dot{Q} \\ \dot{R} \end{pmatrix} = -\begin{pmatrix} \frac{1}{J_x} & 0 & 0 \\ 0 & \frac{1}{J_y} & 0 \\ 0 & 0 & \frac{1}{J_z} \end{pmatrix} \begin{pmatrix} RQ(J_z - J_y) \\ PR(J_x - J_z) \\ PQ(J_y - J_x) \end{pmatrix} + \begin{pmatrix} \frac{1}{J_x} & 0 & 0 \\ 0 & \frac{1}{J_y} & 0 \\ 0 & 0 & \frac{1}{J_z} \end{pmatrix} \begin{pmatrix} L \\ M \\ N \end{pmatrix} \tag{2-14}$$

where

$$\begin{aligned} L &= (F_2 - F_4)l - k_{d4}\dot{\phi} \\ M &= (F_1 - F_3)l - k_{d5}\dot{\theta} \\ N &= (F_1 + F_3)l - (F_2 + F_4)l - k_{d6}\dot{\psi} \end{aligned} \tag{2-15}$$

Therein, F_3 and F_1 are the thrust of the forward and rear rotors, F_4 and F_2 are the thrust of right and left rotors; $k_{d4}\dot{\phi}$, $k_{d5}\dot{\theta}$ and $k_{d6}\dot{\psi}$ denote the moments caused by drag along body axis x_B , y_B , and z_B respectively, k_{d4} , k_{d5} , and k_{d6} are coefficients, and l represents distance from the rotor to the center of gravity.

Rewriting Eq. (2-14) by employing Eq. (2-15), the moment equations can be obtained as follows:

$$\dot{P} = \frac{1}{J_x}\left[(F_2 - F_4)l - k_{d4}\dot{\phi} - RQ\left(J_z - J_y\right)\right]$$

$$\dot{Q} = \frac{1}{J_y}[(F_1 - F_3)l - k_{d5}\dot{\theta} - PR(J_x - J_z)] \tag{2-16}$$

$$\dot{R} = \frac{1}{J_z}[(F_1 - F_2 + F_3 - F_4)l - k_{d6}\dot{\psi} - PQ(J_y - J_x)]$$

As known previously, the quadrotor's angular velocity is $\omega_B = \begin{pmatrix} P \\ Q \\ R \end{pmatrix}$ where P, Q, R represent three angular velocity vectors of body respectively. The relation between the Euler angle derivatives and the quadrotor's angular velocity can be shown as below:

$$\omega_B = \begin{pmatrix} P \\ Q \\ R \end{pmatrix} = L_x(\phi)L_y(\theta)\begin{pmatrix} 0 & 0 & \dot{\psi} \end{pmatrix}^T + L_x(\phi)\begin{pmatrix} 0 & \dot{\theta} & 0 \end{pmatrix}^T$$

$$+\begin{pmatrix} \dot{\phi} & 0 & 0 \end{pmatrix}^T = \begin{pmatrix} 1 & 0 & -\sin\theta \\ 0 & \cos\phi & \sin\phi\cos\theta \\ 0 & -\sin\phi & \cos\phi\cos\theta \end{pmatrix}\begin{pmatrix} \dot{\phi} \\ \dot{\theta} \\ \dot{\psi} \end{pmatrix}$$

Then the above equation can be rewritten as:

$$\begin{pmatrix} \dot{\phi} \\ \dot{\theta} \\ \dot{\psi} \end{pmatrix} = \begin{pmatrix} 1 & \sin\phi\tan\theta & \cos\phi\tan\theta \\ 0 & \cos\phi & -\sin\phi \\ 0 & \dfrac{\sin\phi}{\cos\theta} & \dfrac{\cos\phi}{\cos\theta} \end{pmatrix}\begin{pmatrix} P \\ Q \\ R \end{pmatrix} \tag{2-17}$$

By assuming that the pitch angle and roll angle are small, the Euler angle derivatives become an identity matrix

$$\begin{pmatrix} \dot{\phi} \\ \dot{\theta} \\ \dot{\psi} \end{pmatrix} = \begin{pmatrix} 1 & 0 & 0 \\ 0 & 1 & 0 \\ 0 & 0 & 1 \end{pmatrix}\begin{pmatrix} P \\ Q \\ R \end{pmatrix}$$

Therefore, Eq. (2-16) can be simplified as:

$$\begin{aligned}
\ddot{\phi} &= \frac{1}{J_x}[(F_2 - F_4)l - k_{d4}\dot{\phi} - \dot{\theta}\dot{\psi}(J_z - J_y)] \\
\ddot{\theta} &= \frac{1}{J_y}[(F_1 - F_3)l - k_{d5}\dot{\theta} - \dot{\phi}\dot{\psi}(J_x - J_z)] \\
\ddot{\psi} &= \frac{1}{J_z}[(F_1 - F_2 + F_3 - F_4)l - k_{d6}\dot{\psi} - \dot{\theta}\dot{\phi}(J_y - J_x)]
\end{aligned} \tag{2-18}$$

Finally, all the equations are summarized below for easy reference:

Force equations:

$$\begin{aligned}
\dot{u} &= \frac{1}{m}(mg\sin\theta - k_{d1}\dot{x}) + \dot{\psi}v - \dot{\theta}w \\
\dot{v} &= \frac{1}{m}(-mg\sin\phi\cos\theta - k_{d2}\dot{y}) + \dot{\phi}w - \dot{\psi}u \\
\dot{w} &= \frac{1}{m}[(F_1 + F_2 + F_3 + F_4) - mg\cos\phi\cos\theta - k_{d3}\dot{z}] + \dot{\theta}u - \dot{\phi}v
\end{aligned} \tag{2-19}$$

Moment equations:

$$\begin{aligned}
\ddot{\phi} &= \frac{1}{J_x}[(F_2 - F_4)l - k_{d4}\dot{\phi} - \dot{\theta}\dot{\psi}(J_z - J_y)] \\
\ddot{\theta} &= \frac{1}{J_y}[(F_1 - F_3)l - k_{d5}\dot{\theta} - \dot{\phi}\dot{\psi}(J_x - J_z)] \\
\ddot{\psi} &= \frac{1}{J_z}[(F_1 - F_2 + F_3 - F_4)l - k_{d6}\dot{\psi} - \dot{\theta}\dot{\phi}(J_y - J_x)]
\end{aligned} \tag{2-20}$$

Navigation equations:

$$\begin{aligned}
\ddot{x} &= \frac{F_1 + F_2 + F_3 + F_4}{m}(\cos\psi\sin\theta\cos\phi + \sin\psi\sin\phi) - \frac{k_{d1}\dot{x}}{m} \\
\ddot{y} &= \frac{F_1 + F_2 + F_3 + F_4}{m}(\sin\psi\sin\theta\cos\phi - \cos\psi\sin\phi) - \frac{k_{d2}\dot{y}}{m} \\
\ddot{z} &= \frac{F_1 + F_2 + F_3 + F_4}{m}\cos\theta\cos\phi - \frac{k_{d3}\dot{z}}{m} - g
\end{aligned} \tag{2-21}$$

Force equations (Eq. (2-19)) describe the relation between velocities and forces associated with the body frame. Moment equations (Eq. (2-20)) show the moments expressed with angular velocity and angular acceleration. Navigation equations (Eq. (2-21)) present the quadrotor UAV's position in the earth frame.

2.3 Summary

After briefly describing the operational mechanism of the quadrotor UAV, this chapter provides an elaborate derivation procedure of the quadrotor UAV's mathematical model by utilizing Newton's Second Law. The derived equations in this chapter are force equations, moment equations and navigation equations. The following chapters will adopt moment equations and altitude equation in navigation equations to design a Lyapunov-based controller and a Lyapunov-based adaptive controller respectively.

CHAPTER 3

LYAPUNOV-BASED CONTROL WITH UNCERTAINTY

As pointed out in Chapter 1 through literature review, the existing nonlinear controllers investigated for quadrotor UAVs are feedback linearization, sliding mode control and backstepping control. Feedback linearization makes it possible to utilize all of the linear methods by eliminating the nonlinear characters in the original system. The limitation here is that feedback linearization requires a highly precise mathematic model but mathematical model cannot reflect the real physical model precisely. The sliding mode control is insensitive to the modeling errors, parametric uncertainties and other disturbances, and the response is quick. However, the sliding mode control can bring the chattering phenomenon [46]. The backstepping control method has the flexibility to avoid nonlinear cancellations which makes the controller more practical in the real life [47].

In this thesis, the Lyapunov-based method is used for the quadrotor UAV control design.

3.1 Controller Design

For the quadrotor UAV system defined in Eqs. (2-20) and (2-21), the effect caused by the drag can be ignored, since the speed of the quadrotor UAV is slow, which means that drag coefficients $k_{di} = 0$ [12, 22].

By defining the virtual control signals, $\begin{pmatrix} u_1 \\ u_2 \\ u_3 \\ u_4 \end{pmatrix} = \begin{pmatrix} F_1 + F_2 + F_3 + F_4 \\ F_2 - F_4 \\ F_1 - F_3 \\ F_1 + F_3 - F_2 - F_4 \end{pmatrix}$, the altitude and the moment equations in Eqs. (2-20) and (2-21) can be rewritten as follows:

$$\ddot{z} = \frac{u_1}{m}\cos\theta\cos\phi - g$$

$$\ddot{\phi} = \frac{1}{J_x}[u_2 l - \dot{\theta}\dot{\psi}(J_z - J_y)]$$

$$\ddot{\theta} = \frac{1}{J_y}[u_3 l - \dot{\phi}\dot{\psi}(J_x - J_z)]$$

$$\ddot{\psi} = \frac{1}{J_z}[u_4 l - \dot{\theta}\dot{\phi}(J_y - J_x)]$$

The above system changes into a standard affine nonlinear form:

$$\ddot{\mathrm{X}} = \Psi + \Phi U \tag{3-1}$$

where X is the state space vector of the system and it can be defined as:

$$\mathrm{X} = \begin{pmatrix} z & \phi & \theta & \psi \end{pmatrix}^T$$

with the virtual control inputs

$$U = \begin{pmatrix} u_1 \\ u_2 \\ u_3 \\ u_4 \end{pmatrix} = \begin{pmatrix} F_1 + F_2 + F_3 + F_4 \\ F_2 - F_4 \\ F_1 - F_3 \\ F_1 + F_3 - F_2 - F_4 \end{pmatrix}$$

and

$$\Psi = \begin{pmatrix} -g \\ \dfrac{-\dot{\theta}\dot{\psi}(J_z - J_y)}{J_x} \\ \dfrac{-\dot{\phi}\dot{\psi}(J_x - J_z)}{J_y} \\ \dfrac{-\dot{\theta}\dot{\phi}(J_y - J_x)}{J_z} \end{pmatrix} \Phi = \begin{pmatrix} \dfrac{\cos\theta\cos\phi}{m} & 0 & 0 & 0 \\ 0 & \dfrac{l}{J_x} & 0 & 0 \\ 0 & 0 & \dfrac{l}{J_y} & 0 \\ 0 & 0 & 0 & \dfrac{l}{J_z} \end{pmatrix} \tag{3-2}$$

According to Eqs. (3-1) and (3-2), the whole system is:

$$\begin{pmatrix} \ddot{z} \\ \ddot{\phi} \\ \ddot{\theta} \\ \ddot{\psi} \end{pmatrix} = \begin{pmatrix} -g \\ \dfrac{-\dot{\theta}\dot{\psi}(J_z - J_y)}{J_x} \\ \dfrac{-\dot{\phi}\dot{\psi}(J_x - J_z)}{J_y} \\ \dfrac{-\dot{\theta}\dot{\phi}(J_y - J_x)}{J_z} \end{pmatrix} + \begin{pmatrix} \dfrac{\cos\theta\cos\phi}{m} & 0 & 0 & 0 \\ 0 & \dfrac{l}{J_x} & 0 & 0 \\ 0 & 0 & \dfrac{l}{J_y} & 0 \\ 0 & 0 & 0 & \dfrac{l}{J_z} \end{pmatrix} \begin{pmatrix} u_1 \\ u_2 \\ u_3 \\ u_4 \end{pmatrix} \tag{3-3}$$

As a first step, we will address the issue related to the design of the virtual control signal U for the altitude tracking. Then, as the basis on the design of U, the real control signal F can be obtained by using their relationship defined in Eq. (3-2).

Now introduce the altitude error in Eq. (3-4) where z is the actual altitude and z_r is the desired one [47]

$$\begin{aligned} e &= z_1 = z_r - z \\ z_2 &= a(z_1) - \dot{z} \end{aligned} \tag{3-4}$$

where $a(z_1)$ is the function to make z_1 approach to zero.

Then the derivative of z_1 equals to

$$\dot{z}_1 = \dot{z}_r - \dot{z} \tag{3-5}$$

and Eq. (3-5) becomes the following by combining Eq. (3-4):

$$\dot{z}_1 = \dot{z}_r - \dot{z} = \dot{z}_r + z_2 - a(z_1) \tag{3-6}$$

Select the Lyapunov function $V_1 = \frac{1}{2} z_1^2$, then the derivative of V_1 is:

$$\begin{aligned} \dot{V}_1 &= z_1 \dot{z}_1 = z_1[\dot{z}_r + z_2 - a(z_1)] \\ &= z_1[\dot{z}_r - a(z_1)] + z_1 z_2 \end{aligned} \tag{3-7}$$

Choose the stabilizing function as shown in Eq. (3-8), it has

$$a(z_1) = \dot{z}_r + k_a z_1 \; (k_a > 0) \tag{3-8}$$

where k_a is defined as a positive constant.

Then Eq. (3-7) becomes:

$$\begin{aligned} \dot{V}_1 &= z_1 \dot{z}_1 = z_1[\dot{z}_r + z_2 - a(z_1)] \\ &= -k_a z_1^2 + z_1 z_2 \end{aligned} \tag{3-9}$$

The next step is to build the Lyapunov function V_2 to make $z_2 \to 0$

$$V_2 = V_1 + \frac{1}{2} z_2^2$$

From Eqs. (3-4), (3-6) and (3-8), the derivative of V_2 is:

$$\begin{aligned} \dot{V}_2 &= (-k_a z_1^2 + z_2 z_1) + z_2(\ddot{z}_r + k_a \dot{z}_1 - \ddot{z}) \\ &= -k_a z_1^2 + z_2[z_1 + \ddot{z}_r + k_a(z_2 - k_a z_1) - \ddot{z}] \end{aligned} \tag{3-10}$$

In order to make $\dot{V}_2$ negative, choose

$$z_1 + \ddot{z}_r + k_a(z_2 - k_a z_1) - \ddot{z} = -k_b z_2 \; (k_b > 0) \tag{3-11}$$

where k_b is a positive constant.

By employing Eq.(3-11), Eq. (3-10) can be converted to

$$\begin{aligned}\dot{V}_2 &= (-k_a z_1^2 + z_2\, z_1) + z_2(\ddot{z}_r + k_a \dot{z}_1 - \ddot{z}) \\ &= -k_a z_1^2 + z_2[z_1 + \ddot{z}_r + k_a(z_2 - k_a z_1) - \ddot{z}] \\ &= -k_a z_1^2 - k_b z_2^2\end{aligned}$$

and Eq. (3-11) can be rewritten as follows:

$$\ddot{z} = \ddot{z}_r + (1 - k_a^2)\, z_1 + (k_a + k_b) z_2 \;(k_a > 0, k_b > 0) \tag{3-12}$$

Introduce the altitude equation in Eq. (3-3) into Eq. (3-12) and solve it, then one obtains:

$$u_1 = \frac{m}{\cos\theta \cos\phi}[\ddot{z}_r + (1 - k_a{}^2) z_1 + (k_a + k_b) z_2 + g]$$

After the derivation procedure of the altitude control law, the same process is followed for the roll control law u_2, pitch control law u_3, and yaw control law u_4.

To simplify the control laws, consider all of the controller parameters k_a and k_b for each control law are same. Finally, the control laws of the altitude and the angles are presented as follows:

$$\begin{aligned}u_1 &= \frac{m}{\cos\theta \cos\phi}[\ddot{z}_r + (1 - k_a{}^2) z_1 + (k_a + k_b) z_2 + g] \\ u_2 &= \frac{1}{l}(J_z - J_y)\dot{\theta}\dot{\psi} + \frac{J_x}{l}[\ddot{\phi}_r + (1 - k_a{}^2) z_3 + (k_a + k_b) z_4] \\ u_3 &= \frac{1}{l}(J_x - J_z)\dot{\phi}\dot{\psi} + \frac{J_y}{l}[\ddot{\theta}_r + (1 - k_a{}^2) z_5 + (k_a + k_b) z_6] \\ u_4 &= \frac{1}{l}(J_y - J_x)\dot{\theta}\dot{\phi} + \frac{J_z}{l}[\ddot{\psi}_r + (1 - k_a{}^2) z_7 + (k_a + k_b) z_8]\end{aligned} \tag{3-13}$$

In Eq. (3-13), the virtual control inputs u_1, u_2, u_3, u_4 have been designed, which guarantees the stability of the closed-loop system. For the complete quadrotor system shown in the Eq. (2-20) and Eq. (2-21), the thrust forces F can thus be obtained with the relationship:

$$U = \begin{pmatrix} u_1 \\ u_2 \\ u_3 \\ u_4 \end{pmatrix} = \begin{pmatrix} F_1 + F_2 + F_3 + F_4 \\ F_2 - F_4 \\ F_1 - F_3 \\ F_1 + F_3 - F_2 - F_4 \end{pmatrix}$$

In the next section, an extensive simulation study will be conducted to confirm the above developed control approach.

3.2 Simulations

By employing the Lyapunov-based control approach with controller gains $k_a = 1$ & $k_b = 3$ and $k_a = 5$ & $k_b = 30$ respectively, this section will apply the quadrotor's control laws to the simulations. The uncertainty will not be considered in Section 3.2.1 while it will be taken into account in Section 3.2.2. The overall simulation time is 30 seconds. The definitions of the initial and desired conditions are shown as follows:

- Initial position: $z = 0$ (meter)
- Initial Euler angle: (30, 30, 30) (degree)
- Desired Euler angle: (10, 10, 10) (degree)
- Desired altitude: $z_r = 1 + 0.1t$

The parameters of the quadrotor UAV used in the dynamic modeling are in Table 3-1.

Table 3-1 Physical parameters of the quadrotor UAV [23]

Symbol	Description	Value	Units
m	Mass of quadrotor	0.6120	kg
l	Distance from cg	0.305	m
J_x	Moment of inertia	0.0154	$kg*m^2$
J_y	Moment of inertia	0.0154	$kg*m^2$
J_z	Moment of inertia	0.0309	$kg*m^2$

3.2.1 Simulations of the Utilization of Different Controller Gains

This section discusses and compares the altitude and Euler angle performance by different controller gains $k_a = 1$ & $k_b = 3$ and $k_a = 5$ & $k_b = 30$ without system parameter uncertainty.

Simulation results with $k_a = 1$ & $k_b = 3$

Figure 3-1 and Figure 3-2 present altitude and Euler angle performances when employing controller gains $k_a = 1$ & $k_b = 3$ without uncertainty. It can be seen that the altitude reaches a steady state around 3 seconds and Euler angle steady state errors are close to zero. Moreover, the yaw angle error has an overshoot before it becomes stable.

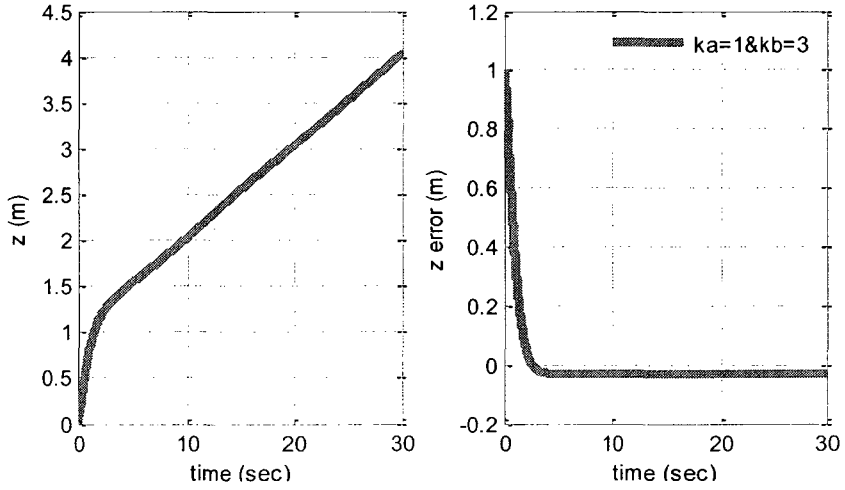

Figure 3-1 Altitude and altitude error without uncertainty and with controller gains 1 & 3

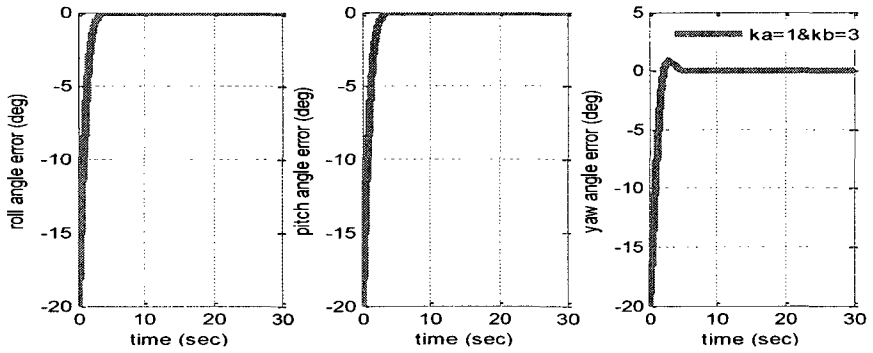

Figure 3-2 Euler angle errors without uncertainty with controller gains 1 & 3

Simulation results with $k_a = 5$ & $k_b = 30$

Based on controller gains $k_a = 5$ & $k_b = 30$, the altitude and altitude error reaches a steady state around 1 second, as shown in Figure 3-3. Meanwhile, Euler angle errors are convergent to zero without overshoot as shown in Figure 3-4.

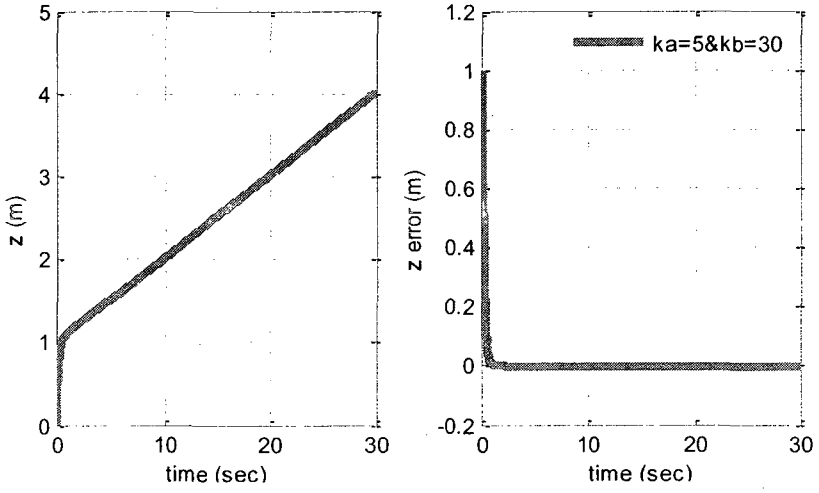

Figure 3-3 Altitude and altitude error without uncertainty and with controller gains 5 & 30

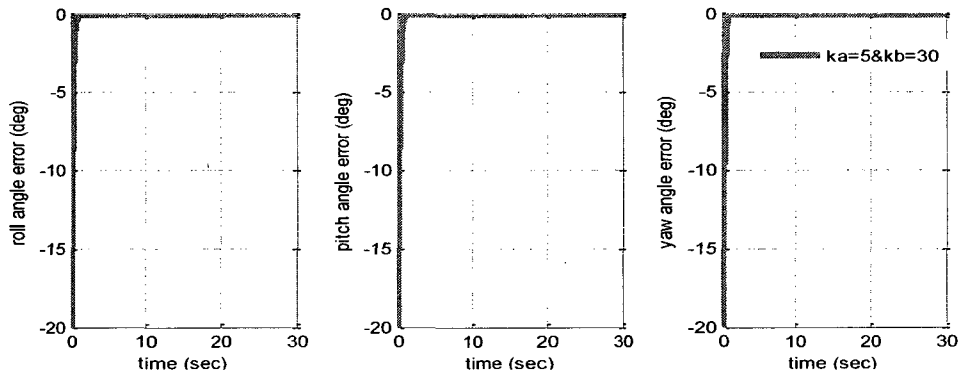

Figure 3-4 Euler angle errors without uncertainty with controller gains 5 & 30

Comparison between controller gains $k_a = 1$ & $k_b = 3$ and $k_a = 5$ & $k_b = 30$

Figure 3-5 and Figure 3-6 reveal the performance difference when making use of the Lyapunov-based method, with different controller gains for the quadrotor UAV. It is obvious that the appropriate controller gains can reach a steady state more quickly and have less error.

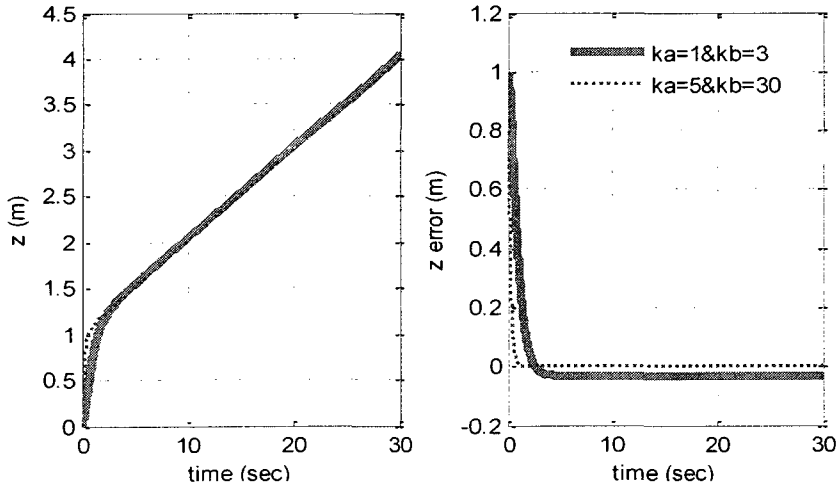

Figure 3-5 Altitude and altitude error comparison without uncertainty between controller gains 1 & 3 and 5 & 30

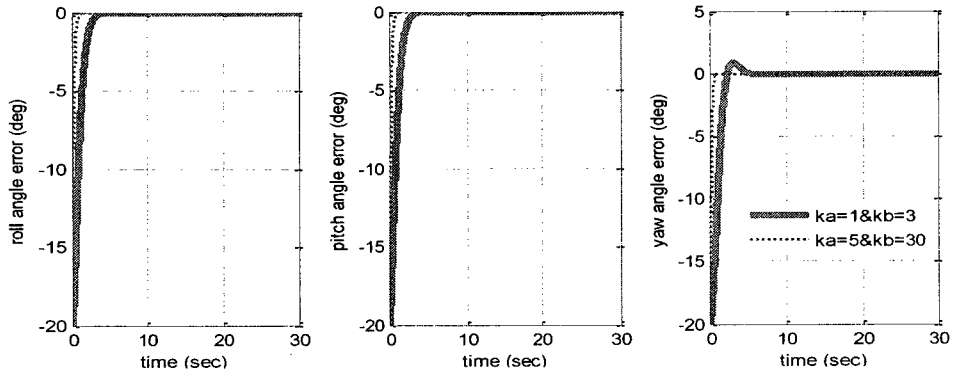

Figure 3-6 Euler angle errors comparison without uncertainty between controller gains 1 & 3 and 5 & 30

3.2.2 Simulations with Uncertainty

The uncertainty discussed here is considered as it affects the system by decreasing the system parameters in the mass and inertia moments of the quadrotor UAV [13, 16, 26, 33]. The quadrotor UAV model can be

$$\begin{aligned}
\ddot{z} &= \frac{u_1}{m}\cos\theta\cos\phi - g \\
\ddot{\phi} &= \frac{1}{J_x'}[u_2 l - \dot{\theta}\dot{\psi}(J_z' - J_y')] \\
\ddot{\theta} &= \frac{1}{J_y'}[u_3 l - \dot{\phi}\dot{\psi}(J_x' - J_z')] \\
\ddot{\psi} &= \frac{1}{J_z'}[u_4 l - \dot{\theta}\dot{\phi}(J_y' - J_x')]
\end{aligned} \tag{3-14}$$

When system uncertainty is 50%, it means that the system parameters (mass and inertial moments) $m' = 0.5m, J_x' = 0.5J_x, J_y' = 0.5J_y, J_z' = 0.5J_z$ where m, J_x, J_y, J_z are the system parameters under normal cases. The same method is used for 80% system parameter uncertainty.

Simulations of the Lyapunov-based control approach with controller gains $k_a = 1$ & $k_b = 3$ and $k_a = 5$ & $k_b = 30$ will be implemented for the quadrotor UAV respectively, when

a) There is no uncertainty considered.

b) Uncertainty decreases 50% of the system parameters.

c) Uncertainty decreases 80% of the system parameters.

Suppose that uncertainty influences the system from the time of 5 seconds (t_u=5s). In the following figures, the thick solid line denotes a case without uncertainty, the dot-dash line shows the case where uncertainty decreases 50% of the system parameters, and the thin solid line is a case where uncertainty decreases 80% of system parameters.

Simulation results based on the Lyapunov-based method with $k_a = 1$ & $k_b = 3$

When uncertainty affects the quadrotor system, the Lyapunov-based control scheme, with controller gains $k_a = 1$ & $k_b = 3$, cannot accommodate these changes as shown in Figure 3-7 and Table 3-2 (the altitude steady-state error under 50% uncertainty is 2.3876/4=59.7%).

Table 3-2 Euler angle errors and altitude error comparison when employing the Lyapunov-based method with $k_a = 1$ & $k_b = 3$

Uncertainty type	Roll angle error (degree)	Pitch angle error (degree)	Yaw angle error (degree)	z error (m)
No uncertainty	-3.4461e-13	-3.4461e-13	-2.2561e-12	-0.0312
50% uncertainty	-3.4461e-13	-3.4461e-13	-2.2561e-12	2.3876
80% uncertainty	-3.4461e-13	-3.4461e-13	-2.2561e-12	10.9144

When uncertainty becomes especially stronger and reaches up to 80% of system parameter reductions, the altitude changes greatly than when dealing with a case which is uncertainty free shown clearly in Table 3-2.

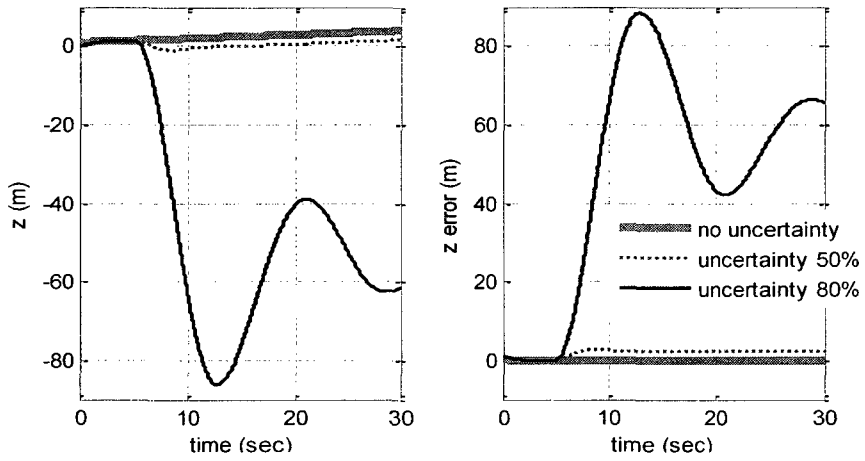

Figure 3-7 Altitude and altitude error with uncertainty under controller gains 1 & 3

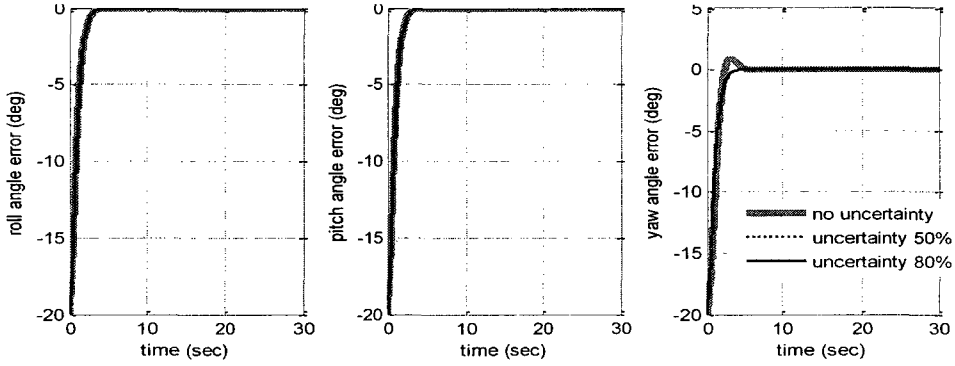

Figure 3-8 Euler angle errors with uncertainty under controller gains 1 & 3

Simulation results based on the Lyapunov-based method with $k_a = 5$ & $k_b = 30$

Table 3-3 Euler angle errors and altitude error comparison when employing the Lyapunov-based method with $k_a = 5$ & $k_b = 30$

Uncertainty type	Roll angle error (degree)	Pitch angle error (degree)	Yaw angle error (degree)	z error (m)
No uncertainty	-1.5454e-13	-1.5454e-13	-8.5265e-14	-8.268e-4
50% uncertainty	-1.5454e-13	-1.5454e-13	-8.5265e-14	0.0632
80% uncertainty	-1.5454e-13	-1.5454e-13	-8.5265e-14	1.5369

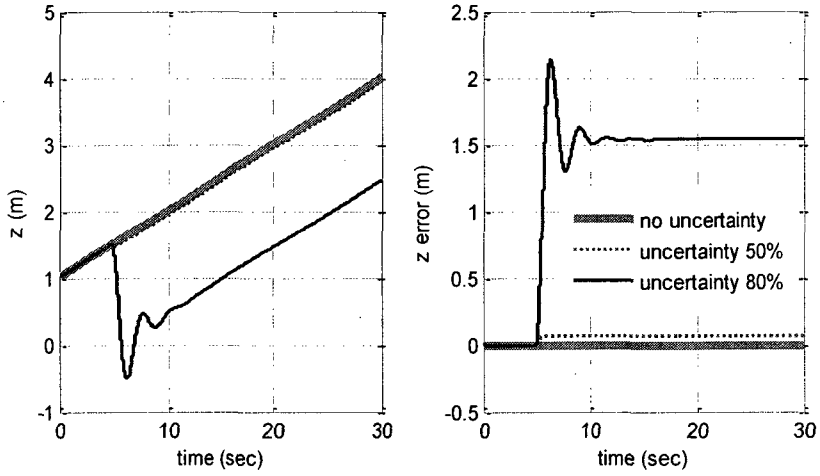

Figure 3-9 Altitude and altitude error with uncertainty under controller gains 5 & 30

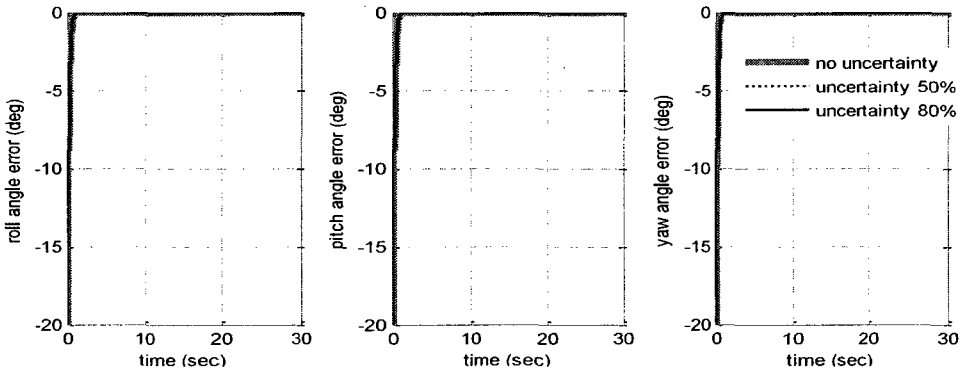

Figure 3-10 Euler angle error with uncertainty under controller gains 5 & 30

For the altitude, the controller gain with $k_a = 1$ & $k_b = 3$ cannot meet the performance requirement (the altitude steady-state error is over 5%) anymore (see Figure 3-7 and Table 3-2) when uncertainty decreases 50% and 80% of the system parameters. However, the system with controller gains $k_a = 5$ & $k_b = 30$ can still accommodate the worst uncertainty case (80% of the system parameters reduction). The altitude steady-state error

is 1.5369/4=0.384. Comparing Figure 3-7 & Figure 3-9 and Table 3-2 & Table 3-3, it is evident that the controller with suitable controller gains will possess a stronger ability to handle the uncertainties.

3.3 Summary

After derivation of the quadrotor control laws designed by a Lyapunov-based control approach, the effects of the uncertainties have been analyzed for quadrotor UAV control. The simulation results demonstrate that a Lyapunov-based method with controller gains $k_a = 1$ & $k_b = 3$ and $k_a = 5$ & $k_b = 30$ are executable without uncertainty.

System performances become worse when the uncertainty level is increased. In addition, when the uncertainty reaches 50% and 80% reductions of the system parameters, the controller with controller gains $k_a = 1$ & $k_b = 3$ cannot handle them any more since the altitude error exceed the requirement. The Lyapunov-based method with $k_a = 5$ & $k_b = 30$ achieves better results either with uncertainty or without uncertainty. Therefore, a system with appropriate controller gains is capable of convergeing the steady-state more quickly and achieving less errors.

CHAPTER 4

LYAPUNOV-BASED PASSIVE FAULT TOLERANT CONTROL OF THE QUADROTOR UAV

In pure control system theory, control signals from the controller directly act on the system as shown in Figure 4-1. However, in practical systems, control signals are unable to impact the system plant in a straight forward manner unless they pass through the actuator as demonstrated in Figure 4-2.

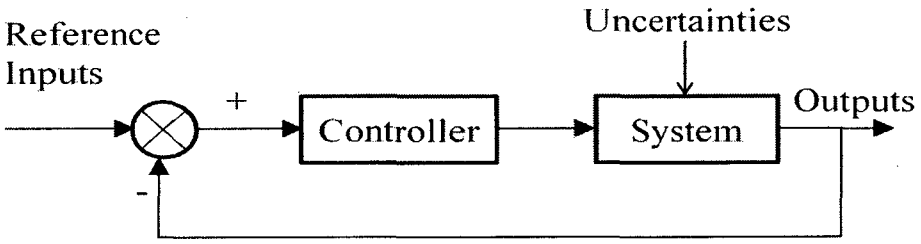

Figure 4-1 Control system diagram in theory

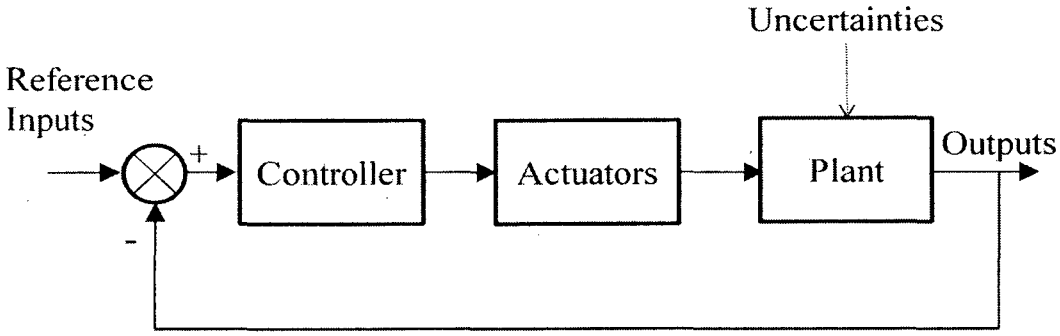

Figure 4-2 A practical control system without consideration of fault

Figure 4-2 shows the practical control system diagram considering the fault-free actuator. The control signals sent to the plant do not directly originate from the controller outputs, but are from the actuators physically connected to the plant.

As a system component, malfunction or damage could occur in system actuators during their life cycle. Actuators of a system will have malfunctions due to aged materials or other reasons. This in turn may cause various faults, such as a partial loss of control effectiveness, stuck at a certain location or a float with no corresponding response to the required control signals sent by the controller. Partial loss is represented as the efficiency reduction of one or multiple actuators; stuck failure is a case that actuator becomes immovable to somewhere; and a floating fault corresponds to randomly movable control surfaces without providing the moments/forces to the aircraft/UAV. These kinds of actuator malfunctions are very dangerous for the quadrotor UAVs, which lead to unacceptable performance for the degraded system and even a crash of the UAV.

This thesis focuses on one or multiple actuator partial loss effects for the quadrotor UAV, based on the consideration of less hardware redundancy available in the quadrotor UAV. However, the developed control approach can be applied for handling stuck and floating types of failures in other types of UAVs with higher hardware redundancy.

The quadrotor UAV holds four actuators, according to the vehicle's physical structure. Therefore, it is very important to make clear how the actuator causes an impact on a quadrotor UAV because of malfunctions.

When introducing the actuator to generate the thrust of each rotor, we obtain [48]:

$$F_i = \frac{\rho}{4}\omega_i^2 R^3 abc(\theta_t - \varphi_t) \tag{4-1}$$

where ρ is the air density, ω is the rotor speed, R is the rotor radius, a is the airfoil lift curve scope, b is the blade number of a rotor, c is the lift coefficient, θ_t is the pitch angle at the blade tip, and φ_t is the inflow angle at the tip. Since the quadrotor UAV has fixed pitch rotors, θ_t can be seen as a constant. To simplify the system, φ_t has been ignored by setting it to zero when the airflow direction changes are a result due to the quadrotor motions through the air. Since all of the parameters are constant, except the rotor speed ω_i, the actuator generating the thrust can be simplified as:

$$F_i = b_i \omega_i^2 \tag{4-2}$$

where b_i is defined as the coefficient of ith actuator. When faults occur, b_i in Eq. (4-2) will have a reduced value by decreasing certain percentage corresponding to certain level of actuator partial fault or loss of its effectiveness. Finally, these partial losses have an effect on the entire quadrotor UAV system due to the dynamic change induced by the fault.

Since actuator faults can easily occur in the quadrotor UAV, the strategies on how to overcome or reduce the fault influences on the UAV are a main concern in the development that follows. This chapter will introduce fault tolerant control (FTC) concepts and design a passive fault tolerant control system (PFTCS) for the quadrotor UAV by employing the Lyapunov-based method with reliable controller gains $k_a = 5$ & $k_b = 30$.

4.1 Introduction

Over the last four decades, more and more researchers have been brought into the FTCS field since the safety and reliability requirements have been increased dramatically, especially for safety-critical engineering systems, such as manned and unmanned aerial or aerospace systems, autonomous robots and vehicles, ground, surface and underwater vehicles, nuclear reactors and power plants, chemical or petrochemical processes, medical devices and so on [34].

The FTC concept can be traced back to 1971, and it is marked as the novel theory of Niederlinski [49]. As a part of the FTCS, fault detection and diagnose (FDD) schemes have made better progress than FTCS. Great incentives to the development of the FTCS came from the aerospace field. This was motivated by the following two airplane accidents in 1970s; one happened on May 25, 1979 and resulted in 271 deaths or injuries. Fortunately, another one with an elevator jammed at 19 degrees up on Flight 1080 on April 12, 1977 has been successfully overcome and the L-1011 airplane landed safely because of the clever use of actuation redundancy in the airplane by the pilot. Since then, the American Air Forces and NASA (National Aeronautics and Space Administration) initiated research in FTCS field in order to ensure that combat and civilian aircrafts can land safely even with multiple control surface impairments [34].

Before going into details about the concepts and design techniques of the FTCS, the terminology of faults, FTCS and PFTCS, will be explained respectively. There are two different definitions for fault: 1) "A fault is an unpermitted deviation of at least one characteristic property (feature) of the system from the acceptable, usual, standard condition" and "A failure is a permanent interruption of a system's ability to perform a

required function under specified operation conditions" [50]; 2) Another definition says that "A fault is regarded as any kind of malfunction in a system, and which may lead to system instability or result in unacceptable performance degradation" [51]. [50] points out that one or more faults result in failure. Therefore, a failure is a rather worse type of malfunction than a fault. This thesis adopts the concept from [51] which indicates faults shown here can be any malfunctions, and that faults and failures are of the same terminology in this thesis.

There are two ways to classify the faults [52, 34]. Depending on the faulty components, faults can happen at sensors, actuators, system or plant components; depending on the effects on the system performance, faults can be permanent faults (remain until the component is repaired or replaced), transient faults (a temporary malfunction of the components), and intermittent faults (repeated occurrences of transient faults). Faults that frequently occur in aircrafts are control loss of one or more actuators/sensors, partial or full hydraulic loss, partial or full control surface losses, engine efficiency loss, aircraft control surface stuck to some degree, and others.

FTCS (Fault Tolerant Control Systems) are known as the control systems that possess the ability to accommodate system component faults/failures automatically and maintain overall system stability and acceptable performances in the event of such failures [34]. The ideal FTCS is to design the controller with a desirable structure to meet the requirements of the performance, robustness and reliability, not only under fault-free cases but also in the presence of various fault cases. The FTCS are divided into Passive Fault Tolerant Control Systems (PFTCS) and Active Fault Tolerant Control Systems

(AFTCS). AFTCS can also be called Reconfigurable Fault Tolerant Control Systems (RFTCS) because of the control reconfiguration feature of the FTCS [34].

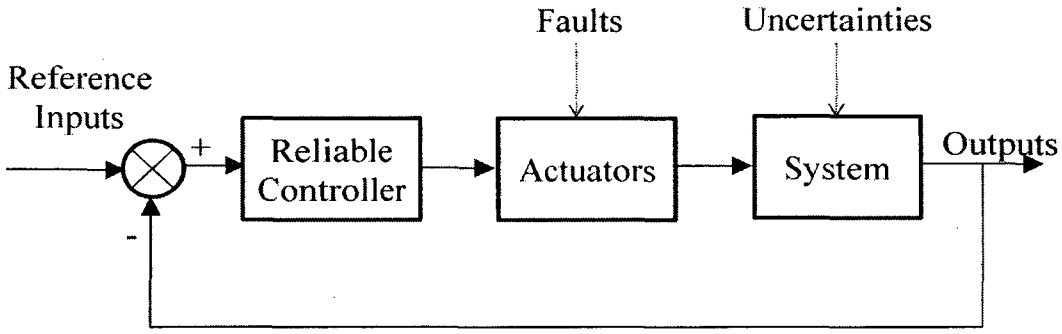

Figure 4-3 PFTCS structure

There are differences between conventional control systems (Figure 4-2) and the PFTCS structure (Figure 4-3). Figure 4-2 includes reference inputs, controller, actuators, system plant and sensors. Since Figure 4-2 deals with control system without considering faults, the stability and robustness requirements for the controller are not so strict. However, faults occurrence is a very common event, although rare, in the real life. Controllers designed with a consideration for the faults demands more robust and more reliable control schemes which enable the system to counteract certain, but different level faults. Therefore, FTCS design is more challenging since the controller should be designed for achieving acceptable stability, performance and also reliability during both systems' normal and fault conditions. As far as these requirements are concerned, Figure 4-3 replaces the controller in Figure 4-2 with a reliable/fault-tolerant controller. The objective of a reliable/fault-tolerant controller is to be capable of accommodating the degraded system in the event of component impairments and maintaining acceptable

stability and performance requirements while keeping good/acceptable stability, performance and robustness requirements under system normal operation conditions.

PFTCS are designed to be able to tolerate a certain class of component faults without the need of online fault information (or called Fault Detection and Diagnose (FDD) scheme) [51, 34]. PFTCS can be applied as a fixed controller to cover system operation conditions under both normal and fault cases. In this instance, PFTCS can compensate for certain faults, and usually the fault types and locations have been known and provided prior to the designed reliable/fault-tolerant controller being implemented/embedded in the system. Without the benefit of the online fault information, a system with such a reliable/fault-tolerant controller is classified as a PFTCS which adopts robust control strategies for handling faults, as similar as handling uncertainties in the system, with the objective of guaranteeing system stability, acceptable performance and robustness under both normal and fault conditions. The robustness of a PFTCS depends on the original closed-loop system under fault-free conditions.

4.2 Fault Tolerant Control System Design for the Quadrotor UAV

Section 4.1 introduces the actuators' fault occurrence and fault types, as well as the motivations behind the development of FTCS research. Furthermore, Section 4.2 reviews the current control strategies studied in the FTCS field, and shows which kinds of aircraft and fault scenarios have been studied in existing research works. This section will design the passive fault tolerant control system for the quadrotor UAV based on the Lyapunov-based controller developed in Chapter 3.

Figure 4-4 presents the PFTCS structure of the quadrotor UAV which includes blocks of the Reliable/Fault-tolerant Controller, the Actuator, and the Quadrotor UAV. Reference inputs and the quadrotor UAV outputs are altitude and Euler angles. The reliable controller block in Figure 4-3 is replaced with an overall controller block using the Lyapunov-based method in Figure 4-4.

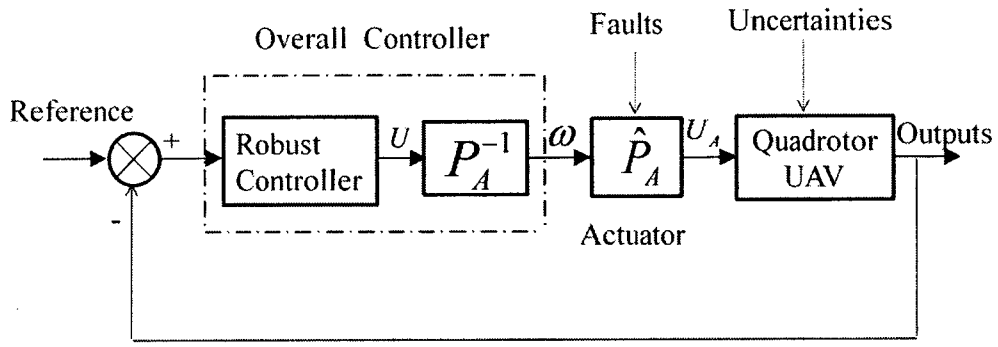

Figure 4-4 PFTCS of a quadrotor UAV

In Figure 4-4, the relation between ω and U_A is shown as below, according to Eqs. (3-2) and (4-2):

$$U_A = \hat{P}_A \omega = \begin{pmatrix} F_1 + F_2 + F_3 + F_4 \\ F_2 - F_4 \\ F_1 - F_3 \\ F_1 + F_3 - F_2 - F_4 \end{pmatrix} = \begin{pmatrix} \hat{b}_1 & \hat{b}_2 & \hat{b}_3 & \hat{b}_4 \\ 0 & \hat{b}_2 & 0 & -\hat{b}_4 \\ \hat{b}_1 & 0 & -\hat{b}_3 & 0 \\ \hat{b}_1 & -\hat{b}_2 & \hat{b}_3 & -\hat{b}_4 \end{pmatrix} \begin{pmatrix} \omega_1^2 \\ \omega_2^2 \\ \omega_3^2 \\ \omega_4^2 \end{pmatrix} \tag{4-3}$$

where ω is $\omega = \begin{pmatrix} \omega_1^2 & \omega_2^2 & \omega_3^2 & \omega_4^2 \end{pmatrix}^T$, the actuator matrix $\hat{P}_A$ equals

$$\hat{P}_A = \begin{pmatrix} \hat{b}_1 & \hat{b}_2 & \hat{b}_3 & \hat{b}_4 \\ 0 & \hat{b}_2 & 0 & -\hat{b}_4 \\ \hat{b}_1 & 0 & -\hat{b}_3 & 0 \\ \hat{b}_1 & -\hat{b}_2 & \hat{b}_3 & -\hat{b}_4 \end{pmatrix} \tag{4-4}$$

and $\hat{b}_1, \hat{b}_2, \hat{b}_3, \hat{b}_4$ in Eq. (4-4) denotes changeable coefficients b_1, b_2, b_3, b_4 when the actuator faults take place.

As far as the concerned controller design, we still prefer using the virtual control U for the convenience. Therefore, the relationship between ω and U can be obtained by Eqs. (3-2) and (4-2) as:

$$\omega = \begin{pmatrix} \omega_1^2 \\ \omega_2^2 \\ \omega_3^2 \\ \omega_4^2 \end{pmatrix} = P_A^{-1} U = \frac{1}{4} \begin{pmatrix} \frac{1}{b_1} & 0 & \frac{2}{b_1} & \frac{1}{b_1} \\ \frac{1}{b_2} & \frac{2}{b_2} & 0 & -\frac{1}{b_2} \\ \frac{1}{b_3} & 0 & -\frac{2}{b_3} & \frac{1}{b_3} \\ \frac{1}{b_4} & -\frac{2}{b_4} & 0 & -\frac{1}{b_4} \end{pmatrix} \begin{pmatrix} u_1 \\ u_2 \\ u_3 \\ u_4 \end{pmatrix} \tag{4-5}$$

Matrix P_A^{-1} is represented in Eq. (4-5) as:

$$P_A^{-1} = \frac{1}{4} \begin{pmatrix} \frac{1}{b_1} & 0 & \frac{2}{b_1} & \frac{1}{b_1} \\ \frac{1}{b_2} & \frac{2}{b_2} & 0 & -\frac{1}{b_2} \\ \frac{1}{b_3} & 0 & -\frac{2}{b_3} & \frac{1}{b_3} \\ \frac{1}{b_4} & -\frac{2}{b_4} & 0 & -\frac{1}{b_4} \end{pmatrix} \tag{4-6}$$

where b_1, b_2, b_3, b_4 are constants unlike $\hat{b}_1, \hat{b}_2, \hat{b}_3, \hat{b}_4$ which are changeable in Eq. (4-4). In other words, the values of b_1, b_2, b_3, b_4 equal those of $\hat{b}_1, \hat{b}_2, \hat{b}_3, \hat{b}_4$, if there is no fault. From Figure 4-4, the relationship between U_A and U can be obtained as:

$$U_A = \hat{P}_A \omega = P_A^{-1} \hat{P}_A U \tag{4-7}$$

It is clear that P_A^{-1} is the inverse matrix of $\hat{P}_A$ if there is no fault occurrence. At this point, Eq. (4-7) is $U_A = \hat{P}_A \omega = P_A^{-1} \hat{P}_A U = U$ which are the fault-free situations discussed in Chapter 3. Moreover, it can be reflected that Figure 4-4 is the same as Figure 4-1 without occurrence of faults, which means that signal U from the controller block in Figure 4-4 can be directly applied to the quadrotor UAV. On the other hand, when the actuator faults do happen, the actuator matrix $\hat{P}_A$ will decrease in percentage. Consequently, the partial loss impacts to the actuator matrix can affect the quadrotor system, which can be expressed as $U_A = \hat{P}_A \omega = P_A^{-1} \hat{P}_A U$.

In the following section, as the fixed controller of PFTCS, the Lyapunov-based control method with fixed controller gains developed in Chapter 3 will be illustrated to accommodate most of the possible quadrotor partial losses.

4.3 Simulations of the Passive Fault Tolerant Control by the Lyapunov-based Method with Controller Gains $k_a = 5$ & $k_b = 30$

The section will show the simulation results which employ the Lyapunov-based method with controller gains $k_a = 5$ & $k_b = 30$ as the fixed controller of the PFTCS to accommodate most of the possible quadrotor partial losses.

The overall simulation time is 30 seconds, and the faults occur at 10 seconds. The definitions of the initial and desired conditions are the same as shown in Chapter 3:

- Initial position: $z = 0$ (meter)
- Initial Euler angles: (30, 30, 30) (degree)
- Desired Euler angles: (10, 10, 10) (degree)
- Desired altitude: $z_r = 1 + 0.1t$ (meter)

The parameters of the quadrotor UAV used in dynamic modeling are given as Table 3-1.

As mentioned in Section 4.1, when designing a PFTCS, potential faults that may occur in the system and fault effects will be taken into consideration at the fault-tolerant controller design stage. Control schemes/parameters will not be changed anymore once the controller has been designed and implemented in the system. In other words, only one controller will be utilized through the entire system operation period and with potential fault conditions predetermined. It is expected that the designed fault-tolerant controller can accommodate different kinds of anticipated faults. As a result, this control strategy can maintain system stability and obtain acceptable performances under both healthy and faulty system operation conditions.

Partial loss fault is an often occurring component fault in the engineering system, which can result in the instability of the system [53]. The quadrotor UAV has four actuators, and it is a complex and highly coupled system. Simulations given later will demonstrate the stability and performance of the control schemes under different levels of partial loss faults. The fault scenarios of possible actuator partial loss discussed in the following sections can be seen clearly through Eq. (4-8):

$$U_A = \begin{pmatrix} u_{A1} \\ u_{A2} \\ u_{A3} \\ u_{A4} \end{pmatrix} = \hat{P}_A \omega = \begin{pmatrix} \hat{b}_1 & \hat{b}_2 & \hat{b}_3 & \hat{b}_4 \\ 0 & \hat{b}_2 & 0 & -\hat{b}_4 \\ \hat{b}_1 & 0 & -\hat{b}_3 & 0 \\ \hat{b}_1 & -\hat{b}_2 & \hat{b}_3 & -\hat{b}_4 \end{pmatrix} \begin{pmatrix} \omega_1^2 \\ \omega_2^2 \\ \omega_3^2 \\ \omega_4^2 \end{pmatrix} \quad (4\text{-}8)$$

- Quad actuators ($\hat{b}_1, \hat{b}_2, \hat{b}_3, \hat{b}_4$) under 50% and 80% partial loss respectively
- Actuator 1 ($\hat{b}_1$) under 50% and 80% partial loss respectively
- Actuator 2 ($\hat{b}_2$) under 50% and 80% partial loss respectively
- Actuator 3 ($\hat{b}_3$) under 50% and 80% partial loss respectively
- Actuator 4 ($\hat{b}_4$) under 50% and 80% partial loss respectively
- Actuator 1 & 4 ($\hat{b}_1$ & $\hat{b}_4$) under 50% and 80% partial loss respectively
- Actuator 2 & 3 ($\hat{b}_2$ & $\hat{b}_3$) under 50% and 80% partial loss respectively
- Actuator 3 & 4 ($\hat{b}_3$ & $\hat{b}_4$) under 50% and 80% partial loss respectively
- Actuator 2 & 3 & 4 ($\hat{b}_2$ & $\hat{b}_3$ & $\hat{b}_4$) under 50% and 80% partial loss respectively

How each type of fault affects the outputs (the altitude and Euler angles) can be derived by Eq. (4-8). The influences are shown in Table 4-1 where u_{A1} is related to altitude alternations and u_{A2}, u_{A3}, u_{A4} are related to roll angle, pitch angle, and yaw angle alternations respectively. For example, quad actuator partial losses only affect u_{A1} since $\hat{b}_1$ & $\hat{b}_2$ & $\hat{b}_3$ & $\hat{b}_4$ are decreased by the same percentage of their efficiency. These analysis results will be proven in simulation results in the following sections.

Table 4-1 Fault effects on the UAV

Fault Types	u_{A1}	u_{A2}	u_{A3}	u_{A4}
$\hat{b}_1$, $\hat{b}_2$, $\hat{b}_3$, $\hat{b}_4$ partial loss	decrease	**no effect**	**no effect**	**no effect**
$\hat{b}_1$ partial loss	decrease	**no effect**	decrease	decrease
$\hat{b}_2$ partial loss	decrease	decrease	**no effect**	*increase*
$\hat{b}_3$ partial loss	decrease	**no effect**	*increase*	decrease
$\hat{b}_4$ partial loss	decrease	*increase*	**no effect**	*increase*
$\hat{b}_1$, $\hat{b}_4$ partial loss	decrease	*increase*	decrease	**no effect**
$\hat{b}_2$, $\hat{b}_3$ partial loss	decrease	decrease	*increase*	**no effect**
$\hat{b}_3$, $\hat{b}_4$ partial loss	decrease	decrease	*increase*	**no effect**
$\hat{b}_2$, $\hat{b}_3$, $\hat{b}_4$ partial loss	decrease	**no effect**	*increase*	*increase*

In the simulation figures of the successive sections, the thicker solid line denotes a fault free situation, the dotted-dash line represents 50% partial loss and the thin solid line shows 80% partial loss. As can be seen, the requirements for the altitude and angle steady-state errors are smaller than 5%.

4.3.1 **Quad Actuators Loss Effects on Altitude**

The quad rotor partial losses will be discussed first since it only affects the altitude when all of the actuators are decreased the same efficiency simultaneously. Table 4-1 clearly demonstrates that the partial loss influences the attitude if quad actuators lose the same efficiency at the same time. Three kinds of partial loss (fault free, losing 50% and 80% efficiency) are executed in the simulation.

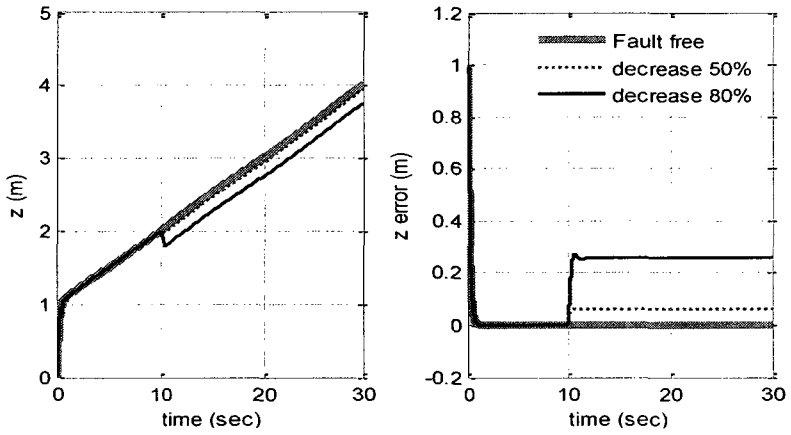

Figure 4-5 Altitude and altitude error comparison when quad rotors are under fault free, 50% and 80% partial loss

Table 4-2 Altitude and altitude error when quad rotors are under fault free, 50% and 80% partial loss with $k_a = 5$ & $k_b = 30$ (unit: m)

Fault type	Roll angle error (degree)	Pitch angle error (degree)	Yaw angle error (degree)	z error (m)
Fault free	-1.5454e-13	-1.5454e-13	-8.5265e-14	-8.2687e-4
50% loss	-1.5454e-13	-1.5454e-13	-8.5265e-14	0.0632
80% loss	-1.5454e-13	-1.5454e-13	-8.5265e-14	0.2555

Figure 4-5 shows the performances when the quadrotor is under fault free (thick line), 50% partial loss (dotted-dash line) and 80% partial loss (thin line). As the partial loss becomes more serious (80% partial loss), the errors of the altitude increase correspondingly. The final stable altitude value according to the desired trajectory is 4 meters since the running time is 30 seconds. Therefore, the steady-state error can be analyzed as shown in Table 4-2. It can be seen from the table that the altitude steady-state error exceeds 5% tolerance when losing 80% efficiency (0.2555/4=6.4%).

4.3.2 Actuator 1 Partial Loss

Actuator 1 partial loss affects pitch angle and yaw angle at the same time, and Figure 4-7 and Table 4-3 prove this analysis. Moreover, these angle changes have an effect on the altitude. When an 80% partial loss fault occurs at 10 seconds, the peak taking place on the pitch angle and yaw angle causes corresponding altitude oscillation.

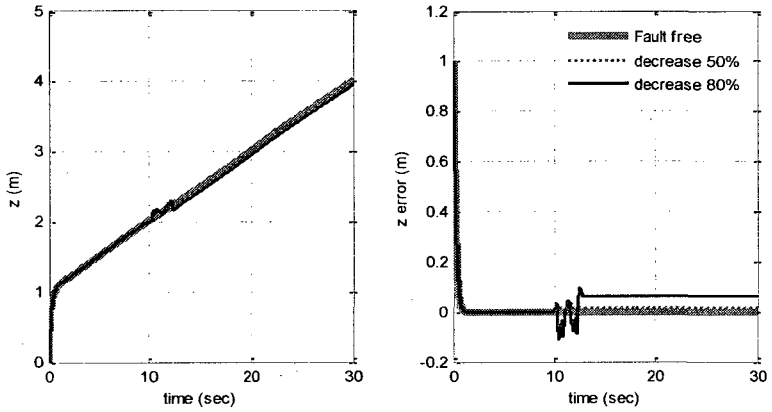

Figure 4-6 Altitude and altitude error comparison when actuator 1 is under fault free, 50% and 80% partial loss

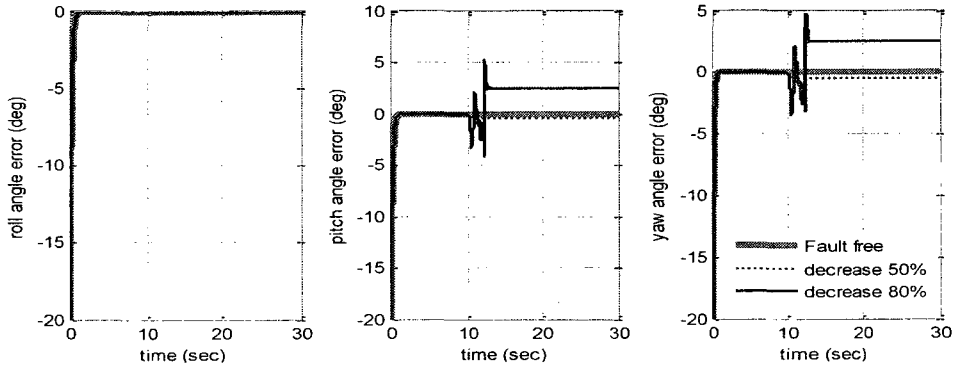

Figure 4-7 Euler angle errors comparison when actuator 1 is under fault free, 50% and 80% partial loss

In fact, the altitude steady-state errors under different fault levels increase when the faults worsen, but they still satisfy 5% requirements even decreasing 80% efficiency.

Table 4-3 Euler angle errors and altitude error comparison when actuator 1 is under fault free, 50% and 80% partial loss

Fault type	Roll angle error (degree)	Pitch angle error (degree)	Yaw angle error (degree)	z error (m)
Fault free	-1.5454e-13	-1.5454e-13	-8.5265e-14	-8.2687e-4
50% loss	-1.5454e-13	-0.4430	-0.4430	0.0152
80% loss	-1.5454e-13	-2.5235	-2.5235	0.0632

From Figure 4-6, Figure 4-7 and Table 4-3, it is clear that a Lyapunov-based control strategy with fixed controller gains (k_a= 5 & k_b= 30) can handle the 50% partial loss acceptably. However, Euler angle performances are not qualified (2.5235/10=25.235%) when actuator 1 loses 80% efficiency.

4.3.3 Actuator 2 Partial Loss

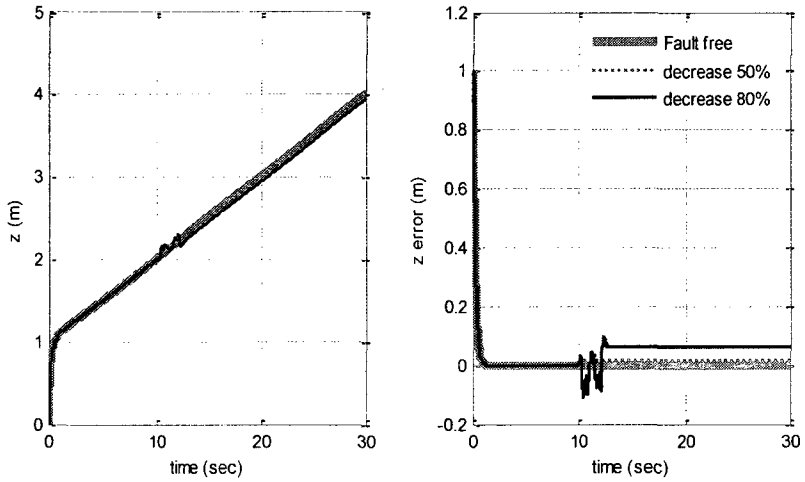

Figure 4-8 Altitude and altitude error comparison when actuator 2 is under fault free, 50% and 80% partial loss

The altitude and Euler angles are still convergent to the steady-state values even when a partial loss of actuator 2 happens at 10 seconds, but with some oscillations. Actuator 2

partial loss affects roll angle and yaw angle simultaneously, and these influences cause altitude changes since the quadrotor UAV is highly coupled system.

Roll angle and yaw angle change greatly when 80% partial loss takes place, because the Lyapunov-based control method with fixed controller gains has limited capability to deal with this severe fault. Table 4-4 shows the large angle steady-state errors when 80% efficiency loss happens.

Table 4-4 Euler angle errors and altitude error comparison when actuator 2 is under fault free, 50% and 80% partial loss

Fault type	Roll angle error (degree)	Pitch angle error (degree)	Yaw angle error (degree)	z error (m)
Fault free	-1.5454e-13	-1.5454e-13	-8.5265e-14	-8.2687e-4
50% loss	-0.443	-1.5454e-13	0.443	0.0152
80% loss	8.5384	-1.5454e-13	-8.5384	0.0632

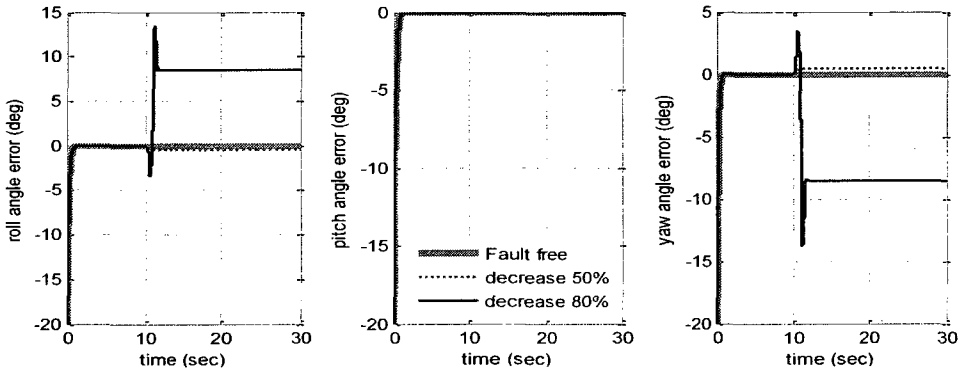

Figure 4-9 Euler angle errors comparison when actuator 2 is under fault free, 50% and 80% partial loss

In comparison with altitude, Euler angles have more oscillations since the altitude peak is caused by the trigonometric function of the dramatic angle alternations which can be seen from the altitude equations in Eq. (2-21) and Eq. (2-20).

4.3.4 Actuator 3 Partial Loss

When comparing the actuator 3 Euler angle errors (Table 4-5) with those of actuator 1 (Table 4-3) and actuator 2 (Table 4-4) when partial loss reaches 80%, Euler angle errors of actuator 3 are smaller than those of actuator 1 and actuator 2, and the response under 80% efficiency loss is smoother (no peak, Figure 4-11). This leads to no position errors, peak and oscillation (Figure 4-10).

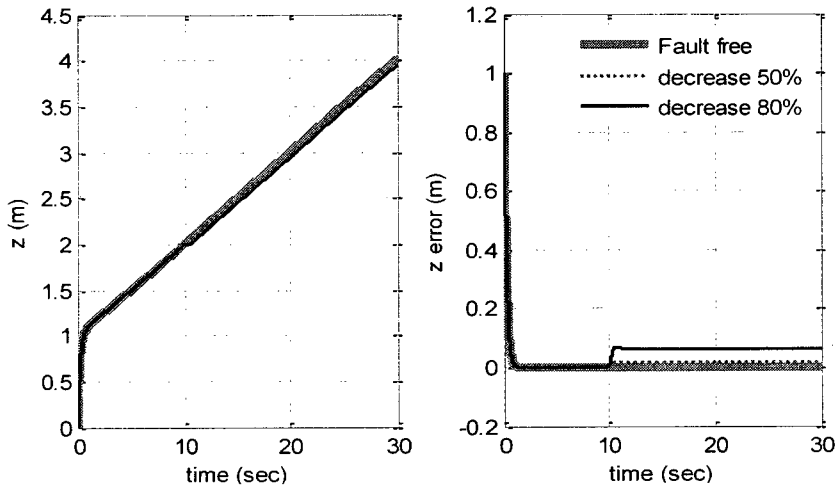

Figure 4-10 Altitude and altitude error comparison when actuator 3 is under fault free, 50% and 80% partial loss

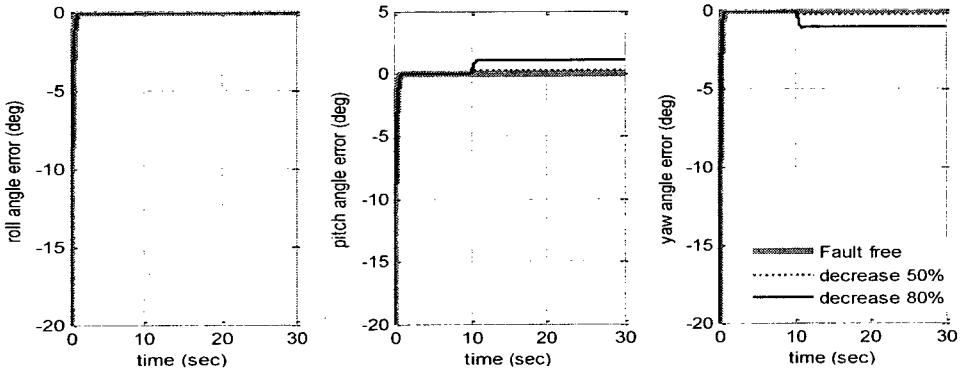

Figure 4-11 Euler angle errors comparison when actuator 3 is under fault free, 50% and 80% partial loss

Table 4-5 Euler angle errors and altitude error comparison when actuator 3 is under fault free, 50% and 80% partial loss

Fault type	Roll angle error (degree)	Pitch angle error (degree)	Yaw angle error (degree)	z error (m)
Fault free	-1.5454e-13	-1.5454e-13	-8.5265e-14	-8.2687e-4
50% loss	-1.5454e-13	0.2457	-0.2457	0.0152
80% loss	-1.5454e-13	1.0410	-1.0410	0.0632

Nevertheless, the angle steady-state errors still exceed the 5% requirements (1.0410/10=10.41%) under an 80% partial loss fault.

4.3.5 Actuator 4 Partial Loss

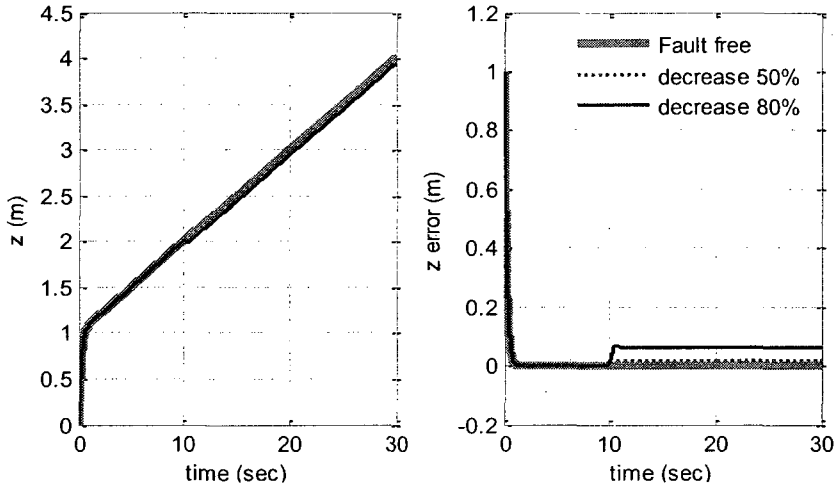

Figure 4-12 Altitude and altitude error comparison when actuator 4 is under fault free, 50% and 80% partial loss

Table 4-6 Euler angle errors and altitude error comparison when actuator 4 is under fault free, 50% and 80% partial loss

Fault type	Roll angle error (degree)	Pitch angle error (degree)	Yaw angle error (degree)	z error (m)
Fault free	-1.5454e-13	-1.5454e-13	-8.5265e-14	-8.2687e-4
50% loss	0.2457	-1.5454e-13	0.2457	0.0152
80% loss	1.0410	-1.5454e-13	1.0410	0.0632

Similar to the cases with other single actuator partial losses, the 50% partial loss has small altitude errors and angle errors which can be exhibited from Figure 4-12, Figure 4-13, and Table 4-6. Furthermore, when the 80% efficiency is reduced, the quadrotor system with the Lyapunov-based controller reacts to the fault smoothly at 10 seconds, unlike the system responses of actuator 1 and actuator 2 partial losses cases which result in dramatic changes in altitude and Euler angles at 10 seconds. However, the Euler angle steady-state errors under actuator 4 partial loss go beyond 5% too as those of actuator 3 demonstrated.

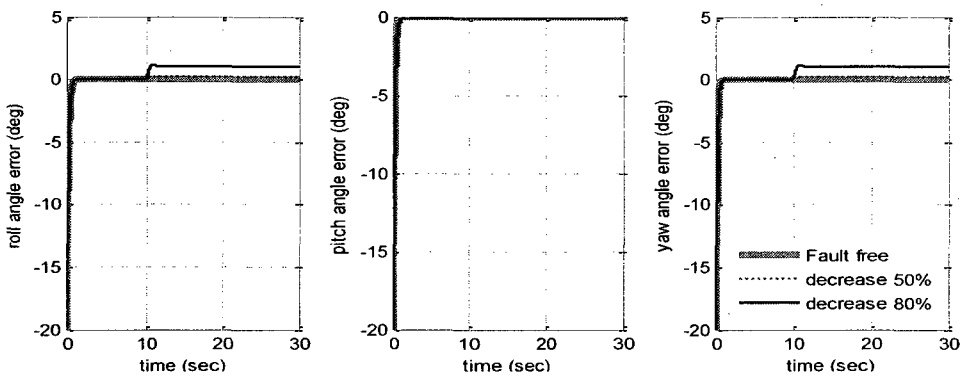

Figure 4-13 Angle error comparison when actuator 4 is under fault free, 50% and 80% partial loss

4.3.6 **Actuator 1 & 4 Partial Loss**

From this section, cases with more than one actuator partial losses are discussed, which induces more serious faults affecting the performance of the quadrotor UAV. The following shows the partial losses occurring on actuator 1 and actuator 4 simultaneously. When actuator 1 and actuator 4 lose 80% efficiency concurrently, this causes a small angle peak which is convergent to 2.4692 (24.692% steady-state angle error in Table 4-7). However, the altitude steady-state error still reaches the satisfied value (0.1273/4=3.18%)

without a peak but some small vibrations, when the worst partial loss (80% partial loss) has an influence on the quadrotor UAV at 10 seconds.

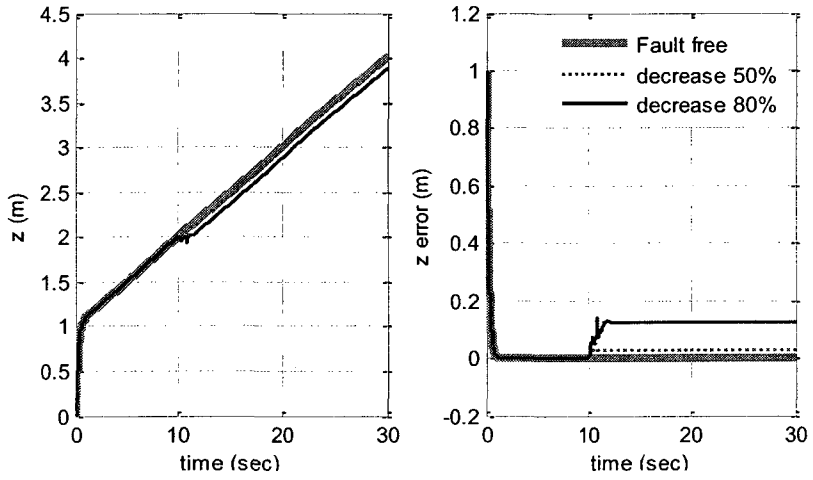

Figure 4-14 Altitude and altitude error when actuators 1 & 4 are under fault free, 50% and 80% partial loss

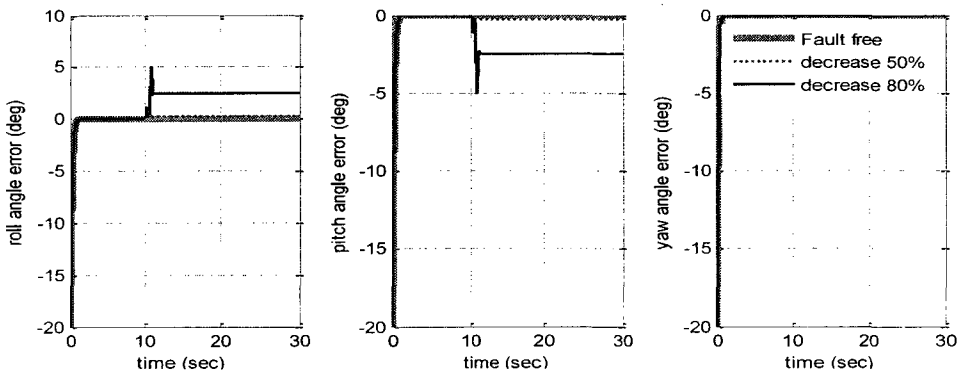

Figure 4-15 Euler angle errors comparison when actuators 1 & 4 are under fault free, 50% and 80% partial loss

Comparing the single partial loss case with the dual-actuator partial loss case under the 80% efficiency reduction, actuator 1 partial loss, actuator 2 partial loss, and actuator 1 & actuator 4 partial losses lead to the small altitude oscillations as shown in Figure 4-6, Figure 4-8 and Figure 4-14. Furthermore, the altitude steady-state errors of dual-actuator

partial losses are greater than those of the single actuator partial loss (see Table 4-3 and Table 4-7). The caused oscillations are because partial loss results in the roll angular acceleration and pitch angular acceleration more negative (shown in Eq. (2-20)). A similar occurrence takes place with actuator 2 & 3 partial loss as presented in the following section.

Table 4-7 Euler angle errors and altitude error comparison when actuators 1 & 4 are under fault free, 50% and 80% partial loss

Fault type	Roll angle error (degree)	Pitch angle error (degree)	Yaw angle error (degree)	z error (m)
Fault free	-1.5454e-13	-1.5454e-13	-8.5265e-14	-8.2687e-4
50% loss	0.3236	-0.3236	-1.5454e-13	0.0312
80% loss	2.4692	-2.4692	-1.5454e-13	0.1273

4.3.7 Actuator 2 & 3 Partial Loss

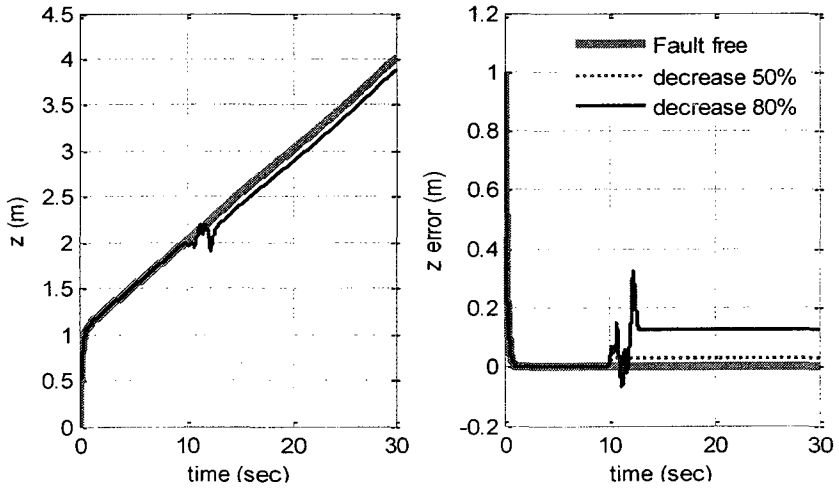

Figure 4-16 Altitude and altitude error when actuators 2 & 3 are under fault free, 50% and 80% partial loss

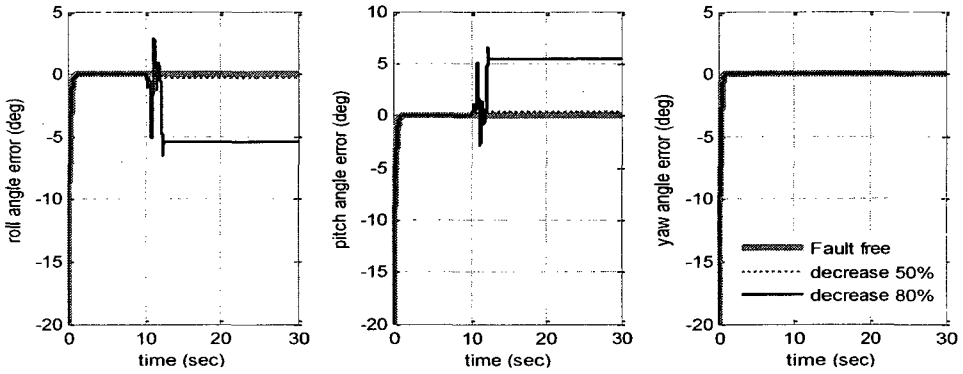

Figure 4-17 Euler angle errors comparison when actuators 2 & 3 are under fault free, 50% and 80% partial loss

When the 80% partial loss affects the system, the altitude steady-state error is convergent to the steady-state values and meets the 5% requirement. Nevertheless, the altitude error has a great peak (Figure 4-16) while the Euler angle errors encounter the peak too (Figure 4-17). Additionally, the angle steady-state errors do not satisfy the requirement, which greatly exceeds the steady-state error requirement (54.371% as shown in Table 4-8).

Table 4-8 Euler angle errors and altitude error comparison when actuators 2 & 3 are under fault free, 50% and 80% partial loss

Fault type	Roll angle error (degree)	Pitch angle error (degree)	Yaw angle error (degree)	z error (m)
Fault free	-1.5454e-13	-1.5454e-13	-8.5265e-14	-8.2687e-4
50% loss	-0.3236	0.3236	-8.5265e-14	0.0312
80% loss	-5.4371	5.4371	-8.5265e-14	0.1273

When comparing the performances of the single actuator and the dual actuator faults, the errors increase dramatically when more actuators have faults (for example, Table 4-3 vs. Table 4-8). Moreover, the 50% partial loss of actuator 1 & 4 results in the same altitude error and Euler angle errors as actuator 2 & 3 demonstrated (as shown in Table 4-7 and Table 4-8).

4.3.8 Actuator 3 & 4 Partial Loss

The quadrotor UAV with the PFTCS structure accommodates the partial loss of actuator 3 & 4 well because small angle errors do not result in the peak of the altitude error (as shown in Figure 4-18 and Figure 4-19).

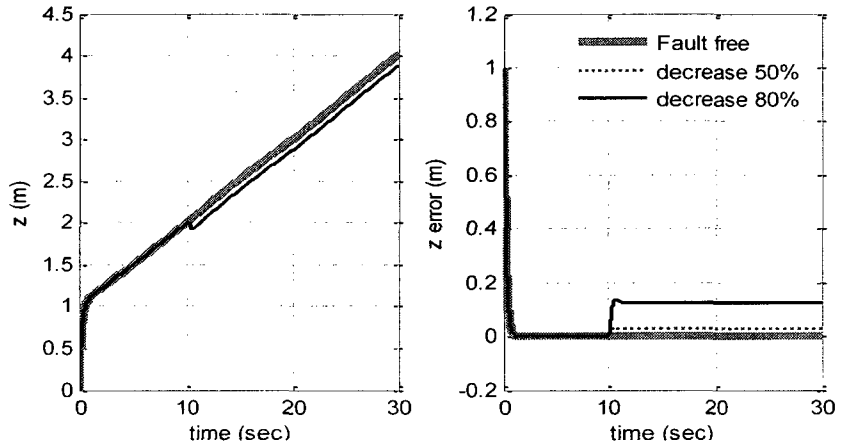

Figure 4-18 Altitude and altitude error when actuators 3 & 4 are under fault free, 50% and 80% partial loss

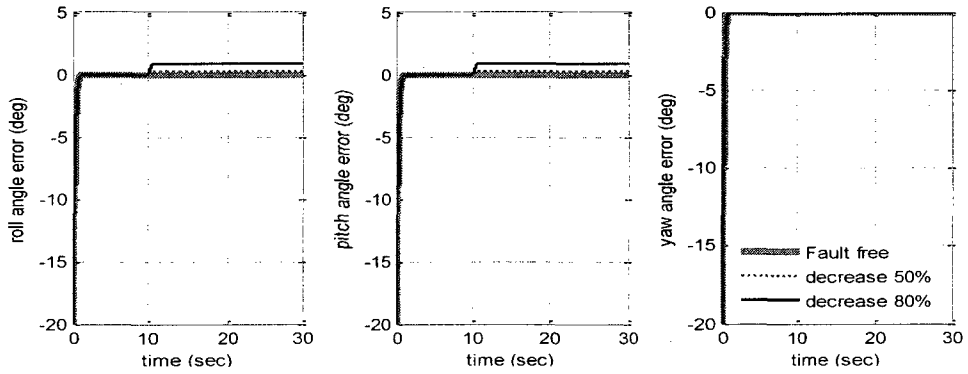

Figure 4-19 Euler angle errors comparison when actuators 3 & 4 are under fault free, 50% and 80% partial loss

However, roll angle error and pitch angle error exceed the required performance (0.8360/10=8.36% in Table 4-9) under 80% partial loss.

Table 4-9 Euler angle errors and altitude error comparison when actuators 3 & 4 are under fault free, 50% and 80% partial loss

Fault type	Roll angle error (degree)	Pitch angle error (degree)	Yaw angle error (degree)	z error (m)
Fault free	-1.5454e-13	-1.5454e-13	-8.5265e-14	-8.2687e-4
50% loss	0.2217	0.2217	-8.5265e-14	0.0312
80% loss	0.8360	0.8360	-8.5265e-14	0.1273

4.3.9 Actuator 2 & 3 & 4 Partial Loss

The partial loss of actuator 2 & 3 & 4 affects roll angle and pitch angle. When the partial loss reaches 80%, the system accommodates the faults well, regardless the altitude (Figure 4-20) and Euler angles (Figure 4-21). However, the angle steady-state errors are 10.4%, which does not make it eligible for the objective (5% requirement).

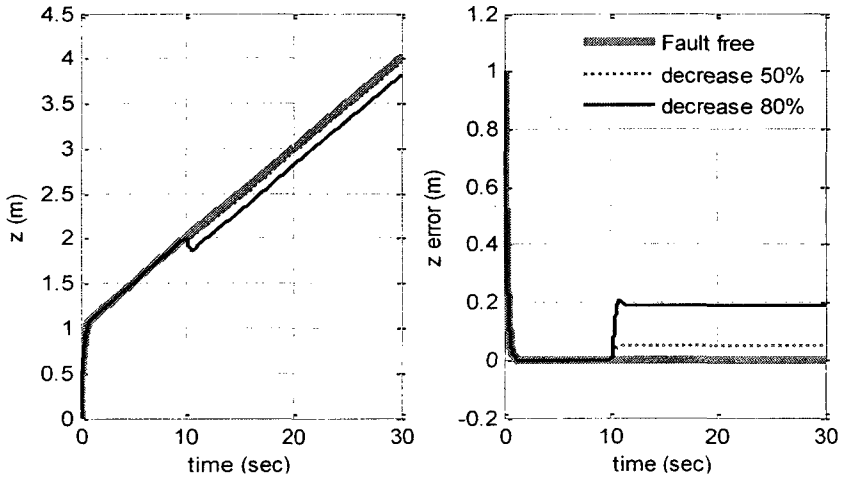

Figure 4-20 Altitude and altitude error comparison when actuators 2 & 3 & 4 are under fault free, 50% and 80% partial loss

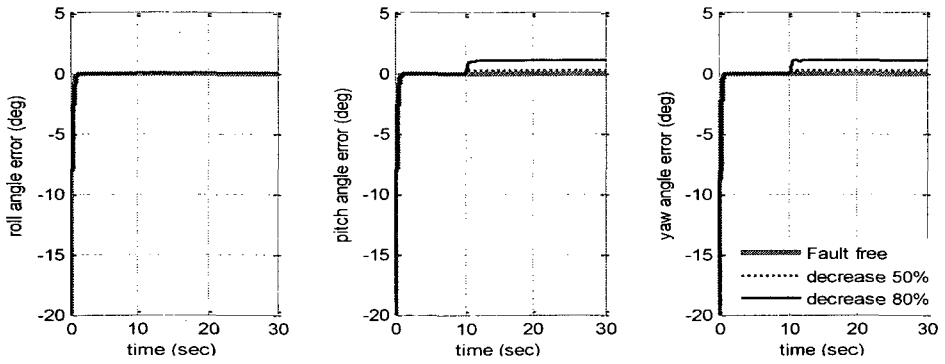

Figure 4-21 Euler angle errors comparison when actuators 2 & 3 & 4 are under fault free, 50% and 80% efficiency

Table 4-10 Euler angle errors and altitude error comparison when actuators 2 & 3 & 4 are under fault free, 50% and 80% partial loss

Fault type	Roll angle error (degree)	Pitch angle error (degree)	Yaw angle error (degree)	z error (m)
Fault free	-1.5454e-13	-1.5454e-13	-8.5265e-14	-8.2687e-4
50% loss	8.7041e-14	0.2457	0.2457	0.0472
80% loss	5.5067e-14	1.0410	1.0410	0.1914

4.4 Summary

By Lyapunov-based control approach, this chapter introduces the PFTCS into quadrotor UAV control system design in order to maintain UAV's stability and performance when faults occur.

The following section will summarize the simulation results based on the passive fault tolerant control (PFTC) method from single actuator partial loss, dual actuator partial losses, triple actuator partial losses, and quad actuator partial losses respectively.

Single actuator partial loss

Combining Table 4-3 to Table 4-6 into Table 4-11, the altitude errors rise with the increase of the partial loss level, and they are the same for each single actuator at the same partial fault level. For example, the altitude steady-state error in Table 4-11 is the same at 50% or 80% partial loss. The 80% single actuator partial loss of actuator 1 and actuator 2 causes oscillations of Euler angles and altitude. Furthermore, the angle oscillations of actuator 2 are greater than those of actuator 1, which cause bigger angle errors in actuator 2 than actuator 1. For the 50% efficiency reduction of actuator 1 and actuator 2, the absolute values of the changed angle errors are the same. In the meantime, the absolute values of the changed angle errors are the same for actuator 3 and actuator 4, regardless the 50% partial loss or 80% partial loss. Moreover, actuator 3 and actuator 4 with 80% partial loss are without oscillation on angles and altitude compared with actuator 1 and actuator 2.

Table 4-11 Comparison of the single actuator partial loss

Fault	Changed angle errors (degree)			Altitude errors (m)
Actuator 1	Fault free	-1.5454e-13 (roll and pitch)	-8.5265e-14 (yaw)	-8.267e-4
	50% loss	-0.4430 (pitch)	-0.4430 (yaw)	0.0152
	80% loss	-2.5235 (pitch)	-2.5235 (yaw)	0.0632
Actuator 2	50% loss	-0.4430 (roll)	0.4430 (yaw)	0.0152
	80% loss	-8.5384 (roll)	8.5384 (yaw)	0.0632
Actuator 3	50% loss	0.2457 (pitch)	-0.2457 (yaw)	0.0152
	80% loss	1.0410 (pitch)	-1.0410 (yaw)	0.0632
Actuator 4	50% loss	0.2457 (roll)	0.2457 (yaw)	0.0152
	80% loss	1.0410 (roll)	1.0410 (yaw)	0.0632

Dual-actuator partial losses

When combining Table 4-7 to Table 4-9 into Table 4-12, it is evident that the altitude errors increase with the rise of partial loss level, and they are the same at the same partial loss level. Actuator 1 & 4 and actuator 2 & 3 cause oscillations of Euler angles and altitude. In addition, the angle oscillation of actuator 2 & actuator 3 is greater than that of actuator 1 & actuator 4, which causes bigger angle errors in actuator 2 & 3 than in actuator 1 & 4. For the 50% efficiency reduction of actuator 1 & 4 and actuator 2 & 3, the absolute values of changed angle errors are the same. At the same time, the absolute values of the changed angle errors are the same for actuator 3 & 4, regardless the 50% partial loss or 80% partial loss. Moreover, actuator 3 & 4 under 80% partial loss is without oscillation on angles and altitude compared with other dual groups.

The Euler angle errors of the dual actuator partial loss are less than those of the single actuator.

Table 4-12 Comparison of dual-actuator partial losses

Fault	Changed angle errors (degree)			Altitude errors (m)
Actuators 1& 4	Fault free	-1.5454e-13 (roll and pitch)	-8.5265e-14 (yaw)	-8.267e-4
	50% loss	0.3236 (roll)	-0.3236 (pitch)	0.0312
	80% loss	2.4692 (roll)	-2.4692 (pitch)	0.1273
Actuators 2& 3	50% loss	-0.3236 (roll)	0.3236 (pitch)	0.0312
	80% loss	-5.4371 (roll)	5.4371 (pitch)	0.1273
Actuators 3 & 4	50% loss	0.2217 (roll)	0.2217 (pitch)	0.0312
	80% loss	0.8360 (roll)	0.8360 (pitch)	0.1273

Triple-actuator partial losses

In Table 4-10, it is clear that altitude errors increase with the augmentation of partial loss.

Quad-actuator partial loss

Altitude errors increase with the increase of partial loss.

Comparison

As shown in Table 3-3, Table 4-10, Table 4-11, and Table 4-12, when uncertainty decreases 50% or 80% of the system parameters, this has a greater impact on the altitude than corresponding 50% or 80% partial loss, in spite of single, dual, triple and quad actuator partial losses.

For different quantity of partial loss faults (single, dual, triple and quad actuators), under the same partial loss level (50% or 80% partial loss), the altitude steady-state error of the quad-actuator partial loss is the largest one, while the single actuator partial loss has the smallest one. Chapter 5 will utilize the new proposed control strategy to improve the performance of quad rotor partial losses.

CHAPTER 5

LYAPUNOV-BASED ADAPTIVE CONTROL APPROACH FOR FAULT TOLERANT CONTROL OF THE QUADROTOR UAV

Chapter 3 utilizes the Lyapunov-based method with fixed controller gains $k_a = 1$ & $k_b = 3$ and $k_a = 5$ & $k_b = 30$ to deal with normal flight situation with system parameter uncertainties. In Chapter 4, the Lyapunov-based method with controller gains $k_a = 5$ & $k_b = 30$ is further applied to the quadrotor UAV, within the framework of PFTCS to handle anticipated actuator partial loss faults. The good performances under not serious actuator partial losses have been obtained. Nevertheless, the Lyapunov-based control strategy with fixed controller gains has limitations in handling severe quadrotor partial loss faults as shown in simulations of Chapter 4.

Therefore, the objective of this chapter is to develop a Lyapunov-based adaptive control design approach for fault tolerant control of the quadrotor UAV.

5.1 Lyapunov-based Adaptive Control Approach

This section discusses the background and the Lyapunov-based adaptive controller design.

5.1.1 Background

Before designing the Lyapunov-based adaptive controller, the existing works will first be introduced. The adaptive control scheme has many applications in control systems, such as optimal parameter tuning [54], backstepping control based on the adaptive PID control [55], decentralized adaptive control systems based on backstepping strategy [43], and adaptive backstepping control scheme of a class of uncertain nonlinear systems [56]. The control platform in these papers is the F-16/MATV (multi-axis thrust vectoring) aircraft which updates the aerodynamic forces and moment coefficients by B-spine neutral networks [57], the UAV which applies an online approximation based on the backstepping control approach under model error, faults, battle damage and actuator constraints [58], and the missile employing adaptive backstepping technique [59].

5.1.2 **Lyapunov-based Adaptive Control Approach**

In Chapter 3, the controlled quadrotor UAV, introduced in Eq. (3-1) to Eq. (3-3), is represented as follows:

$$\ddot{\mathrm{X}} = \Psi + \Phi U_c$$

where X is the state space vector of the system and can be defined as:

$$\mathrm{X} = \begin{pmatrix} z & \phi & \theta & \psi \end{pmatrix}^T$$

with the virtual control inputs

$$U_c = \begin{pmatrix} u_{c1} \\ u_{c2} \\ u_{c3} \\ u_{c4} \end{pmatrix}$$

with

$$\Psi = \begin{pmatrix} -g \\ -\dot{\theta}\dot{\psi}(J_z - J_y) \\ -\dot{\phi}\dot{\psi}(J_x - J_z) \\ -\dot{\theta}\dot{\phi}(J_y - J_x) \end{pmatrix} \quad \Phi = \begin{pmatrix} \frac{\cos\theta\cos\phi}{m} & 0 & 0 & 0 \\ 0 & \frac{l}{J_x} & 0 & 0 \\ 0 & 0 & \frac{l}{J_y} & 0 \\ 0 & 0 & 0 & \frac{l}{J_z} \end{pmatrix}$$

Considering the actuator partial loss $U_c = B^* U$ shown in Figure 5-1, the controlled system can be represented as:

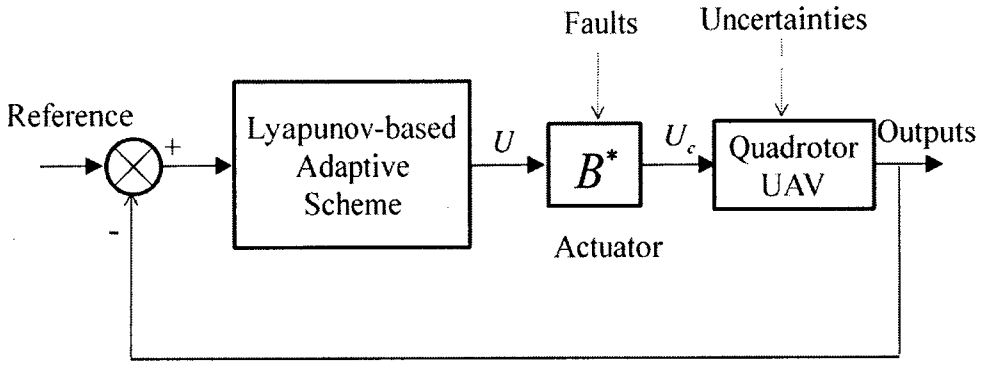

Figure 5-1 Control diagram by utilizing the Lyapunov-based adaptive approach

$$\begin{pmatrix} \ddot{z} \\ \ddot{\phi} \\ \ddot{\theta} \\ \ddot{\psi} \end{pmatrix} = \begin{pmatrix} -g \\ \frac{-\dot{\theta}\dot{\psi}(J_z - J_y)}{J_x} \\ \frac{-\dot{\phi}\dot{\psi}(J_x - J_z)}{J_y} \\ \frac{-\dot{\theta}\dot{\phi}(J_y - J_x)}{J_z} \end{pmatrix} + \begin{pmatrix} b_1^* \frac{\cos\theta\cos\phi}{m} & 0 & 0 & 0 \\ 0 & b_2^* \frac{l}{J_x} & 0 & 0 \\ 0 & 0 & b_3^* \frac{l}{J_y} & 0 \\ 0 & 0 & 0 & b_4^* \frac{l}{J_z} \end{pmatrix} \begin{pmatrix} u_1 \\ u_2 \\ u_3 \\ u_4 \end{pmatrix} \quad (5\text{-}1)$$

where control effectiveness matrix B^* is defined as $B^* = \begin{pmatrix} b_1^* & 0 & 0 & 0 \\ 0 & b_2^* & 0 & 0 \\ 0 & 0 & b_3^* & 0 \\ 0 & 0 & 0 & b_4^* \end{pmatrix}$ with $b_i^* \in (0,1]$.

Remark: The value of b_i^* $(i = 1,2,3,4)$ can reflect effects caused by the actuator partial loss. When the actuators work normally $b_i^* = 1$ $(i = 1,2,3,4)$, this situation has been addressed in Chapter 3. When the actuators work under partial loss, $0 < b_i^* < 1$ $(i = 1,2,3,4)$, the system performance will be affected due to the change of b_i^* $(i = 1,2,3,4)$. In this chapter, considering the actual conditions, the values of b_i^* $(i = 1,2,3,4)$ will be estimated by using adaptive control method, and the corresponding control approach will still ensure the robustness of the system.

Similar to with the Lyapunov-based control design, the following design procedure will utilize the altitude tracking control as an example [60].

The motion equation of the altitude is

$$\ddot{z} = b_1^* \frac{u_1}{m} \cos\theta \cos\phi - g \tag{5-2}$$

The control objective is to design a control law for u_1 to force the system in z to follow a specified desired trajectory z_r i.e., $z \to z_r$ as $t \to \infty$. The desired trajectory satisfies the following assumption:

Assumption 1: The desired trajectory $\mathbf{z}_r = [z_r, \dot{z}_r]^T$ is continuous and available, and $[z_r, \dot{z}_r, \ddot{z}_r]^T \in \Omega_d \subset R^3$ with Ω_d is a compact set.

For presenting the developed adaptive control law, the following definitions are required:

$$\tilde{\alpha}_1 = \hat{\alpha}_1 - \alpha_1 \tag{5-3}$$

where $\hat{\alpha}$ is an estimate of α_1, which is defined as

$$\alpha_1 \overset{\Delta}{=} \frac{1}{b_1^*} \tag{5-4}$$

Given the plant, the following control law is proposed

$$u_1 = \hat{\alpha}_1 u_{c1} \tag{5-5}$$

with

$$u_{c1} = \frac{m}{\cos\theta\cos\phi}(-c_{12}y_{12} - y_{11} + g + \ddot{z}_r + \dot{\beta}_1) \tag{5-6}$$

where

$$\begin{aligned} y_{11}(t) &= z(t) - z_r(t) \\ y_{12}(t) &= \dot{z}(t) - \dot{z}_r(t) - \beta_1 \\ \beta_1(t) &= -c_{11}y_{11}(t) \end{aligned} \tag{5-7}$$

and the parameter $\hat{\alpha}_1$ will be updated by the following adaptation law:

$$\dot{\hat{\alpha}}_1 = -\gamma_1 \frac{u_{c1}}{m}\cos\theta\cos\phi y_{12} \tag{5-8}$$

where parameters c_{11}, c_{12} and γ are positive constants.

For the plant given in Eq. (5-2), subject to Assumption 1, the adaptive controller specified by (5-7) and (5-8) ensures that the signal $z(t)$ is bounded and $z(t) \to z_r(t)$ as $t \to \infty$.

Proof: By utilizing the backstepping design procedure, the following Lyapunov candidate can be selected as

$$V(t)=\frac{1}{2}y_{11}^2+\frac{1}{2}y_{12}^2+\frac{b_1^*}{2\gamma}\tilde{\alpha}_1^{\,2} \tag{5-9}$$

The derivative $\dot{V}$ is given by

$$\begin{aligned}\dot{V} &= y_{11}\dot{y}_{11}+y_{12}\dot{y}_{12}+\frac{b_1^*}{\gamma}\tilde{\alpha}_1\dot{\hat{\alpha}}_1 \\ &\le y_{11}\dot{y}_{11}+y_{12}(\ddot{z}(t)-\ddot{z}_r(t)-\dot{\beta}_1)+\frac{b_1^*}{\gamma}\tilde{\alpha}_1\dot{\hat{\alpha}}_1 \\ &\le y_{11}\dot{y}_{11}+y_{12}(b_1^*\frac{u_1}{m}\cos\theta\cos\phi-g-\ddot{z}_r(t)-\dot{\beta}_1)+\frac{b_1^*}{\gamma}\tilde{\alpha}_1\dot{\hat{\alpha}}_1\end{aligned} \tag{5-10}$$

According to the definition of $\tilde{\alpha}_1$ in Eq. (5-3), we have

$$\hat{\alpha}_1 u_{c1}=(\tilde{\alpha}_1 u_{c1}+\alpha_1 u_{c1}) \tag{5-11}$$

then the inequality (Eq. (5-10)) can be deduced by Eq. (5-11) as

$$\begin{aligned}\dot{V} &\le y_{11}\dot{y}_{11}+y_{12}(b_1^*\frac{(\tilde{\alpha}_1 u_{c1}+\alpha_1 u_{c1})}{m}\cos\theta\cos\phi-g-\ddot{z}_r(t)-\dot{\beta}_1)+\frac{b_1^*}{\gamma}\tilde{\alpha}_1\dot{\hat{\alpha}}_1 \\ &\le y_{11}\dot{y}_{11}+y_{12}(b_1^*\frac{\cos\theta\cos\phi}{m}\tilde{\alpha}_1 u_{c1}+\frac{\cos\theta\cos\phi}{m}u_{c1}-g-\ddot{z}_r(t)-\dot{\beta}_1)+\frac{b_1^*}{\gamma}\tilde{\alpha}_1\dot{\hat{\alpha}}_1\end{aligned} \tag{5-12}$$

By using the control law Eq. (5-6) and the adaptation law (5-8), we have

$$\begin{aligned}\dot{V} \le\ & y_{11}\dot{y}_{11}+y_{12}(b_1^*\frac{\cos\theta\cos\phi}{m}\tilde{\alpha}_1 u_{c1}+\frac{\cos\theta\cos\phi}{m}u_{c1} \\ & -g-\ddot{z}_r(t)-\dot{\beta}_1)+\frac{b_1^*}{\gamma}\tilde{\alpha}_1\dot{\hat{\alpha}}_1 \le -c_{11}y_{11}^2-c_{12}y_{12}^2\end{aligned} \tag{5-13}$$

Eq. (5-9) and Eq. (5-13) imply that V is non-increasing. Hence, y_{1i} $(i=1,2)$ are bounded. By applying the Lasalle-Yoshizawa theorem, it further follows that $y_{1i}(i=1,2)\to 0$ as $t\to\infty$, which implies that $\lim_{t\to\infty}[z(t)-z_r(t)]=0$.

Similarly, the control laws and adaptation laws for the roll angle, pitch angle and yaw angle can be obtained separately.

For roll angle, system plant is:

$$\ddot{\phi} = \frac{1}{J_x}[b_2^* u_2 l - \dot{\theta}\dot{\psi}(J_z - J_y)] \tag{5-14}$$

the control law and adaptive law are designed as

$$u_2 = \hat{\alpha}_2 u_{c2} \tag{5-15}$$

with

$$u_{c2} = \frac{J_x}{l}[-c_{22}y_{22} - y_{21} + \dot{\beta}_2 + \ddot{\phi}_r + \frac{1}{J_x}\dot{\theta}\dot{\psi}(J_z - J_y)] \tag{5-16}$$

where

$$\begin{aligned} y_{21}(t) &= \phi(t) - \phi_r(t) \\ y_{22}(t) &= \dot{\phi}(t) - \dot{\phi}_r(t) - \beta_2 \\ \beta_2(t) &= -c_{21}y_{21}(t) \end{aligned} \tag{5-17}$$

and the adaptive law for roll angle is:

$$\dot{\hat{\alpha}}_2 = -\gamma_2 \frac{u_{c2}}{J_x} l y_{22} \tag{5-18}$$

For pitch angle, the equation is expressed as below:

$$\ddot{\theta} = \frac{1}{J_y}[b_3^* u_3 l - \dot{\phi}\dot{\psi}(J_x - J_z)] \tag{5-19}$$

the control law and adaptive law are designed as

$$u_3 = \hat{\alpha}_3 u_{c3} \tag{5-20}$$

with

$$u_{c3} = \frac{J_y}{l}[-c_{32}y_{32} - y_{31} + \dot{\beta}_3 + \ddot{\theta}_r + \frac{1}{J_y}\dot{\phi}\dot{\psi}(J_x - J_z)] \tag{5-21}$$

where

$$\begin{aligned} y_{31}(t) &= \theta(t) - \theta_r(t) \\ y_{32}(t) &= \dot{\theta}(t) - \dot{\theta}_r(t) - \beta_3 \\ \beta_3(t) &= -c_{31}y_{31}(t) \end{aligned} \tag{5-22}$$

And the adaptive law for pitch angle is:

$$\dot{\hat{\alpha}}_3 = -\gamma_3 \frac{u_{c3}}{J_y} l y_{32} \tag{5-23}$$

For yaw angle, the yaw angular acceleration equals

$$\ddot{\psi} = \frac{1}{J_z}[b_4^* u_4 l - \dot{\theta}\dot{\phi}(J_y - J_x)] \tag{5-24}$$

the control law and adaptive law are designed as

$$u_4 = \hat{\alpha}_4 u_{c4} \tag{5-25}$$

with

$$u_{c4} = \frac{J_z}{l}[-c_{42}y_{22} - y_{41} + \dot{\beta}_4 + \ddot{\psi}_r + \frac{1}{J_z}\dot{\theta}\dot{\phi}(J_y - J_x)] \tag{5-26}$$

where

$$\begin{aligned} y_{41}(t) &= \psi(t) - \psi_r(t) \\ y_{42}(t) &= \dot{\psi}(t) - \dot{\psi}_r(t) - \beta_4 \\ \beta_4(t) &= -c_{41}y_{41}(t) \end{aligned} \tag{5-27}$$

and the adaptive law for yaw angle is

$$\dot{\hat{\alpha}}_4 = -\gamma_4 \frac{u_{c4}}{J_z} l y_{42} \tag{5-28}$$

where $c_{ij}(i = 1,2,3,4, j = 1,2)$ and $\gamma_i(i = 1,2,3,4)$ are positive constants.

5.2 Simulations

This section will demonstrate the methodology presented in previous Section 5.1 by using the quadrotor UAV nonlinear system. The control objective is to make the system state vector $X = (z \quad \phi \quad \theta \quad \psi)^T$ follow the desired Euler angle (10, 10, 10) (degree) and the desired altitude $z_r = 1 + 0.1t$ under varying faults and uncertainties.

The parameters of the quadrotor UAV used in simulations are given in Table 3-1.

Physical parameters of the quadrotor UAV

Symbol	Description	Value	Units
m	Mass of quadrotor	0.6120	kg
l	Distance from cg	0.305	m
J_x	Moment of inertia	0.0154	$kg*m^2$
J_y	Moment of inertia	0.0154	$kg*m^2$
J_z	Moment of inertia	0.0309	$kg*m^2$

Choose the initial altitude z = 0 (meter), the initial Euler angle: (30, 30, 30) (degree), and the initial condition of the derivative of the Euler angles and altitude as:

$$\dot{z}(t) = 0, \ \dot{\phi}(t) = 0, \ \dot{\theta}(t) = 0, \ \dot{\psi}(t) = 0$$

The control constants are chosen by iterative simulation instead of analytical strategy. The control constants employed for the adaptive laws and control laws are selected as:

$$\gamma_1 = 0.01, \ c_{11} = 302, \ c_{12} = 18$$
$$\gamma_2 = 0.015, \ c_{21} = 416, \ c_{22} = 14$$
$$\gamma_3 = 0.0146, \ c_{31} = 408, \ c_{32} = 15$$
$$\gamma_4 = 0.013, \ c_{41} = 390, \ c_{42} = 12.8$$

5.2.1 Simulations under Normal Condition

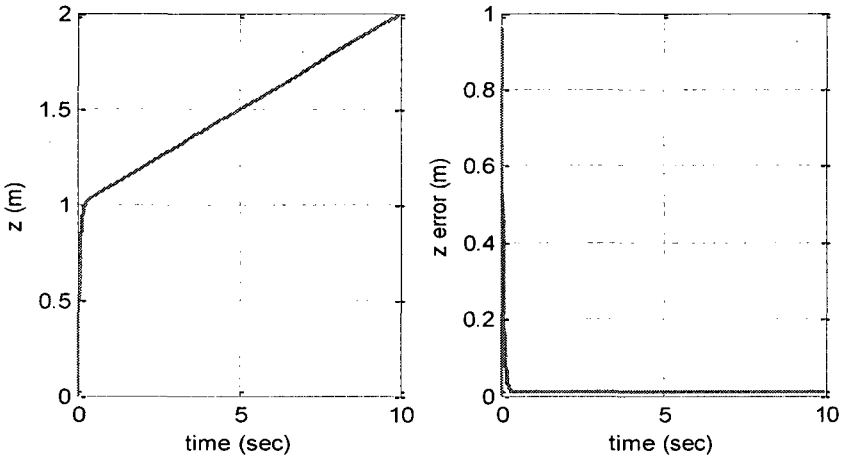

Figure 5-2 Altitude and altitude error with normal case

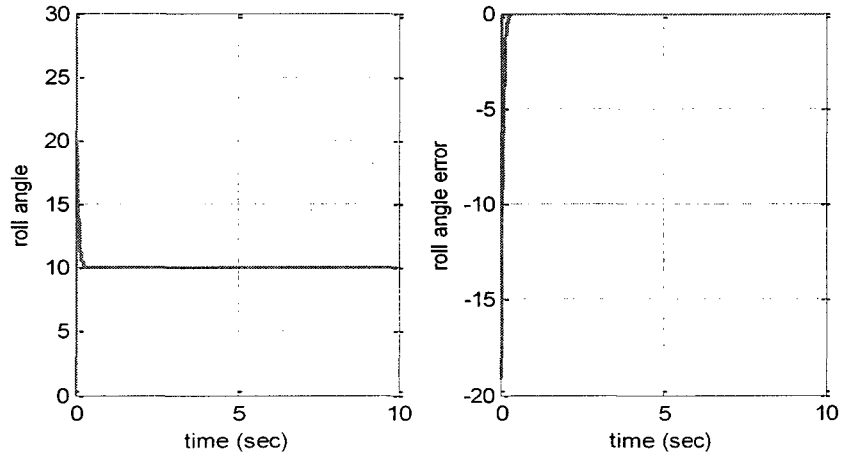

Figure 5-3 Roll angle and roll angle error with normal case

The tracking errors and outputs of the Euler angles and altitude in these figures achieve excellent performance, which can be seen from Figure 5-2 to Figure 5-5. They demonstrate that the proposed control scheme is executable under normal cases without considering uncertainty and partial loss.

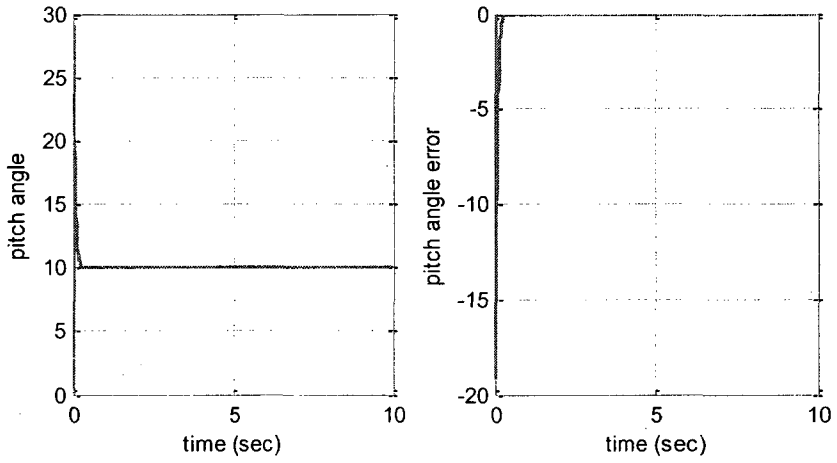

Figure 5-4 Pitch angle and pitch angle error with normal case

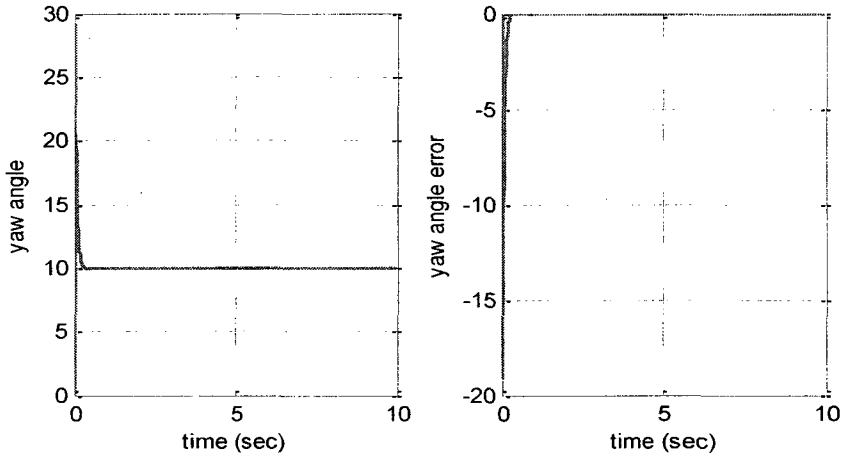

Figure 5-5 Yaw angle and yaw angle error with normal case

5.2.2 **Simulations with Uncertainty**

Considering the uncertainty in a system parameter, namely as mass and inertial moments, the equations of motion for the quadrotor UAV model can be expressed as

$$
\begin{aligned}
\ddot{z} &= \frac{u_1}{m'}\cos\theta\cos\phi - g \\
\ddot{\phi} &= \frac{1}{J_x'}[u_2 l - \dot{\theta}\dot{\psi}(J_z' - J_y')] \\
\ddot{\theta} &= \frac{1}{J_y'}[u_3 l - \dot{\phi}\dot{\psi}(J_x' - J_z')] \\
\ddot{\psi} &= \frac{1}{J_z'}[u_4 l - \dot{\theta}\dot{\phi}(J_y' - J_x')]
\end{aligned}
\tag{5-29}
$$

where m', J_x', J_y', J_z' are mass and inertial moments with parameter uncertainty respectively.

When system uncertainty is 50%, it means that the system parameters (mass and inertial moments) $m' = 0.5m, J_x' = 0.5J_x, J_y' = 0.5J_y, J_z' = 0.5J_z$ where m, J_x, J_y, J_z are the system parameters under normal cases. The same method is used for 80% system parameter uncertainty. The system parameter uncertainty is added at 5 seconds.

Figure 5-6 shows system performance under situations which are uncertainty free, and uncertainty under 50% and 80% of system parameters reductions. The Lyapunov-based adaptive controller has strong robustness so that it can be fast to converge to be stable. Moreover, higher uncertainty has almost the same performance as the uncertainty free case, which is clearly shown in Figure 5-6 since 80% uncertainty performance overlaps with the one which has 50% uncertainty or the one which is uncertainty free.

Comparing Figure 5-6 with Figure 3-7 and Figure 3-9 when a 80% uncertainty occurs in the quadrotor UAV, Figure 3-7 shows that the system is not convergent to the stable value at 30 seconds with unacceptable error. In addition, Figure 3-9 shows that the system can be converged to be stable. However, the overshoot and the altitude steady-

state error are greater than those in Figure 5-6. The excellent system performance shown in Figure 5-6 is not only its convergent speed, but also its steady-state error which is almost zero.

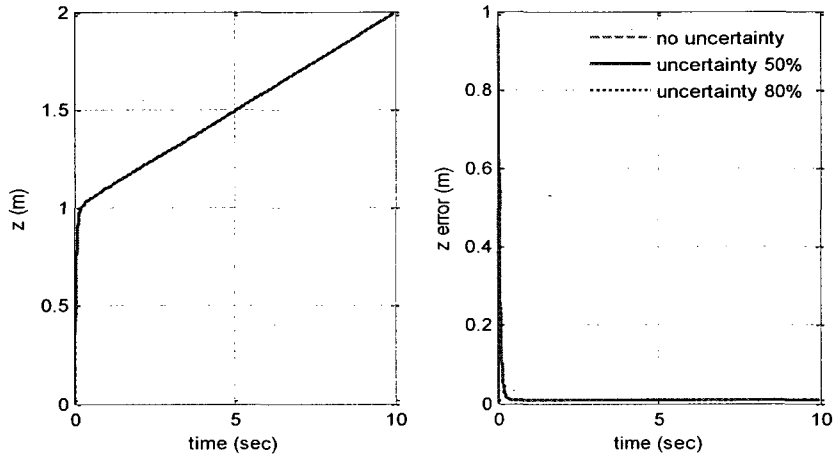

Figure 5-6 Altitude and altitude errors comparison among no uncertainty, decreasing 50% and 80% system parameters

5.2.3 Simulations with Partial Loss Faults

Simulations in this Section will evaluate the performance with quadrotor partial losses. Three working conditions will be discussed: 1) no partial loss $b_1^* = 1$, 2) partial loss decreases 50% $b_1^* = 0.5$ and 3) 80% $b_1^* = 0.2$. Partial loss occurs at 5 seconds.

As shown in Figure 5-7, the severe partial loss situation discussed is 80% quadrotor partial losses. When comparing the 80% partial loss with the fault-free case, their altitude errors only show a little difference, which means that the adaptive controller has strong ability to overcome the variable partial losses and achieve a satisfactory performance.

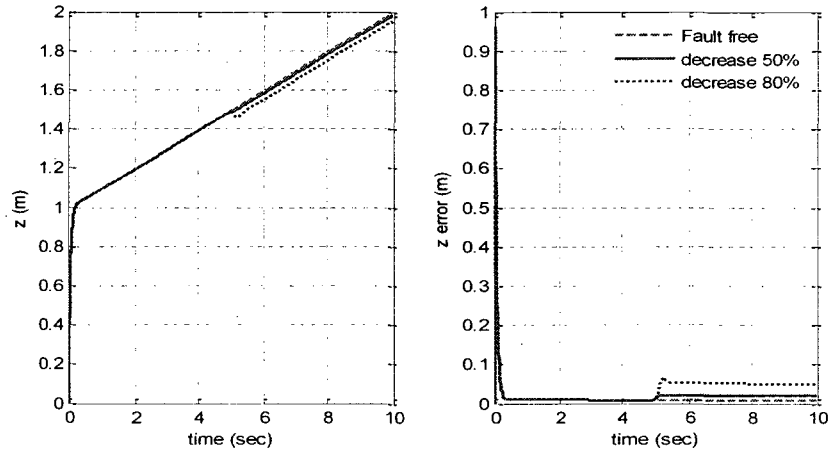

Figure 5-7 Altitude and altitude errors comparison among fault free, 50% and 80% partial loss of the quadrotors

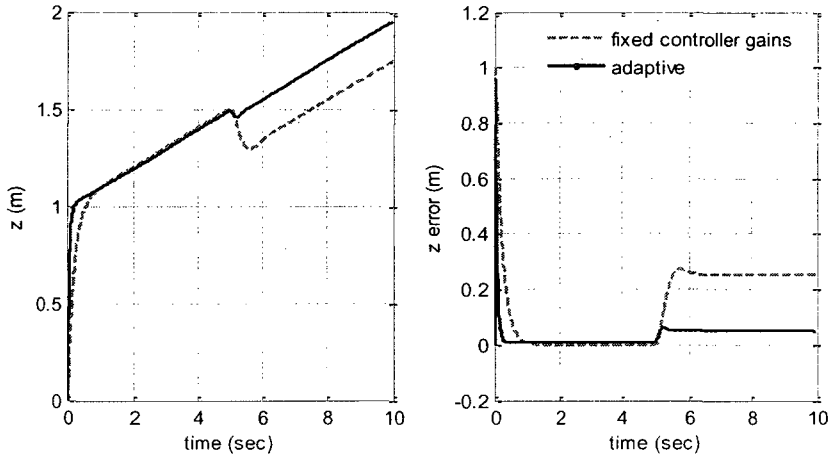

Figure 5-8 Altitude and altitude errors comparison with 80% partial loss by employing different control scheme

In Figure 5-8, dotted line denotes the performance of Lyapunov-based control approach with fixed controller gains, and the solid line presents the performance of Lyapunov-based adaptive control. By comparing the performances under 80% quadrotor partial losses, it can be seen that the Lyapunov-based control method with controller

gains 5 & 30 has certain robustness to accommodate the faults. However, this approach causes more overshoot and steady-state errors. Therefore, the Lyapunov-based adaptive control method has more advantages to deal with the 80% partial loss.

5.2.4 Simulations with Partial Loss Fault Combined with Uncertainty

This section reveals the simulation results which are 50% uncertainty combined with 80% partial loss and 80% uncertainty combined with 80% partial loss respectively. Note that partial loss and system uncertainty will happen simultaneously at 5 seconds. The performances shown in Figure 5-9 illustrate that the Lyapunov-based adaptive control scheme has strong robustness to handle uncertainty and partial loss simultaneously.

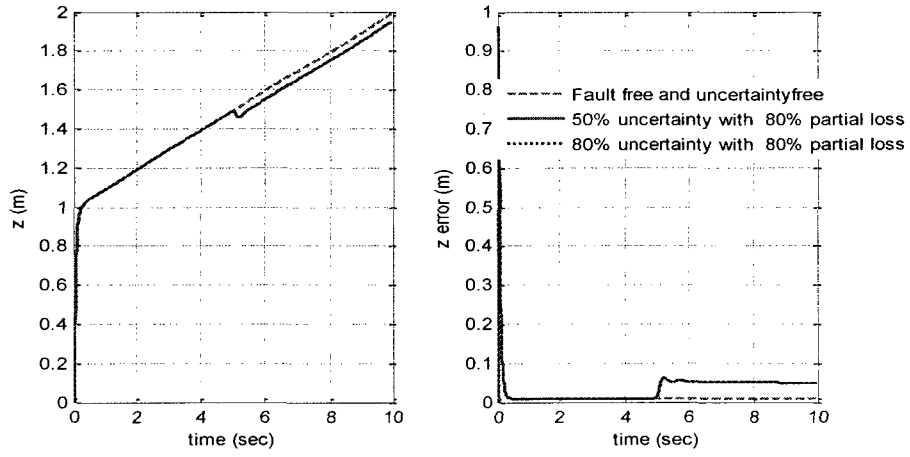

Figure 5-9 Altitude and altitude errors comparison of quad rotors among fault free, uncertain 50% and 80% respectively combined 80% partial loss

5.3 Summary

This chapter has designed the Lyapunov-based adaptive controller and utilizes it for fault tolerant control of the quadrotor UAV. The simulations are implemented with normal case, uncertainty at different levels of quadrotor partial losses. Furthermore, simulations of the severe fault scenarios, 80% partial loss combined with 50% uncertainty and 80% uncertainty respectively have been presented.

The simulation results in this chapter demonstrate that the Lyapunov-based adaptive controller can effectively overcome the effects of not only uncertainty and partial loss, but also the combined severe situations. When comparing the Lyapunov-based control with fixed controller gains, the Lyapunov-based adaptive control approach clearly has advantages in achieving better fault-tolerant capability.

CHAPTER 6

IMPLEMENTATION OF LYAPUNOV-BASED CONTROL APPROACH ON THE QBALL-X4 TEST-BED

This chapter will apply the Lyapunov-based control approach on the Qball-X4 test-bed. Before the test results are exposed, Qball-X4 will be introduced briefly from its structures and features viewpoints.

6.1 Qball-X4

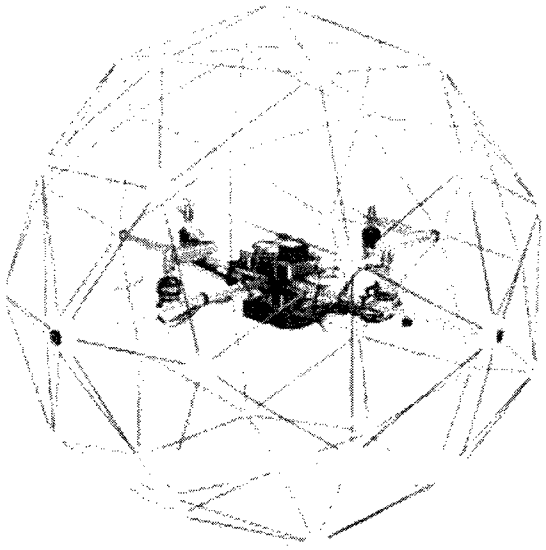

Figure 6-1 Qball-X4 [61]

The Quanser Qball-X4 is a quadrotor unmanned aerial vehicle within a protective carbon fiber cage, which was specially designed and developed by Quanser Inc. through an NSERC Strategic Project Grant (SPG) funded to Concordia University. Its special features include that the designed UAV is a good test-bed for universities and/or research

institutes to be used for different research topics. Qball-X4 are mainly composed of Qball-X4 architecture as shown in Figure 6-1, HIQ DAQ (QuaRC aerial vehicle data acquisition card), Gumstix, Real-time Control Software, and two 3-cell, 2500mAh Lithium-Polymer batteries [61].

Qball-X4, shown in Figure 6-1, has quad rotors and is protected by the carbon fiber cage. Since this test-bed is designed for the universities' research, there are potential to inject possible actuator faults or propeller damages when the developed and unmatured approaches are executed on the Qball-X4. The fiber cage specially protects for these kinds of damages, such as other moving vehicles in the same room, obstacles. The tests in our lab strongly benefit this feature as this design reduced great maintenances.

The HIQ DAQ is a data acquisition card of the Qball-X4. All the data from the on-board sensors and outputting motor commands are obtained from HIQ DAQ. This card may have an optional daughterboard with the I/O (input/output) devices.

Gumstix is chosen for the QuaRC target computer because of its small size like its name exposed, reasonable price and plenty of linux open source code [62]. QuaRC is the real-time control software and connected with Matlab/Simulink, which is very convenient for the researchers to develop their own algorithm on the console. QuaRC in the host computer can generate codes, and these codes are sent to target computer (Gumstix) by wireless network. Meanwhile, it sends/receives scope data, and update runtime parameters.

The test environment includes six cameras to provide position of the Qball-X4 quadrotor UAV. After the process in the host computer, all of the codes will be

downloaded to the target computer on board of UAV by the wireless network. Then Qball-X4 quadrotor UAV is capable of flying autonomously.

6.2 Test Results of Lyapunov-based Control Method on Qball-X4

The Simulink model of Qball-X4 UAV is a highly complex function combination. The position commands block is concerned more since the position controller is in inside. The following will execute the Lyapunov-based control method on controlling the Qball-X4's altitude by replacing the existing LQR controller from Quanser Inc. Figure 6-2 shows the control structure for Qball-X4 [63].

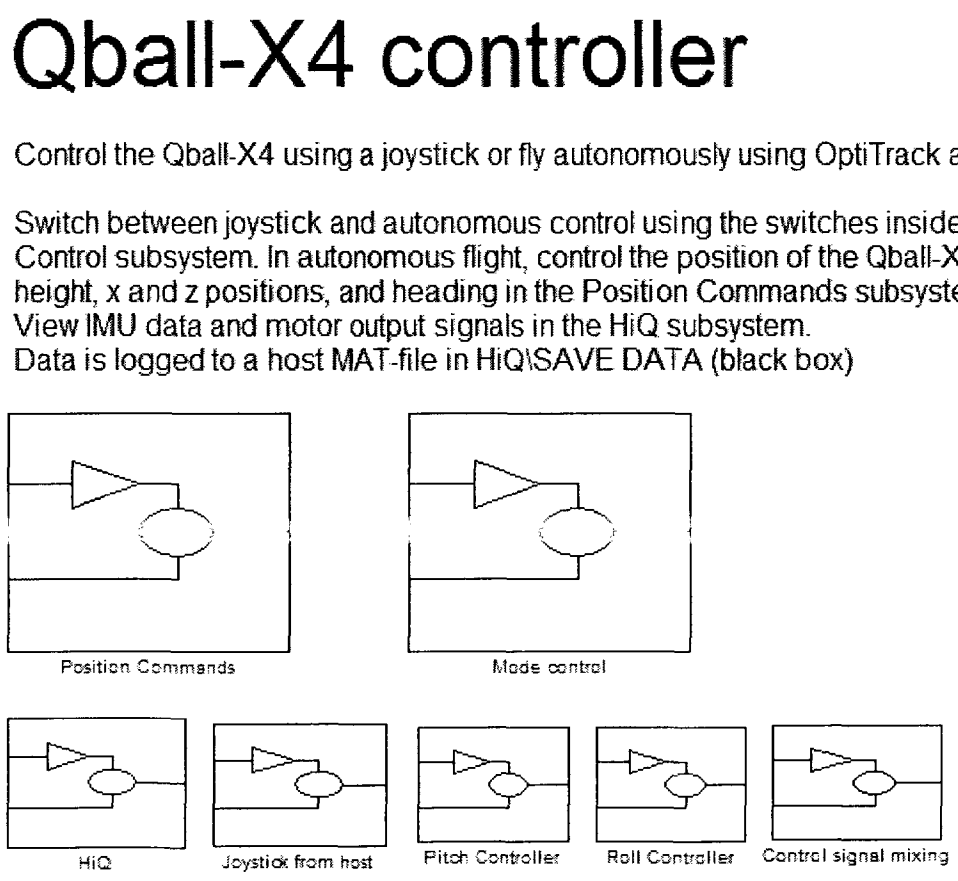

Figure 6-2 Qball-X4 controller [63]

Through plenty of test data, it shows that the results are sensitive to the battery level. The following will present three groups test results in real time manner under full charge, stable voltage, and lower voltage in sequence, and the test results under different battery levels are related to altitude, corresponding battery output, altitude control law and PWM output from each rotor respectively. The test condition is set as Zr = 0.4, the initial altitude $Z(0)$ = 0, and Euler angles are not taken into account in order to simplify the test condition. Due to safety issue, the running time starts around 5 seconds. The following experiments will choose controller gains k_a= 1.8 & k_b=0.9 during the test to verify the power effect on the system.

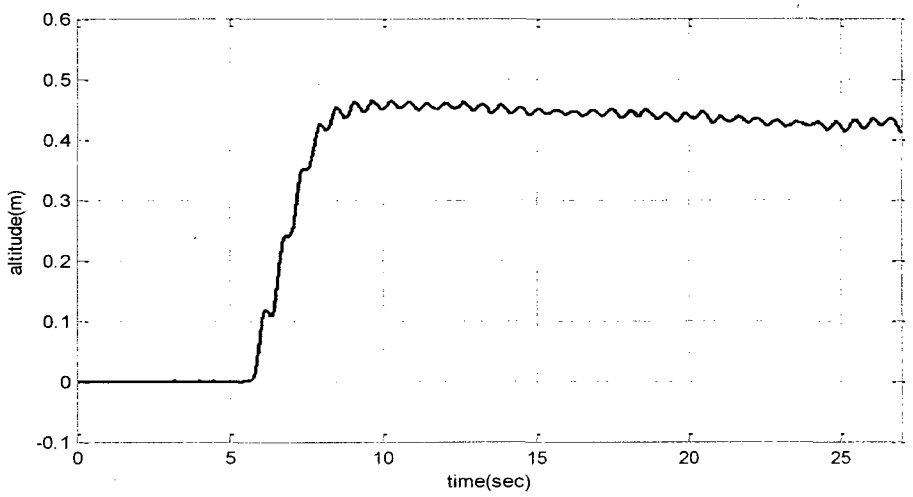

Figure 6-3 Altitude under full battery

The experiment of the first group concerns the performance of UAV under full battery charge. The battery is a nonlinear output with lots of oscillation as shown in Figure 6-4, and it assigns the power to each rotor. Moreover, PWM output of each rotor has many oscillations as shown in Figure 6-5. Since the thrust is generated by the PWM, this nonlinear PWM output makes the system to be controlled more difficult. The altitude has

the tendency to be stable shown in Figure 6-3. However, the overshoot is bigger and the vehicle takes a long time to reach to the stable status. Meanwhile, the altitude control law tries to make altitude reach to the desired value as shown in Figure 6-5. But the result is not so satisfactory.

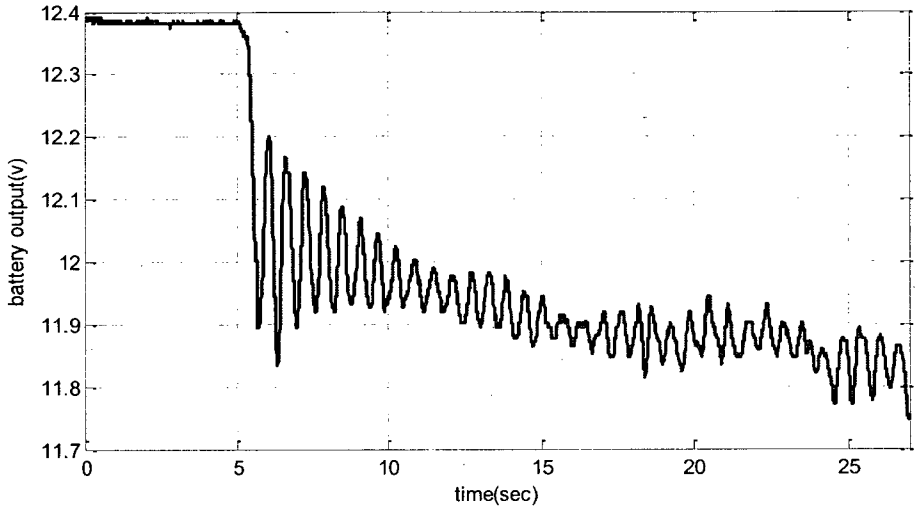

Figure 6-4 Battery output

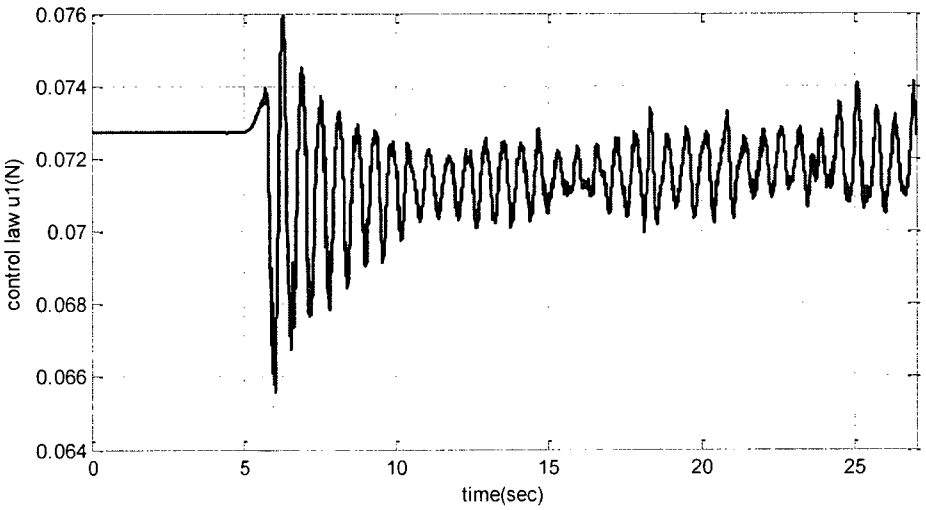

Figure 6-5 Altitude control law under full battery

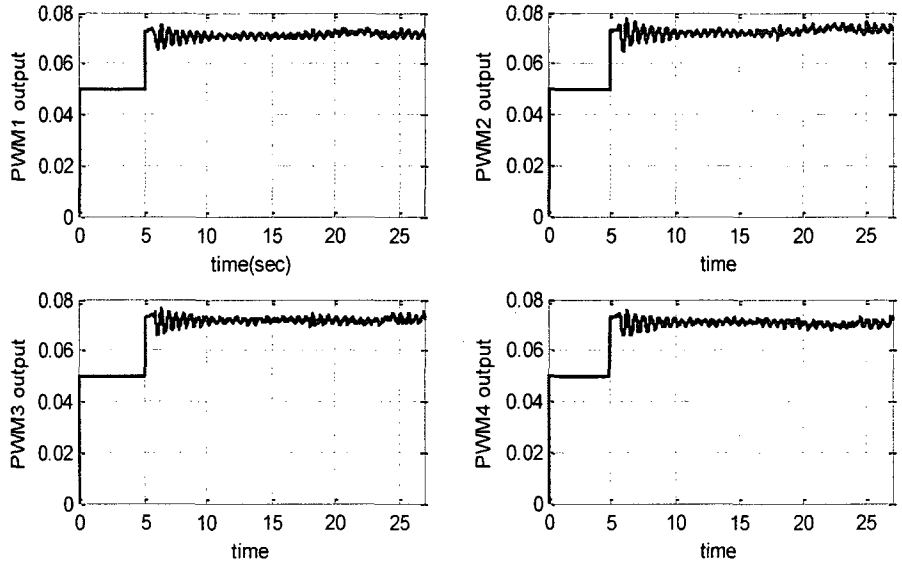

Figure 6-6 PWM output from each rotor under full battery

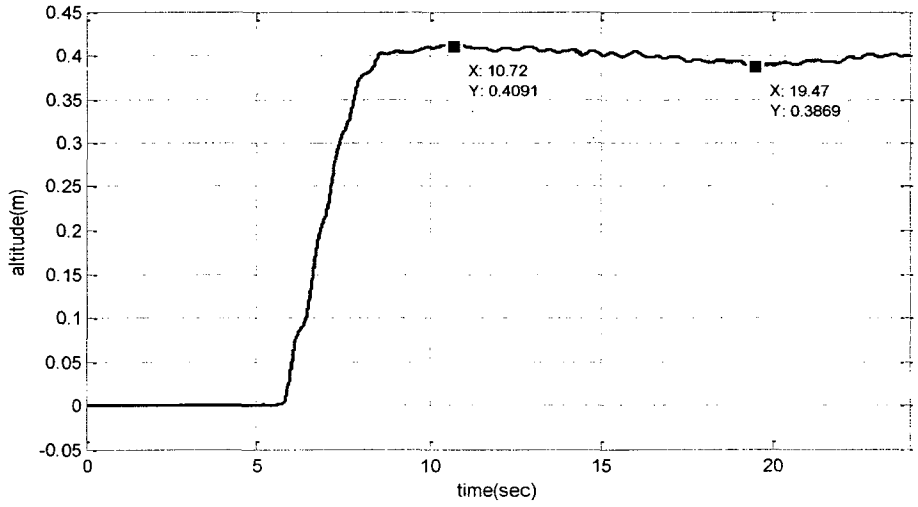

Figure 6-7 Altitude under stable battery voltage

When the battery is more stable, as shown in Figure 6-8 and PWM output in Figure 6-10 that are much smoother without so many nonlinear disturbances, the performance of the Qball-X4 achieves an excellent level. The rising time in Figure 6-7 is about 3 seconds,

the steady-state error is very small with real-time battery and PWM output from each rotor. The top point and the bottom point in Figure 6-7 are only 0.4091 meter (steady-state error is 2.2%) and 0.3869 meter (steady-state error is 3.2%) separately.

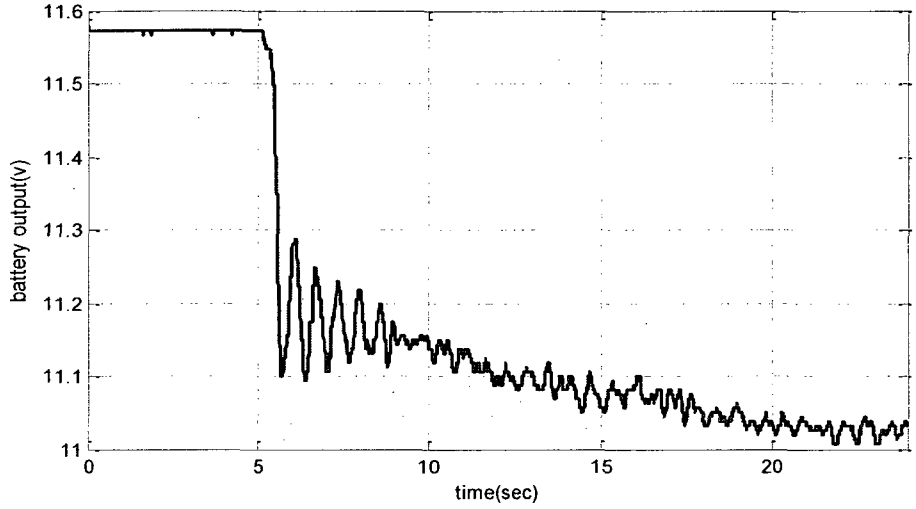

Figure 6-8 Battery output

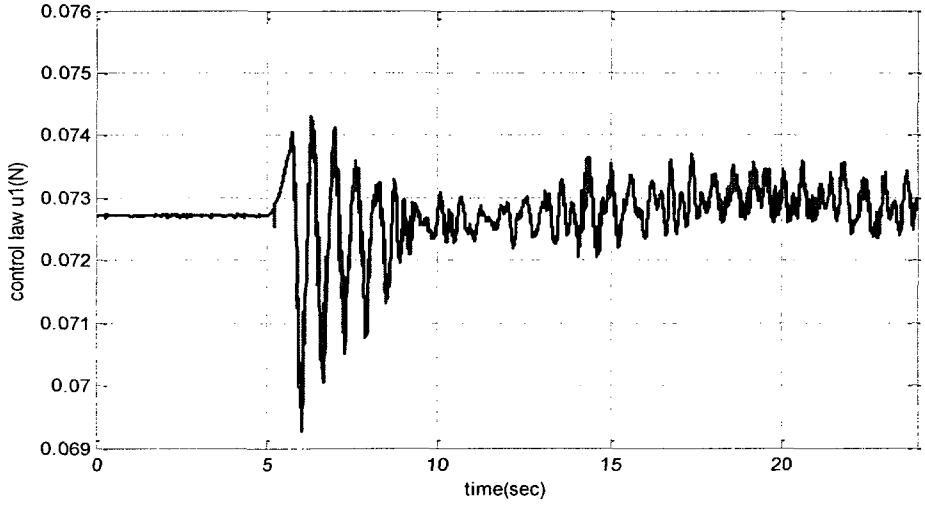

Figure 6-9 Altitude control law under stable battery

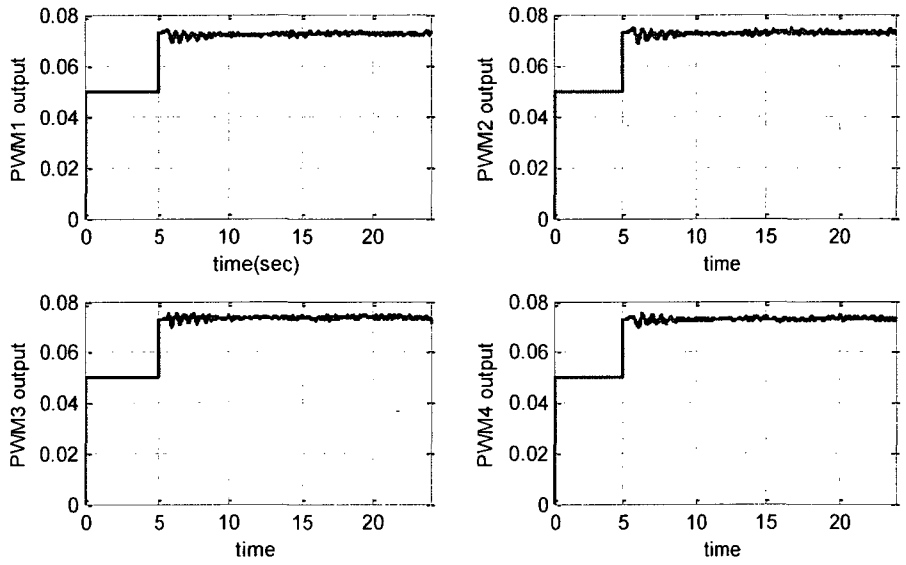

Figure 6-10 PWM output from each rotor under stable battery

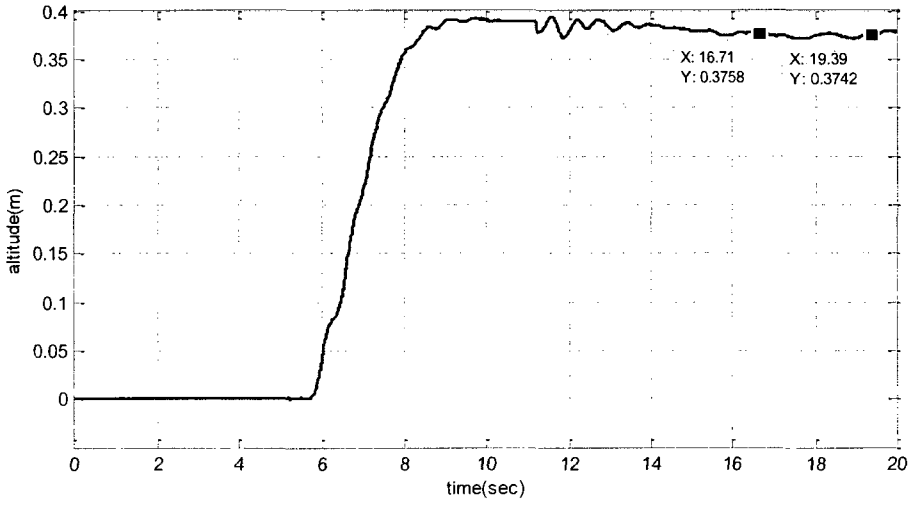

Figure 6-11 Altitude under low battery voltage

The third group discusses about the low battery down to 10.9 voltages which has been warned "low battery" from the system in fact. When the battery reaches below 11 voltages, it will bring more nonlinear disturbances into the system and the performance

cannot be ensured. From Figure 6-11, the steady-state error is 7.5% when the vehicle reaches to the stability. This performance is better than the system with full battery.

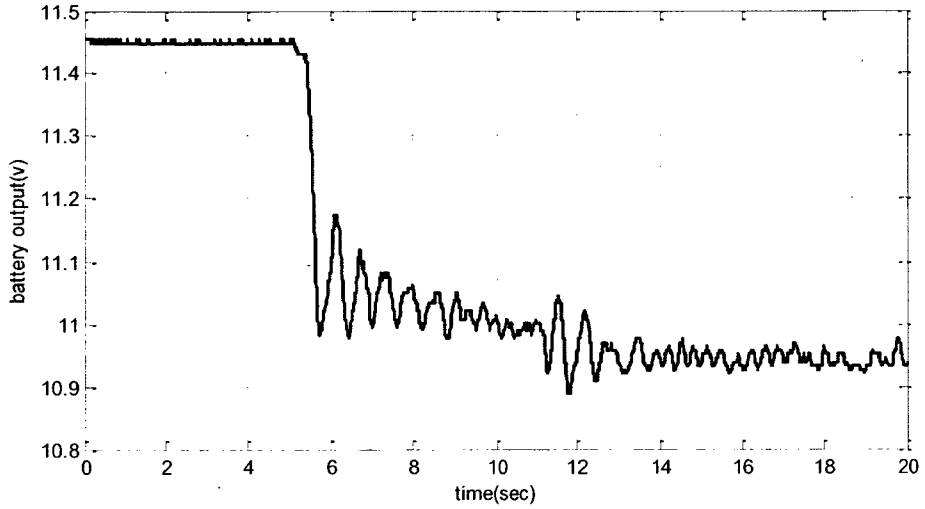

Figure 6-12 Battery output

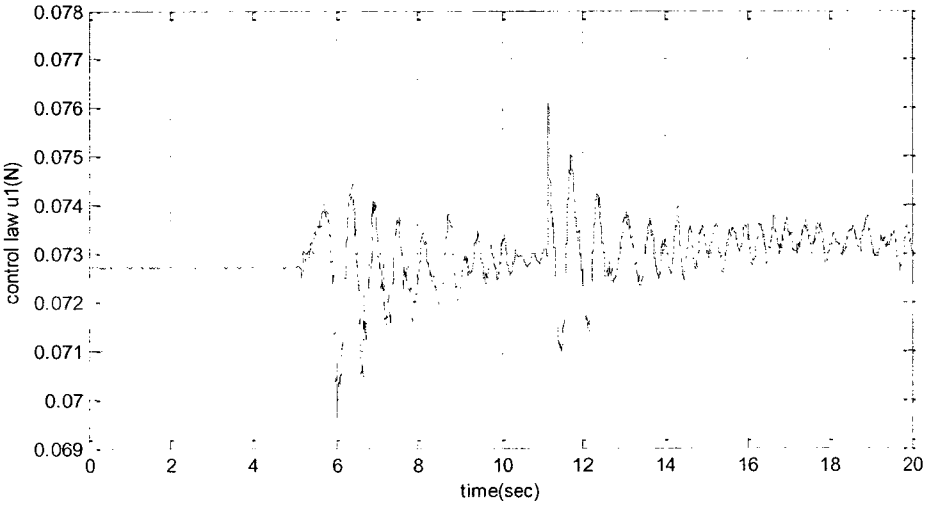

Figure 6-13 Altitude control law under low battery

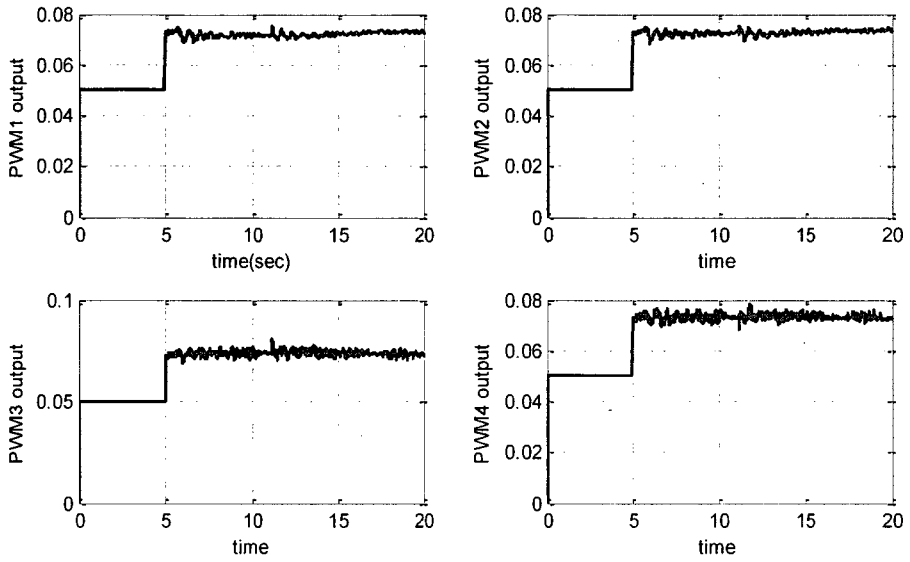

Figure 6-14 PWM output from each rotor under low battery

Comparing the PWM outputs from each rotor in Figure 6-6, Figure 6-10, and Figure 6-14, it is clear that battery change leads to each rotor's PWM outputs change, then correspondingly alters each rotor's thrust and makes the system to be controlled in a difficult way.

If battery output is nonlinear and it cannot ensure the stable power, the power assigned to each rotor cannot provide expected thrust. Since each rotor is drived by its corresponding actuator, unstable battery can be considered as the actuator fault with partial control effectiveness loss. In Chapter 4, various actuator partial loss conditions have been concerned, now this section exposes the practical actuator faults. The test results show that Lyapunov-based control approach is executable on the Qball-X4 test-bed and is capable of tolerating certain faults.

Note that this section doesn't consider the Euler angles' effects on the Qball-X4 test-bed due to the time limitation. The position control combined with rotation control will be developed in the continuous work.

6.3 Summary

The objective of this Qball-X4 experiment on altitude control is to evaluate and demonstrate the capability of the control system to tolerant certain faults. From these test results, it demonstrates that the Qball-X4 quadrotor UAV can flight automatically and stay stable. Nevertheless, there are a lot of factors to affect the performance of Qball-X4 quadrotor UAV since it is a physical vehicle composed of various hardwares, such as the communication between camera and host, the wireless communication between host computer and Qball-X4 UAV, and the calculation speed of the microchip in Gumstix, and so on. However, from many experiment results have been done, it noticed that battery plays an important role in Qball-X4 control performance. The experiment results prove that the Lyapunov-based control method has certain robustness to deal with actuator faults caused by unstable battery.

CHAPTER 7

CONCLUSIONS AND RECOMMENDATIONS

7.1 Contributions

This thesis focuses on fault tolerant control under various actuator partial loss faults by applying a nonlinear control strategy. Based on our best knowledge, there is little FTC (Fault Tolerant Control) work done for the quadrotor UAVs.

The contributions of this thesis are as follows:

- Dynamic modeling of a nonlinear six-degree of mathematical model of a quadrotor UAV is aimed at the system analysis and controls design.
- Design the Lyapunov-based controller, and demonstrated the effectiveness for dealing with the normal situations and the cases with uncertainty.
- Design a passive fault tolerant control system for the quadrotor UAV by employing Lyapunov-based control method and analyze the simulation results under partial loss faults in different position and different quantity of malfunction actuators.
- Design a new Lyapunov-based adaptive controller for fault tolerant control of the quadrotor UAV and analyze the performance under different levels of parameter uncertainties, partial loss faults and combined situations;
- Implement Lyapunov-based control scheme on a real system, Qball-X4 quadrotor UAV and satisfactory flight test results have been obtained.

7.2 Conclusion

This thesis studies the passive fault tolerant control system (PFTCS) by utilizing the Lyapunov-based method and the Lyapunov-based adaptive control approaches using a quadrotor UAV as the research platform. The following conclusions can be drawn based on the research outcomes of this thesis work:

- Quadrotor UAV is a highly coupled system;
- The Lyapunov-based control strategy with fixed controller gains has the limited ability of dealing with severe faults since it cannot handle some actuator partial losses at specific positions;
- The Lyapunov-based adaptive control approach has stronger ability to handle different kind of faults and uncertainties;
- The experiments of the test-bed, Qball-X4, demonstrate that the proposed control approach is executable and capable of tolerating certain faults.

7.3 Recommendations for Future Works

This thesis and the research work mostly concentrate on the partial loss faults of the quadrotor UAV. However, it does not solve the stuck or float fault scenario of the quadrotor UAV since the stuck fault changes the quadrotor's mathematical model, and the corresponding controller is required to be redesigned simultaneously. Therefore, future work will be as follows:

- Utilize the FTCS scheme and redesign the controller under stuck or float faults to accommodate such types of faults;

- Extend the research work discussed in this thesis to other types of UAVs or aircrafts, in order to demonstrate the effectiveness of the proposed method with general UAV applications;
- Test and evaluate the proposed control approaches about position and Euler angle control in the physical quadrotor UAV test-bed, and try to improve the performance combined with the system's physical structure and hardware.

REFERENCES

[1] http://www.aviastar.org/helicopters_eng/oemichen.php (accessed on 2010/04/08).

[2] http://www.aviastar.org/helicopters_eng/bothezat.php (accessed on 2010/04/08).

[3] http://www.aviastar.org/helicopters_eng/convertawings.php (accessed on 2010/04/08).

[4] J. G. Leishman, *Principles of Helicopter Aerodynamics*, New York, NY: Cambridge

[5] http://www.draganfly.com/uav-helicopter/draganflyer-x4/index.php (accessed on 2010/04/08).

[6] http://vertol.mit.edu/index.html (accessed on 2010/04/08).

[7] http://www.draganfly.com/news/2007/11/20/vecpav-autonomous-uav-control-system-draganflyer-helicopters/ (accessed on 2010/04/08).

[8] D. J. Halaas, S. R. Bieniawski, P. Pigg, and J. Vian, "Control and Management of an Indoor, Health Enabled, Heterogenous Fleet," *Proc. of AIAA Infotech@Aerospace Conference*, Seattle, Washington, 6-9 April, 2009 (AIAA 2009-2036).

[9] http://users.encs.concordia.ca/~ymzhang/UAVs.htm (accessed on 2010/04/08).

[10] P. Pounds, R. Mahony, P. Corke, "Modelling and Control of a Quad-Rotor Robot," *In the Proceedings of the Australasian Conference on Robotics and Automation*, Auckland, New Zealand, December, 2006.

[11] G. M. Hoffman, H. Huang, S. L. Waslander, C. J. Tomlin, "Quadrotor Helicopter Flight Dynamics and Control: Theory and Experiment," *In the Conference of the American Institute of Aeronautics and Astronautics*. Hilton Head, South Carolina, August 20-23, 2007.

[12] E. Altug, J. P. Ostrowski and R. Mahony, "Control of a Quadrotor Helicopter using Visual Feedback," *Proceedings of the 2002 IEEE International Conference on Robotics and Automation*, 2002, Vol. 1, pp. 72-77.

[13] V. Mistler, A. Benallegue, and N. K. M' Sirdi, "Exact Linearization and Noninteracting Control of a 4 Rotors Helicopter via Dynamic Feedback," *IEEE International workshop on Robot and Human Interactive Communication*, 2001, pp. 586-593.

[14] D. Lee, T. C. Burg, B. Xian and D. M. Dawson, "Output Feedback Tracking Control of an Underactuated Quad-rotor UAV," *Proceedings of the 2007 American Control Conference*, New York City, USA, July 11-13, 2007, pp. 1775-1780.

[15] A. Tayebi and S. McGilvary, "Attitude Stabilization of a Four-rotor Aerial Robot," *Proceedings of the 2004 IEEE Conference on Decision and Control*, Atlantis, Paradise Island, Bahamas, 2004, vol. 2, pp. 1216-1221.

[16] A. Mokhtari, A. Benallegue and B. Daachi, "Robust Feedback Linearization and GH∞ Controller for a Quadrotor Unmanned Aerial Vehicle," *Journal of Electrical Engineering*, 2006, Vol. 57, No. 1, 20-27.

[17] A. Benallegue, A. Mokhtari and L. Fridman, "Feedback Linearization and High Order Sliding Mode Observer for a Quadrotor UAV," *Proceedings of the 2006 International Workshop on Variable Structure Systems*, Alghero, Italy, June 5-7, 2006, pp. 365-370.

[18] F. Zhou, Z. Zhang, J. Liang, J. Wang, "Feedback Linearization and Continuous Sliding Mode Control for a Quad-rotor," *Proceedings of the 27th Chinese Control Conference*, Kunming, Yunnan, China, July 16-18, 2008, pp.349-353.

[19] I. Kanellakopoulos, P. V. Kokotovic and A. S. Morse, "Systematic Design of Adaptive Controllers for Feedback Linearizable Systems," *IEEE TRANSACTIONS ON AUTOMATIC CONTROL*, Vol. 36, No. 11, November 1991, pp. 1241-1253

[20] Khalil, H. K., *Nonlinear Systems*, Prentice-Hall, Inc., New Jersey, 2nd edition, 1996.

[21] T. Madani and A. Benallegue, "Backstepping Control for a Quadrotor Helicopter," *Proceedings of the 2006 IEEE/RSJ, International Conference on Intelligent Robots and Systems*, Beijing, China, Oct. 9-15, 2006, pp. 3255-3260.

[22] E. Altug, J. P. Ostrowski, C. J. Taylor, "Control of a Quad-rotor Helicopter using Dual Camera Visual Feedback," *The International Journal of Robotics Research*, May 2005, Vol. 24, No. 5, pp. 329-341.

[23] A. A. Mian, M. I. Ahmad and D. B. Wang, "Backstepping based Nonlinear Flight Control Strategy for 6 DOF Aerial Robot," *International Conference on Smart Manufacturing Application*, Kintex, Gyeonggi-do, Korea, April 9-11, 2008, pp.146-151.

[24] G. V. Raffo, M. G. Ortega and F. R. Rubio, "Backstepping/Nonlinear H∞ Control for Path Tracking of a Quad-rotor Unmanned Aerial Vehicle," *2008 American Control Conference*, Westin Seattle Hotel, Seattle, Washington, USA, June 11-13, 2008, pp. 3356-3361.

[25] T. Madani and A. Benallegue, "Backstepping Sliding Mode Control Applied to a Miniature Quadrotor Flying Robot," *Proceedings of IEEE Conference on Industrial Electronics*, Paris, France, 2006, pp.700-705.

[26] M. Sharma, D. G. Ward, "Flight-Path Angle Control via Neuro-Adaptive Backstepping", Barron Associates, Inc., 1160 Pepsi Place Suite 300, Charlottesville, VA 22902.

[27] S. Bouabdallah, P. Murrieri, and R. Siegwart, "Design and Control of an Indoor Micro Quad-rotor," *Proceedings of 2004 IEEE International Conference on Robotics and Automation*, New Orleans, USA, 2004, pp. 4393-4398.

[28] P. Castillo, A. Dzul and R. Lozano "Stabilization of a Mini-rotorcraft having Four Rotors," *Proceedings of the 2004 IEEE International Conference on Industry Technology*, Sendai, Japan, 2004, Vol. 3, pp. 1543-1548.

[29] K. T. Oner, E. Cetinsoy, M. Unel, M. F. Aksit, I. Kandemir, and K. Gulez, "Dynamic Model and Control of a New Quad-rotor Unmanned Aerial Vehicle With Tilt-wing Mechanism," *Proceedings of World Academy of Science, Engineering and Technology*, November 2008, Vol. 35, pp.58-63.

[30] P. Castillo, A. Dzul and R. Lozano, "Real-time Stabilization and Tracking of a Four-rotor Mini-Rotorcraft," *IEEE Transactions on Control Systems Technology*, 2004, Vol. 12, No. 4, pp. 510-516.

[31] F. Kendoul, D. Lara, I. Fantoni-Coichot, and R. Lozano, "Real-Time Nonlinear Embedded Control for an Autonomous Quadrotor Helicopter," *Journal of Guidance, Control, and Dynamics*, July-August 2007, Vol. 30, No. 4, pp.1049-1061

[32] M. Chen and M. Huamezan, "A Combined Mbpc/2DOF H∞ Controller for a Quad-rotor UAV," *AIAA Guidance, Navigation, and Control Conference and Exhibit*, Austin, Texas, August 11-14, 2003.

[33] R. Xu and U. Ozguner, "Sliding Mode Control of a Quad-rotor Helicopter," *Proceedings of the 45th IEEE Conference on Decision & Control*, Manchester Grand Hyatt Hotel, San Diego, CA, USA, December 13-15, 2006, pp. 4957-4962.

[34] Y. M. Zhang and J. Jiang, "Bibliographical Review on Reconfigurable Fault-tolerant Control Systems", *Annual Reviews in Control*, Vol. 32, No. 2, 2008, pp. 229-252.

[35] C. Berbra, S. Lesecq and J. J. Martinez, "A Multi-observer Switching Strategy for Fault-Tolerant Control of a Quadrotor Helicopter," *16th Mediterranean Conference on Control and Automation*, Ajaccio, France, June 25-27, 2008, pp. 1094-1099.

[36] J. T. Qi, Z. Jiang and X. G. Zhao, "Adaptive UKF and Its Application in Fault Tolerant Control of Quadrotor UAV," *AIAA Guidance, Navigation and Control Conference and Exhibit,* August 20-23, 2007, Hilton Head, South Carolina, pp. 1-15.

[37] Y. M. Zhang and J. Jiang, "Active Fault tolerant Control System against Partial Actuator Failures," *IEE Proceedings - Control Theory and Applications*, January 2002, Vol. 149, No. 1, pp. 95-104.

[38] J. D. Boskovic and R. K. Mehra, "A Hybrid Fault-Tolerant Scheme for Flight Control Applications," *AIAA Guidance, Navigation, and Control Conference and Exhibit*, August 6-9, 2001, Montreal, Canada, pp. 1-11.

[39] S. Gayaka and B. Yao, "Accommodation of Partial Actuator Faults using Output Feedback based Adaptive Robust Control," *International Conference on Prognostics and Health Management*, 2008.

[40] G. Tao, S. Chen, and S. M. Joshi, "An Adaptive Actuator Failure Compensation Controller Using Output Feedback," *Proceeding of the American Control Conference*, June 25-27, 2001, Arlington, pp. 3085-3090.

[41] F. Liao, J. L. Wang, and G. H. Yang, "Reliable Robust Flight Tracking Control: An LMI Approach," *IEEE Transaction on Control Systems Technology*, January, 2002, Vol. 10, No.1, pp. 76-89.

[42] G. H. Yang, J. L. Wang and Y. C. Soh, "Reliable LQG Control with Sensor Failures," *IEE Proc.-Control Theory and Applications*, July 2000, Vol. 147, No. 4, pp. 433-438.

[43] K. Ikeda and S. Shin, "Fault Tolerant Decentralized Adaptive Control Systems using Backstepping," *Proceedings of the 34th Conference on Decision & Control*, New Orleans, December 1995, pp. 2340-2345.

[44] B. L. Stevens, F. L. Lewis, *Aircraft Control and Simulation*, Wiley, New York, 2003.

[45] R. Goel, S. M. Shah, N. K. Gupta, and N. Ananthkrishnan, "Modeling, Simulation and Flight Testing of an Autonomous Quadrotor," *Proceedings of ICEAE*, 2009.

[46] C. Edwards and S. K. Spurgeon, *Sliding Mode Control*, Taylor & Francis Ltd, USA, 1998.

[47] M. Krstic, I. Kanellakopoulos and P. Kokotovic, *Nonlinear and Adaptive Control Design*, New York: John Wiley & Sons, 1995.

[48] R. W. Prouty, *Helicopter Performance, Stability and Control*, Krieger Publishing Company, Florida, 1996.

[49] A. Niederlinski, "A Heuristic Approach to the Design of Interacting Multivariable Systems," *Automatic*, 1971, Vol.7, pp. 691-701.

[50] R. Isermann, *Fault-Diagnosis Systems: An Introduction from Fault Detection to Fault Tolerance*, Springer-Verlag, Berlin Heidelberg, 2006.

[51] M. Mahmoud, J. Jiang, Y. M. Zhang, *Active Fault Tolerant Control Systems: Stochastic Analysis and Synthesis*, Springer-Verlag, May 1, 2003.

[52] Y. M. Zhang, *Fault Tolerant Control Systems*, Lecture notes, 2005.

[53] N. E. Wu, Y. M. Zhang and K. M. Zhou, "Detection, Estimation, and Accommodation of Control Effectiveness Loss," *International Journal of Adaptive Control and Signal Processing*, 2000, Vol 14, pp. 775-795.

[54] D. Hazry and M. Sugisaka, "Optimal Parameter Tuning in a Predictive Nonlinear Control Method for a Mobile Robot," *American Journal of Applied Science*, 2006, pp. 1803-1809.

[55] A. R. Benaskeur and A. Desbiens, "Backstepping Based Adaptive PID Control," *IEEE Proceeding*, online no. 20020100.

[56] Y. Feng, Y. X. Wu, Y. M. Hu and C. Y. Su, "Adaptive Backstepping Control of a Class of Uncertain Nonlinear Systems with Prandti-Ishlinskii Hysteresis," *Proceedings of the Fourth International Conference on Machine Learning and Cybernetics*, Guangzhou, August 18-21, 2005, pp. 697-701.

[57] L. Sonneveldt, Q. P. Chu and J. A. Mulder, "Nonlinear Flight Control Design using Constrained Adaptive Backstepping," *Journal of Guidance, Control, and Dynamics*, March-April 2007, Vol. 30, No 2, pp. 322-336.

[58] J. Farrell, M. Sharma, and M. Polycarpou, "Backstepping Based Flight Control with Adaptive Function Approximation," *Journal of Guidance, Control, and Dynamics*, November-December 2005, Vol. 28, No. 6, pp. 1089-1102.

[59] L. Sonneveldt, E. R. V. Ort, Q. P. Chu and J. A. Mulder, "Comparison of Inverse Optimal and Tuning Functions Designs for Adaptive Missile Control," *Journal of Guidance, Control and Dynamics*, July-August 2008, Vol. 31, No. 4, pp. 1176-1182.

[60] C. Y. Su, Q. Q. Wang, X. K. Chen, and S. Rakheja, "Adaptive Variable Structure Control of a Class of Nonlinear Systems With Unknown prandtl-Ishlinskii Hysteresis," *IEEE Trans. on Automatic Control*, December 2005, Vol. 50, No. 12, pp. 2069-2073.

[61] QUANSER INNOVATE EDUCATE, "Quanser Qball-x4 user manual, Document Number 829.

[62] Gunstix: www. Gumstix.com, accessed in June, 2010.

[63] www.quanser.com, accessed in June, 2010